

ISLANDING DETECTION USING COMPUTATIONAL INTELLIGENCE TECHNIQUES IN A SMART DISTRIBUTION NETWORK

Thesis

Submitted in partial fulfillment of the requirements for the degree of

DOCTOR OF PHILOSOPHY

by

M SANTHOSH KUMAR GOUD



DEPARTMENT OF ELECTRICAL AND ELECTRONICS ENGINEERING

NATIONAL INSTITUTE OF TECHNOLOGY KARNATAKA

SURATHKAL, MANGALORE -575025

DECEMBER, 2019

DECLARATION

by the Ph.D. Research Scholar

I hereby *declare* that the Research Thesis entitled **Islanding Detection Using Computational Intelligence Techniques in a Smart Distribution Network** which is being submitted to the National Institute of Technology Karnataka, Surathkal in partial fulfillment of the requirement for the award of the Degree of Doctor of Philosophy in Electrical and Electronics Engineering is a *bonafide report of the research work carried out by me*. The material contained in this Research Thesis has not been submitted to any University or Institution for the award of any degree.

.....

M Santhosh Kumar Goud, 158020EE15F08
Department of Electrical and Electronics Engineering

Place: NITK-Surathkal

Date:

CERTIFICATE

This is to *certify* that the Research Thesis entitled **Islanding Detection Using Computational Intelligence Techniques in a Smart Distribution Network** submitted by M Santhosh Kumar Goud (Register Number: 158020EE15F08) as the record of the research work carried out by him, is *accepted as the Research Thesis submission* in partial fulfillment of the requirements for the award of degree of Doctor of Philosophy.

Dr. Dattatraya N Gaonkar
(Research Guide)

Dr. Shubhanga K N
(Chairman-DRPC, EEE Dept.)

Acknowledgements

It gives me immense pleasure and a great sense of satisfaction to express my heartfelt gratitude to those who made this dissertation possible.

Firstly, I would like to express my deepest gratitude to my supervisor, Dr. Dattatraya N Gaonkar, Associate Professor, Department of Electrical and Electronics Engineering, for his sagacious guidance, encouragement and showing trust in me all the time. He has been a constant source of motivation and support in this entire journey.

I thank National Institute of Technology Karnataka (NITK) for giving me an opportunity to pursue research and Ministry of Human Resource Development(MHRD), Government of India, for awarding research scholarship.

I would like to thank my research progress assessment committee (RPAC) members Dr. Nagendrappa H and Dr. Basavaraju Manu, for their constructive feedback and guidance. Also, I would like to thank Dr. Shubhanga K N, Head of the Department of Electrical and Electronics Engineering, NITK, Surathkal. Thanks also go to Dr. Venkatesa Perumal and Dr. Vinatha U, former HODs for providing the necessary resources in the department to carry out my research. I also wish to thank the non-teaching staff of the EEE department for providing necessary support.

I would like to express my thanks to all my colleagues and friends for making this journey memorable.

I would like to express my deepest gratitude towards my parents Smt. Latha Rani and Sri. Chandrashekar garu and my brothers Shashi and Bhargav for their unconditional love and patience. I can't thank them enough for putting up with all my idiosyncrasies. Their faith and unconditional love towards me are the reason for whatever I have achieved in my

life. I would like to thank my wife Swathi from the bottom of my heart for being supportive, caring, and encouraging. Thank you, I owe it all to you!! I would like to dedicate this dissertation to my Late grandfather Sri. Janakiramulu garu for his love, affection, and fantastic childhood memories.

M SANTHOSH KUMAR GOUD

Abstract

Distributed generation (DG) offers solution to the ever increasing energy needs by generating the energy at the consumer end, in most cases by means of renewable energy sources. A microgrid with DGs will result in an enhanced performance in terms of continuity of the power supply for consumers. Microgrids may operate either in grid-connected or islanded mode. Islanding detection is one of the most important aspect of inter-connecting a DG to the utility. Several islanding detection methods have been proposed over the years to improve the islanding detection in terms of detection time, accuracy. However, with the upcoming trends, such as smart grids, there is an imminent need for incorporating intelligence to the islanding detection methods. Also, it is important for the islanding detection methods to perform well at near zero power mismatch conditions and noisy conditions.

This research work proposes islanding detection methods based on image classification techniques. Time-series data from point of common coupling is acquired and then converted to an image to enable this. A dataset for islanding detection based on several islanding and non-islanding events is created to be used in training and testing the machine learning and deep learning models. Three islanding detection methods are proposed in this research work. The first method is based on HOG feature extraction from the image and SVM classifier. The second method is based on transfer learning method. The third islanding detection method is based on custom designed CNN for islanding detection. In addition to islanding detection, a feature for early islanding detection is also proposed in this research work. Early islanding detection is proposed by monitoring the fault and normal conditions. Once a fault occurs, the time window between the operation of relay contacts and the opening of circuit breakers is utilized to detect the islanding event. All the methods are tested with the islanding dataset that is created which includes near zero power mismatch conditions and noisy data. The proposed methods demonstrate the potential of image classification techniques for islanding detection.

Contents

Acknowledgements	i
Abstract	iii
List of figures	vii
List of tables	xi
Nomenclature	xv
1 INTRODUCTION	1
1.1 Introduction	1
1.2 Classification of islanding detection methods	3
1.3 Local methods	6
1.3.1 Passive methods	6
1.3.2 Active methods	8
1.3.3 Hybrid methods	13
1.4 Remote methods	16
1.5 Signal processing Techniques	17
1.5.1 Fourier transform (FT) based methods	17
1.5.2 Wavelet transform (WT) based methods	18
1.5.3 S-Transform (ST) based techniques	20
1.5.4 Time- Time (TT) Transform based techniques	21
1.5.5 Hilbert Huang Transform (HHT) based techniques	22
1.5.6 Mathematical Morphology based technique	22
1.6 Intelligent techniques	23
1.6.1 Neural Network based techniques	26
1.6.2 Fuzzy logic based techniques	27
1.6.3 Decision tree based techniques	27
1.6.4 Naive Bayesian classifier	28

1.6.5	Support vector machine classifier	29
1.6.6	Random forest classifier	29
1.7	Motivation	37
1.8	Contributions of this research work	37
1.9	Thesis organization	38
2	DATASET GENERATION	42
2.1	Introduction	42
2.2	Supervised learning	42
2.2.1	Need for image dataset	43
2.3	Scalogram	44
2.4	Data set generation	44
2.4.1	System description	46
2.4.2	Parameters used for islanding detection	46
2.4.3	Test cases for islanding and non-islanding events	49
2.5	Summary	56
3	HISTOGRAM OF ORIENTED GRADIENTS FEATURE BASED ISLANDING DETECTION	58
3.1	Introduction	58
3.2	Feature extraction from images	58
3.2.1	Histogram of oriented gradient features	59
3.3	Proposed method	63
3.4	Results and discussions	64
3.5	Summary	70
4	TRANSFER LEARNING BASED ISLANDING DETECTION	72
4.1	Introduction	72
4.2	Need for better features	72
4.2.1	Neural networks for image classification	73
4.2.2	Convolution neural networks	74
4.3	Transfer learning	81
4.4	Proposed islanding detection method	81
4.4.1	AlexNet	82
4.4.2	VGG16	84

4.5	Results and discussion	86
4.6	Summary	88
5	CUSTOM CONVOLUTION NEURAL NETWORK BASED ISLAND- ING DETECTION	90
5.1	Introduction	90
5.2	Proposed CNN based islanding detection method	91
5.3	Results and discussions	92
5.3.1	Design of CNN	92
5.3.2	Custom CNN based IDM results	98
5.4	Summary	105
6	CONCLUSIONS AND FUTURE SCOPE	106
6.1	Conclusions	106
6.2	Future scope	107
	Bibliography	112
	PUBLICATIONS	124

List of Figures

1.1	Islanding phenomenon	3
1.2	Classification of islanding detection methods	5
1.3	Block diagram of passive islanding detection method	6
1.4	Block diagram of active islanding detection method	8
1.5	Block diagram of hybrid islanding detection method	13
1.6	Block diagram of signal processing based islanding detection method	17
1.7	Block diagram of machine learning based islanding detection method	23
1.8	Classification of islanding detection methods - Contribution of this thesis work indicated	39
1.9	Organization of thesis	40
2.1	Supervised learning workflow	43
2.2	Scalogram image of the time-series data obtained from example equation	45
2.3	Schematic of the system used for generating data set	45
2.4	Time line of events after a fault	49
2.5	Scalogram images for concatenated voltages $V_{[abc]}$ for grid connected and islanded modes of operation	50
2.6	Scalogram images for different parameters (a) $dV_{[abc]}/dt$ for grid con- nected and islanded case (b) dV_{neg}/dt for grid connected and islanded case (c) dV_{neg}/dt for normal condition and fault condition (for early islanding detection)	52
2.7	Scalogram images for various non-islanding cases: (a) Sudden switching ON of Inductive load/Induction motor load (b) Sudden switching OFF of Inductive load/Induction motor load (c) Sudden switching ON of Capacitive load (d) Sudden switching OFF of Capacitive load	53
3.1	Feature extraction in supervised learning	59

3.2	Gradient computation for a given pixel	60
3.3	Magnitude allocation for bins based on direction	62
3.4	Final HOG feature vector for 16x16 pixel image	62
3.5	Flowchart of the proposed HOG feature based islanding detection method	63
3.6	(a) Size of HOG feature vector for different block and cell sizes (b) Plot of accuracy for optimizing cell size and block size	65
3.7	(a) $V_{[abc]}$ (b) $\frac{dV_{[abc]}}{dt}$ (c) $\frac{dV_{[neg]}}{dt}$ - Islanding detection (d) $\frac{dV_{[neg]}}{dt}$ - Early islanding detection(Fault) . . .	68
3.8	(a) $V_{[abc]}$ (b) $\frac{dV_{[abc]}}{dt}$ (c) $\frac{dV_{[neg]}}{dt}$ - Islanding detection (d) $\frac{dV_{[neg]}}{dt}$ - Early islanding detection(Fault) . . .	69
4.1	General architecture of ANN	73
4.2	General architecture of a CNN	74
4.3	Example image and filters for convolution operation	75
4.4	Convolution operation in a CNN with Filter 1	76
4.5	Convolution operation in a CNN with Filter 1	76
4.6	Feature map for Filter 1 after convolution operation on entire image .	76
4.7	Feature map for Filter 2 after convolution operation on entire image .	77
4.8	Feature maps for Filter 1 and Filter 2 after convolution operation on entire image	77
4.9	Activation functions (a) Sigmoid function (b) tanh function (c) Recti- fied linear unit (ReLU) function	78
4.10	Feature map transformation after applying ReLU activation	79
4.11	Feature map transformation after applying max pooling	79
4.12	Fully connected layer with class outputs	80
4.13	Islanding detection method using transfer learning classifiers	82
4.14	AlexNet architecture	83
4.15	VGG16 architecture	84
4.16	Training plots of AlexNet and VGG16 for $V_{[abc]}$, $dV_{[abc]}/dt$, dV_{neg}/dt , and early islanding detection based on dV_{neg}/dt for fault conditions .	87
5.1	Proposed islanding detection method with multiple CNN classifiers .	91
5.2	Results for CNN training (a) Plots of training accuracy for all CNNs (b) Plots of training loss for all CNNs	94
5.3	Results for CNN training (a) Plots of training accuracy for all CNNs (b) Plots of training loss for all CNNs	95

5.4	Results for CNN training (a) Plots of training accuracy for all CNNs	
	(b) Plots of training loss for all CNNs	99
5.5	Plots comparing different aspects of AlexNet, VGG16 and custom designed architecture CNN-I	103
5.6	Plots comparing different aspects of AlexNet, VGG16 and custom designed architecture CNN-II	104

List of Tables

1.1	International standards for anti-islanding	4
1.2	Summary of passive islanding detection techniques	8
1.3	Summary of active islanding detection techniques	14
1.4	Summary of various signal processing based islanding detection techniques	24
1.5	Summary of various signal processing based islanding detection techniques - Continued	25
1.6	Summary of intelligent-based islanding techniques – I	31
1.7	Summary of intelligent-based islanding techniques – II	32
1.8	Summary of intelligent-based islanding techniques – III	33
1.9	Summary of intelligent-based islanding techniques – IV	34
1.10	Summary of intelligent-based islanding techniques – V	35
2.1	Details of the system used for generating dataset	47
2.2	Various cases simulated to create data set	54
2.3	Training and testing data used for all islanding detection methods	55
3.1	Classification results for HOG based IDM - for all kernels	66
3.2	Classification results for HOG based IDM - for different kernels	67
4.1	Alexnet architectural details	83
4.2	VGG16 architectural details	85
4.3	Classification results for Transfer Learning	88
5.1	Custom designed CNN-I architectural details	96
5.2	CNN-I training hyperparameter details	96
5.3	Custom designed CNN-II architectural details	97
5.4	CNN-II training hyperparameter details	97

5.5	Classification results for custom CNN based IDM	98
5.6	Activation maps and parameters in CNN-I	101
5.7	Activation maps and parameters in CNN-II	102

Nomenclature

Abbreviations

Symbol	Meaning
AFD	Active frequency drift
AFDFP	Active frequency drift with positive feedback
AI	Artificial intelligence
AIDM	Active islanding detection method
ANN	Artificial neural network
CNN	Convolution neural network
CWT	Continuous wavelet transform
DG	Distributed generation
DFT	Discrete Fourier transform
DL	Deep learning
DT	Decision tree
DWT	Discrete wavelet transform
FFT	Fast Fourier transform
FJ	Frequency jump
FL	Fuzzy logic
FT	Fourier transform
HD	Harmonic distortion
HHT	Hilbert Huang transform
HOG	Histogram of oriented gradients
IDM	Islanding detection method
IG	Induction generator
ML	Machine learning
NDZ	Non-detection zone
NN	Neural network
OUF	Over/Under Frequency
OUV	Over/Under Voltage
PCC	Point of common coupling
PE	Power electronic
PIDM	Passive islanding detection method
PJD	Phase jump detection

PLL	Phase locked loop
PLCC	Power line carrier communication
PNN	Probabilistic neural network
PV	Photovoltaic
RFC	Random forest classifier
ROCOF	Rate of change of Frequency
ROCOFOP	Rate of change of frequency over power
ROCONSV	Rate of change of negative sequence voltage
ROCOP	Rate of change of Power
ROCOV	Rate of change of voltage
SCADA	Supervisory control and data acquisition
SFS	Sandia frequency shift
SG	Synchronous generator
SMS	Slip mode frequency shift
SPD	Signal produced by disconnect
SPIDM	Signal processing based islanding detection method
STFT	Short-time Fourier transform
SVS	Sandia voltage shift
SVM	Support vector machine
VSC	Voltage source converter
VU	Voltage unbalance
WT	Wavelet transform

Symbol Meaning

$V_{[abc]}$	Concatenated pcc voltages
$\frac{dV_{[abc]}}{dt}$	Rate of change of voltages
$\frac{dV_{[neg]}}{dt}$	Rate of change of negative sequence voltage
V	Voltage
V_d	Direct axis voltage
ω_{PLL}	Frequency of Phase Locked Loop
I	Current
i_{CON}	Output current of the converter

f	Frequency
Δf	Frequency deviation
$\frac{\Delta f}{\Delta t}$	Rate of change of frequency
f_{grid}	Nominal grid frequency
f_m	Frequency corresponding to maximum phase angle
P	Active power
ΔP	Active power mismatch
$\frac{\Delta P}{\Delta t}$	Rate of change of power
P_{load}	Active power requirement of load
P_{DG}	Active power supplied by DG
Q	Reactive power
ΔQ	Reactive power mismatch
Q_{load}	Reactive power requirement of load
Q_{DG}	Reactive power supplied by DG
Q_{inv}	Inverter reactive power
Z_1	Negative sequence magnitude
ϕ	Negative sequence phase
HC_{odd}	r.m.s value of the odd harmonic components
HC_{even}	r.m.s value of the even harmonic components
pf	Power factor
θ	Normalized phase angle of voltage

Chapter 1

INTRODUCTION

1.1 Introduction

Traditionally, the configuration of distribution system was designed to operate with only one source supplying the downstream feeder networks (Balamurugan et al., 2012). However, with increasing demand for energy and depleting fossil fuel resources, it has become the need of the hour to come up with solutions to meet the insatiable energy consumption requirements. A rudimentary approach to meet this demand would be to increase the generation capacity. This solution increases the dependency on fossil fuels even more. Also, the transmission and distribution networks need to be updated according to the increased generation, transmission, and distribution capacities. As a result, the increased load demand will further increase the transmission and distribution costs. These challenges can be overcome by transitioning from large conventional, and centralized generation sources to small, renewable, and distributed generation (DG) sources. In other words, distributed generation, mostly with renewable energy sources, at the consumer end, is one such solution to meet the future energy demands (Kunte and Gao, 2008, Lidula and Rajapakse, 2011, Tsang and Chan, 2013). As per (1547.2-2008, 2008), there are two classifications for DG sources. One classification is based on the type of prime mover as stationary and rotating DGs. Second classification is based on grid-interfacing technique. According to this, DGs can be asynchronous, synchronous, or power electronic (PE) interfaced DGs.

Distributed generation or DG refers to comparatively small generation sources that are installed at the consumer end of the distribution network. These DG sources are

distributed across the system. The capacity of DG system can range from kilowatts to few tens of megawatts. Depending on the energy conversion technology, various DG sources can be photovoltaic (PV) panels, wind turbines, micro hydro turbines, micro turbines, or fuel cells. A microgrid is defined as a group of interconnected loads and DG sources within clearly defined electrical boundaries that acts as a single controllable entity with respect to the grid.

The advantages of installing DG sources are manifold.

- **Environment friendly**

Since most of the DG sources are based on renewable energy, such as solar and wind, the carbon emissions are reduced.

- **Cost-effective**

The proximity of DG sources to the load centers ensures reduction in transmission and distribution losses when compared to traditional centralized generation sources. Also, the initial investment, construction, and deployment time for DG sources is very less compared to large scale power plants. Further, there is no need for installing or increasing the capacity of the transmission lines, which again saves a lot of resources.

- **Flexibility**

Owing to their relatively smaller ratings, DG sources normally have fast start-up and shutdown times. Other advantages include easy maintenance, flexibility in terms of operation, control and load management.

However, the intermittent nature of the renewable energy sources not only affects the power quality and the system dynamics but also poses some challenges to seamlessly integrate them to the grid. One such challenge is the islanding phenomenon. Islanding in any distributed generation system is a condition wherein the distributed energy resource is disconnected from the main grid and still continues to supply to the local consumers as depicted in Fig.1.1.

Microgrids can operate either in grid-connected or islanded mode and each mode has strikingly different strategies to achieve optimal performance. In grid-connected mode of operation the primary goal is optimal and economical operation. Islanding can either be planned or unplanned. In planned islanding, a controllable operation, the microgrids still supply power to the local loads to ensure continuity of supply while

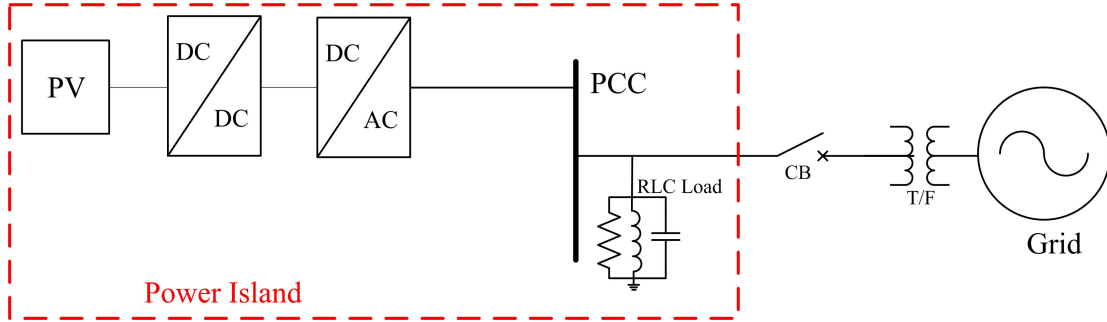


Figure 1.1: Islanding phenomenon

the utility is disconnected. Unplanned islanding on the other hand is an uncontrollable operation and hence it is undesirable. It may occur due to various reasons such as, line tripping, human error, or equipment failure. Unplanned islanding can be a threat to the safety of the personnel working on the system and it can seriously affect the microgrid operation. Hence, islanding must be detected and the DGs must be either disconnected or the mode of operation is changed from grid-connected to islanded mode of operation in case of a planned islanding. Various islanding detection methods have been proposed over the years with a primary goal to detect islanding event adhering to the international standards.

Several international standards currently exist across the globe for interconnecting a DG to the utility. All these standards, more or less, demand stringent requirements for islanding detection in terms of detection time, q-factor, frequency range, and nominal voltage values. These standards are used as a benchmark while developing new techniques for islanding detection. A digest of various international standards is given in Table 1.1.

1.2 Classification of islanding detection methods

Islanding detection techniques can be broadly classified as classical methods, which include all the local methods, such as, passive, active, and hybrid methods, remote methods, signal processing methods, and intelligent/computational intelligence based methods. Classification of islanding detection methods is shown in Fig. 1.2. A brief description of the islanding detection methods is presented here.

Table 1.1: International standards for anti-islanding

Standard	Q	Detection time	Frequency range	Voltage range
IEEE 929-2000	2.5	Within 2s	59.3–60.5 Hz	0.88–1.1 p.u.
IEEE 1547	1	Within 2s	59.3–60 Hz	0.88–1.1 p.u.
IEC 62116	1	Within 2s	59.3–60 Hz	0.88–1.15 p.u.
UL 1741	1	Within 2s	59.3–60.5 Hz	0.88–1.1 p.u.
UK G83/2	0.5	Within 0.5s	47.5–51.5Hz (stage 1)	0.87–1.1 p.u.(stage 1)
(DGs up to 16A/phase)			47–52 Hz (stage 2)	0.8–1.19 p.u.(stage 2)
UK G83/3	0.5	Within 0.5s	47.5–51.5Hz (stage 1)	0.87–1.1 p.u.(stage 1)
(17kW/ph or 50kW/3-ph)			47–52 Hz (stage 2)	0.8–1.19 p.u.(stage 2)
Canadian C22.2 No107-01	2.5	Within 2s	59.5–60.5 Hz	0.88–1.06 p.u.
German VDE 0126-1-1	2	Within 0.2s	47.5–50.2 Hz	0.88–1.1.5 p.u.
French ERDF-NOI- RES 13E	2	Instantly	49.5–50.5 Hz	0.88–1.06 p.u.
Japanese JIs	0	Within 2s (ac- tive IDM)	Setting value	Setting value
		0.5–1s (passive IDM)	Setting value	Setting value
Korean	1	Within 0.5s	59.3–60Hz	0.88–1.1 p.u.

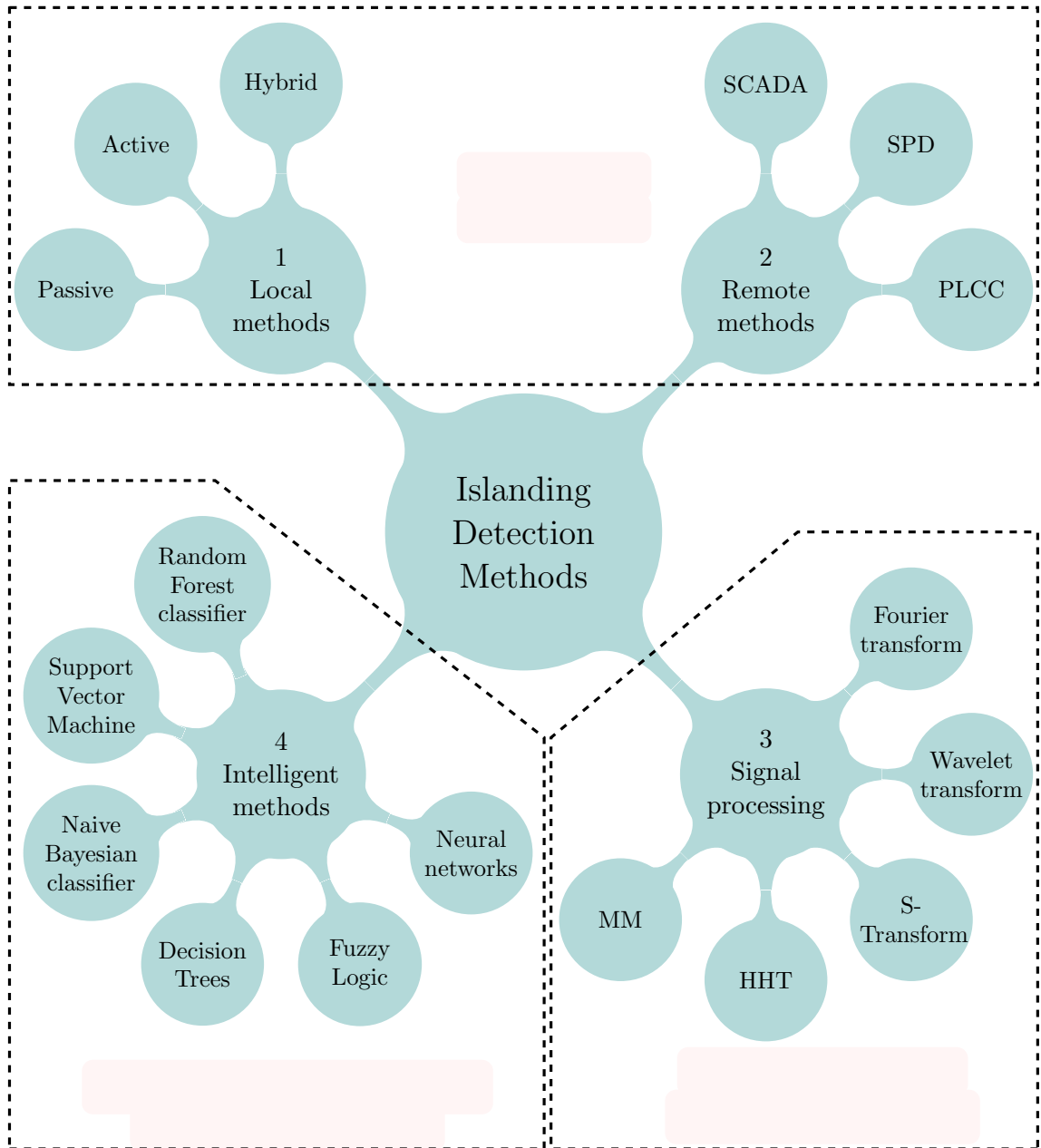


Figure 1.2: Classification of islanding detection methods

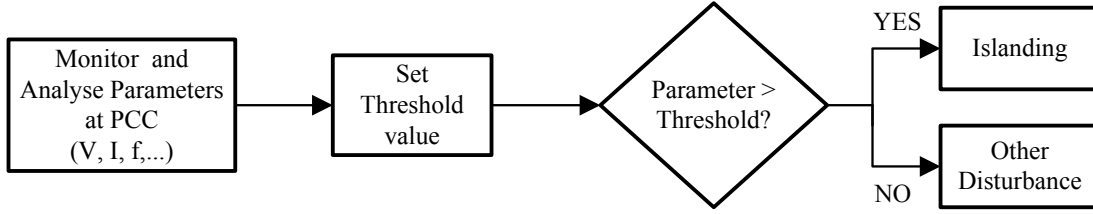


Figure 1.3: Block diagram of passive islanding detection method

1.3 Local methods

1.3.1 Passive methods

Passive methods, as the name suggests, passively monitor a range of electrical quantities at the point of common coupling (PCC) and check if they are below the preset threshold value. If the monitored electrical quantity exceeds the threshold value, which is most likely in the event of loss of grid, an islanding event is detected as depicted in Fig.1.3. A summary of various passive islanding detection techniques is presented in Table 1.2.

1. Voltage unbalance(VU)

During an islanding event, even if the load variations are nominal, an unbalance in the voltage arises as a result of the topological changes in the system. An islanding detection scheme based on this technique is proposed by monitoring the negative and positive sequence components in (Jang and Kim, 2004)

2. Harmonic distortion(HD)

Whenever there is a loss of mains, an immediate effect is changes in the loading of the DG. These changes in loading result in variation of the harmonic content in the current. Therefore, by monitoring the harmonic distortion islanding event can be detected (Jang and Kim, 2004).

3. Over/under voltage and over/under frequency(OUV/OUF)

In grid-connected mode of operation the active and reactive power requirement of the load, P_{load} and Q_{load} , are supplied by the DG (P_{DG} and Q_{DG}) and the mismatch between the two is supplied by the grid.

$$\Delta P = P_{load} - P_{DG} \quad (1.1)$$

$$\Delta Q = Q_{load} - Q_{DG} \quad (1.2)$$

However, in the event of islanding, to maintain the active and reactive power balance, the voltage and frequency will change such that $\Delta P = 0$ and $\Delta Q = 0$, respectively (De Mango et al., 2006). The variation of these two parameters are monitored to detect an island.

4. Rate of change of power(ROCOP)

An islanding event has a direct consequence on the load change, therefore, by monitoring the variations in the power output of the target DG islanding event can be detected (Redfern et al., 1993)

5. Rate of change of frequency

When a distributed generation source is operating in the islanding mode, the power mismatch will lead to a change in the frequency. Therefore, by monitoring the rate of change of frequency over few cycles and comparing it with the threshold value, islanding event can be detected (Redfern et al., 1993, Freitas et al., 2005).

6. Rate of change of frequency over power(ROCOFOP)

ROCOF technique has difficulties detecting the islanding situations especially when the power mismatch between the load and islanded DG is very small. In order to overcome this drawback a method based on df/dP is proposed to detect islanding even under small power mismatch cases (Pai and Huang, 2001).

7. Phase jump detection (PJD)

Phase jump detection essentially monitors the phase difference between output voltage and current of a grid tied inverter. Phase locked loops (PLL) are used to synchronize the inverters with the voltage at the point of common coupling (PCC). This is achieved by a PLL by detecting the zero crossing of the voltage at PCC. However, during an islanding event the inverter output current remains unchanged while the voltage at the PCC, as a consequence of islanding, is no longer stiff. This will result in a phase jump of the voltage since the phase angle of the load is still the same. By detecting this phase jump, islanding event can be detected (PVPS, 2002, Singam and Hui, 2006).

Table 1.2: Summary of passive islanding detection techniques

Technique	NDZ	Impact on power quality	Detection time	Error detection rate
VU	Large	None	53 ms	Low
HD	Large for high Q	None	45 ms	High
OUV/OUF	Large	None	4 ms–2 s	Low
ROCOP	Small	None	24–26 ms	High
ROCOF	Small	None	24 ms	High
ROCOFOP	< ROCOF	None	100 ms	Low
PJD	Large	None	10–20 ms	Low

1.3.2 Active methods

Despite having very short detection times, passive islanding detection methods possess inherent shortcomings, such as, presence of non detection zone (NDZ) and the setting of threshold value for islanding detection. Especially with threshold setting, too low a value will lead to nuisance tripping while slightly larger threshold setting will result in missed islanding event. In order to overcome the shortcomings of passive techniques, active methods are proposed. Active methods take advantage of the fact that response of the grid to a perturbation can vary drastically under normal conditions and islanded conditions. Active islanding, as shown in Fig.1.4, injects a perturbation into the grid parameters, continuously at set intervals, and analyses the response. If the parameter exceeds a set threshold value in the analyzed response, active methods classify it as an islanding event.

Various active islanding detection techniques are presented below and a summary of these techniques is given in Table. 1.3.

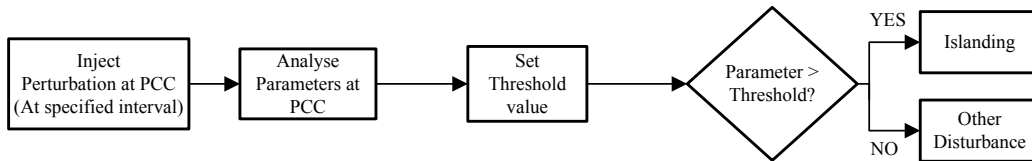


Figure 1.4: Block diagram of active islanding detection method

1. Impedance measurement method

In this method, the magnitude of the inverter output current is continuously varied and the corresponding change in the voltage is monitored. The variation is calculated as dv/di , as equivalent impedance seen from the inverter. If the value exceeds a certain threshold, it will be classified as an islanding event (Ahmad et al., 2013, O’kane and Fox, 1997). However, the difficulties that arise in setting the threshold value makes it impractical to implement.

2. Active frequency drift (AFD) method

Once an inverter is synchronized to the grid, the voltage at the PCC and the inverter current remain fixed. However, when there is a loss of mains, a small disturbance caused in the inverter’s output current will lead to a change in the zero crossing of the voltage giving rise to a change in the phase. This forces the inverter to drift the current to eliminate phase error. This process will lead to a point where the frequency at the PCC is higher than the threshold value leading to detection of an islanding situation (PVPS, 2002).

3. Frequency jump (FJ) method

FJ, just like AFD, also introduces a dead zone in the inverter’s output current waveform, but not in every cycle; for instance, a dead zone in every three cycles. Despite the dead zones introduced to the current waveform, the voltage at PCC remains unchanged when it is connected to the grid. When islanding occurs, the voltage at PCC no longer remains stiff and the islanding is detected by the variation in voltage frequency (PVPS, 2002, Li et al., 2014). Both AFD and FJ techniques fail to perform well for multiple inverters operating in parallel.

4. Active frequency drift with positive feedback (AFDPF) method

A method to minimize the existence of NDZ in AFD is proposed in (Ropp et al., 1999) by employing positive feedback to increase the chopping frequency with increasing frequency deviation from the nominal value as follows:

$$cf_k = cf_{k-1} + F(\Delta\omega_k) \quad (1.3)$$

where: cf_{k-1} and ω_{k-1} are chopping fraction and frequency in the previous cycle respectively, and F is a function which maps sampled frequency error $\Delta\omega_K =$

$\omega_1 - \omega_0$. This function, when properly chosen, adds significant improvements to AFD. However, the power quality is slightly affected and NDZ still prevails for loads with high quality factor.

5. Sandia frequency shift (SFS)

Sandia frequency shift (SFS) is an extension of AFD, wherein a positive feedback is applied to the frequency of the inverter's voltage and its chopping frequency is defined as (PVPS, 2002, Li et al., 2014):

$$cf = cf_0 + K(f_{PCC} - f_{grid}) \quad (1.4)$$

where: cf_0 is the chopping frequency when there is deviation in frequency, K is the accelerating gain, f_{PCC} is the frequency of the voltage at PCC, and f_{grid} is the grid frequency. SFS offers least NDZ in comparison with all the other active methods.

6. Sandia voltage shift (SVS) method

Sandia voltage shift is yet another method that employs positive feedback, in this case to the amplitude of voltage at the PCC, for islanding detection. When the utility is disconnected, by applying a positive feedback to the voltage at PCC, there is a corresponding change in in the inverter's output current and power which can further accelerate the voltage drift to detect the islanding condition (PVPS, 2002, Li et al., 2014). Despite its ease of implementation and efficiency comparable to SFS, Sandia voltage shift has some drawbacks such as, slight degradation of power quality and reduction of inverter's efficiency as a consequence of changing output power and its effect on maximum power point tracking.

7. Slip mode frequency shift (SMS) method

In slip mode frequency (SMS) method, the output current of the utility connected converter, which is expressed as Eq. 1.5, is controlled as a function of the frequency of the voltage at the PCC (Liu et al., 2010, Lopes and Sun, 2006).

$$i_{CON} = I \sin(2\pi ft + \theta_{SMS}) \quad (1.5)$$

where: f and θ_{SMS} are PCC voltage frequency and phase angle for the SMS technique, respectively.

θ_{SMS} is further set as given below:

$$\theta_{SMS} = \frac{2\pi}{360} \theta_m \sin \left(\frac{\pi}{2} \frac{f - f_g}{f_m - f_g} \right) \quad (1.6)$$

where: f_g is the nominal grid frequency, θ_m and f_m are maximum phase angle and the corresponding frequency at which it occurs, respectively.

During grid connected mode of operation, the phase angle between θ_{SMS} is almost zero for rated utility frequency. However, during islanding mode of operation the phase angle is entirely dependent on the external perturbation and the variation in the phase angle can be used to detect an islanding event.

8. Variation of active (P) and reactive(Q) power method

During an islanding condition the changes in the real power output of an inverter, caused due to variation of temperature and/or irradiance, flow into the load. This will directly affect the inverter output current and the voltage at the PCC. The variation of the output power caused by the active power variation injected by inverter can be expressed as follows (Mango et al., 2006):

$$P_{DG} = P_{load} = \frac{V^2}{R} \quad (1.7)$$

The variation in voltage can be derived from Eq. 1.7 as:

$$\Delta V = \frac{\Delta P_{DG}}{2} \cdot \sqrt{\frac{R}{P_{DG}}} \quad (1.8)$$

In Eq. 1.8, since R and P_{DG} are constant, the variation in voltage is directly dependent on variation in P_{DG} . Similarly, relation between variation in reactive power (Q) and variation in frequency is given as:

$$dQ = K_f \cdot (f_n - f) \quad (1.9)$$

where: K_f , f_n , and f are gain, nominal value of frequency and the estimated value of frequency respectively.

9. Negative sequence current injection method

During grid-connected mode of operation, if a negative-sequence current component is injected it will entirely flow into the grid since the grid offers low impedance. Therefore, the injected negative-sequence current will have no effect at all on the voltage at PCC. However, in the event of an islanding condition, the injected negative-sequence current will flow into the local load, resulting in an unbalance in the voltage at the PCC. An islanding event can be detected when the unbalance exceeds the set value (Karimi et al., 2008). The voltage imbalance (VI) to detect islanding event is defined as:

$$VI = \frac{V_n}{V_p} \cdot 100\% \quad (1.10)$$

where: V_n and V_p are instantaneous magnitudes of negative-sequence and positive-sequence voltages in abc reference frame, respectively. The advantages of this method include short detection time, no NDZ, and a higher accuracy than positive-sequence voltage injection method.

10. High frequency signal injection method

An islanding detection method based on injection of high frequency low magnitude voltage signal is proposed in (Reigosa et al., 2012). High frequency impedance can be measured by injecting a various forms of excitation, such as, rotating or a pulsating voltage vector. The advantages of this method are negligible effects on power quality due to the injection of high frequency voltage signal, accurate and fast islanding detection.

11. Virtual capacitor/inductor method

Islanding detection methods are proposed where the grid connected power inverter serves as a virtual capacitor when the frequency is slightly lower than the nominal frequency (Chiang et al., 2012) and as a virtual inductor when the frequency is slightly higher than the nominal frequency (Jou et al., 2007), during an islanding event. Therefore, the amplitude and frequency of the voltage varies even when the real and reactive power mismatch is negligible, resulting in better islanding detection.

12. Phase PLL perturbation

Authors in (Velasco et al., 2011), have proposed a method which adds a current harmonic to the inverter reference current. By modifying the phase signal of the PLL, a perturbation is generated such that the angle of the inverter reference current θ_{INV} becomes 1.11:

$$\theta_{INV} = \theta_{PLL} + k\cos(\theta_{PLL}) \quad (1.11)$$

where: k is the rate of disturbance introduced in the system. Since a PLL is used to generate the perturbation signal, it is always proportional to the injected current. Another advantage of this method is that it does not affect the zero crossing of the signal.

1.3.3 Hybrid methods

As opposed to passive IDMs, active methods could significantly minimize the NDZ and thereby improve the detection accuracy. However, the injection of a disturbance signal, in addition to, increasing the complexity of system, also affects the power quality. In order to avoid continuously injecting a disturbance signal, hybrid techniques are devised by combining passive techniques as a primary detection technique and active method as a secondary detection technique as depicted in Fig.1.5. Hybrid methods inherit the desirable features of both passive and active techniques. The following are various hybrid methods reported in the literature.

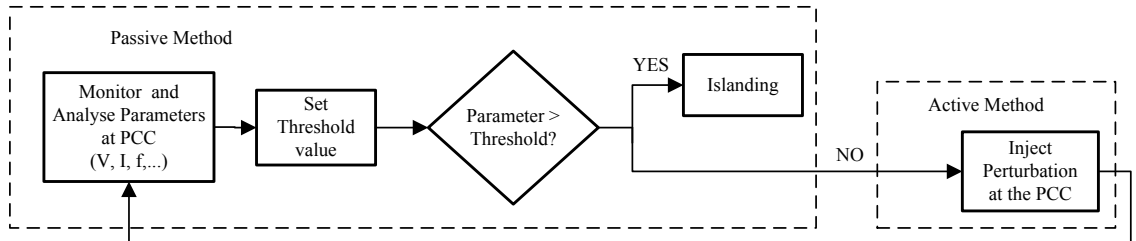


Figure 1.5: Block diagram of hybrid islanding detection method

1. Voltage unbalance and frequency set point method

This islanding detection technique combines positive feedback, an active technique, and voltage unbalance (VU)/THD, a passive method, thus making it a

Table 1.3: Summary of active islanding detection techniques

Technique	NDZ	Impact on power quality	Detection time	Error detection rate
Impedance measurement	Small	Degrades	0.77–0.95 s	Low
AFD	Large for high Q	Degrades	Within 2 s	High
FJ	Small	Degrades	75 ms	Low
AFDPF	Smaller than AFD	Slightly degrades	1 s (approx)	Lower than AFD
SFS	Smallest	Slightly degrades	0.5 s	Low
SVS	Smallest	Slightly degrades	0.5 s	Low
SMS	Small	Degrades	0.4 s (approx)	Low
Variation of P and Q	Small	Degrades	0.3–0.7 s	High
Negative sequence current injection	None	Degrades	60 ms	Low
High frequency signal injection	Smallest	Slightly degrades	few ms	Low
Virtual capacitor	Smallest	Slightly degrades	20–51 ms	Low
Virtual inductor	Smallest	Slightly degrades	13–59 ms	Low
Phase PLL perturbation	Smallest	Negligible	120 ms	Low

hybrid method. At the outset, the three phase voltages are continuously monitored at the output terminal of the DG and voltage unbalance is calculated. Owing to its higher sensitivity, VU is used as a detection parameter instead of THD. Since VU may arise due to an islanding or a sudden variation in load, frequency set point is lowered whenever VU is above the threshold value to properly discriminate an islanding event from other disturbances (Menon and Nehrir, 2007).

2. Voltage and real power shift

This hybrid technique is a combination of average rate of voltage change and real power shift (RPS), a passive and an active method respectively. Initially, voltages are continuously measured at the DG terminals and whenever a $\frac{dV}{dt} \neq 0$ is detected, the magnitude of average rate of change of voltage, Av_5 , for 5 cycles is calculated to check for an islanding. If $Av_5 > V_{SMAX}$, where V_{SMAX} is the maximum set point, then it can be classified as an islanding event, and if $Av_5 < V_{SMIN}$, where V_{SMIN} is the minimum set point, then islanding is not suspected. However, if $V_{SMIN} < Av_5 < V_{SMAX}$, then the change could be due to an islanding or some other disturbance in the system. At this point RPS is used to determine whether the system is islanded or not (Mahat et al., 2009).

3. Voltage fluctuation injection

This hybrid islanding detection scheme comprises of two indices based on passive detection methods, namely, ROCOF and ROCOV, and one parameter, namely correlation factor (CF), that gives the correlation between the variation in the terminal voltage of the DG source and the voltage perturbation source. In this method, the passive islanding detection scheme is used as a primary detection scheme and the active technique is used as a back up scheme (Chang, 2010).

4. Hybrid SFS and Q-f method

In this hybrid method a combination of Q-f droop, a passive method, and SFS, an active method are used. In order to overcome the instability of SFS and to minimize the NDZ, the optimum value of gain is determined by applying Bacterial Foraging optimization algorithm. The Q-f droop curve scheme is further added to the above technique to enhance the overall effectiveness of the hybrid detection technique (Vahedi et al., 2010).

1.4 Remote methods

Remote techniques use communication between the utility and the DG to detect an occurrence of an islanding event. This requires additional instrumentation in order to establish a communication link between the utility and the DG, which is an expensive affair. However, the upside of these methods include the absence of NDZ, no degradation of power quality, and it is effective in multi-DG environment.

1. Power line carrier communication (PLCC)

This technique employs two devices, a signal generator connected at the substation end and a signal detector connected at the target DG terminals. The signal generator continuously transmits a signal through the power line itself to all the distribution feeders. This signal will be detected by the signal detectors present at the DG location. However, if the signal detector fails to detect the signal for more than a set duration, it can be concluded that an islanding has occurred and the DGs will be eventually tripped (Xu et al., 2007). Since the transmitter is expensive, considering the economic aspects, this method is used in cases where the DG system density is high. The detection time of this method is about 200 ms (Wang et al., 2007).

2. Signal produced by disconnect (SPD)

This method is similar to PLCC technique since this method also uses the concept of signal transmission from the utility end to the DG location. However, the difference between the two schemes lies in the fact that SPD uses microwave link, telephone line or other means for communication. Therefore, when the detector at the DG end fails to receive a signal for a set duration, then it will be classified as an islanding event (PVPS, 2002). The disadvantage, however, of this technique is that it requires a huge investment for setting up the communication links.

3. Supervisory control and data acquisition (SCADA)

Islanding detection by means of SCADA is accomplished by measuring the voltage at the target DG location. If a voltage is sensed when the utility is disconnected, SCADA system will take necessary action to tackle the islanding event by sending signals to the corresponding DG (PVPS, 2002). This method

can eliminate NDZ and greatly enhance the efficiency of the system. However, this method suffers with slow detection speeds, increased expenditure on instrumentation and communication links, and a complex installation procedure which is not justified for smaller DGs.

1.5 Signal processing Techniques

On one hand, passive methods offer the advantage of fast response time but on the other, they have a large NDZ which is undesirable. Active methods do not have issues with NDZ as much as passive methods do, but they, in varying degrees, have a negative influence on power quality of the system and hence are employed with caution. Minimization of the NDZ of passive methods can greatly enhance their overall performance and hence make them a viable alternative to active methods. Signal processing(SP) methods come in handy to achieve the task of minimizing NDZ since they are capable of extracting hidden features of any given signal and unveil a great deal of information about the state of the system. Based on the knowledge of the extracted features an islanding event can be classified, as explained further.

SP based IDM, as shown in Fig.1.6, monitors various parameters at the PCC and applies a signal processing technique to derive hidden features, which are further used for islanding detection. Different signal processing methods for islanding detection by feature extraction are explained further and a summary of these techniques is presented in Table. 1.4 and Table. 1.5.

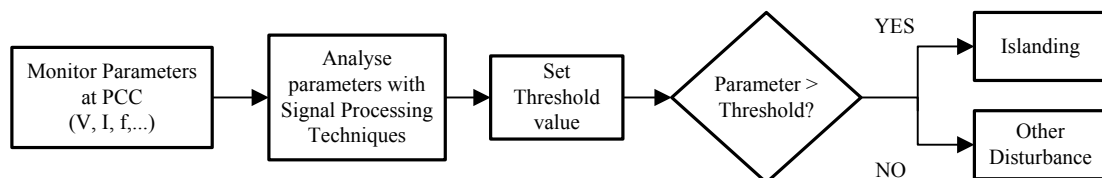


Figure 1.6: Block diagram of signal processing based islanding detection method

1.5.1 Fourier transform (FT) based methods

Fourier transform is a popular technique used for frequency domain analysis, wherein a signal is characterized by a series of sinusoidal signals of different frequencies. However, FT does not have the ability to resolve any momentary information associated with dynamic variations (Karimi et al., 2000). Therefore, to overcome this problem

time–frequency analysis is proposed. Short–time Fourier Transform (STFT), a modification of FT, divides the signal into small frames, wherein each frame can be assumed stationary. A moving window technique is further applied to evaluate all these frames, which allows us to have a time–frequency analysis of the signal (Dash et al., 2003b). The disadvantage, however, is that STFT cannot be applied to non–stationary signals due to the fixed window width (Zhao et al., 2004, Gu and Bollen, 2000). Discrete Fourier Transform (DFT) is a technique that is employed to perform frequency domain analysis on discrete time signals, which are sampled from continuous time signals. Fast Fourier Transform (FFT) is an algorithm that is used to compute the DFT with a significant enhancement of computational efficiency (Ribeiro et al., 2013). In spite of its computational efficiency, FFT suffers from limitations, such as the depiction of high–frequency components as low–frequency components (Lee and Girgis, 1988). An islanding detection method based on DFT is reported in (Kim, 2012) with a detection time of $1ms$ even under the circumstances where the difference between the power generated by the PV and the power consumed load is insignificant. Another islanding detection method reported in (Vatani et al., 2015) employs FFT to calculate the harmonic content of the equivalent reactance seen at the DG location, which is further used as an input feature for an intelligent classifier. FFT with Artificial Neural Network (ANN) to detect islanding event is discussed in (Yin, 2005). Goertzel algorithm, a type of DFT, which has the fastest technique for pitch detection in comparison with DFT and FFT, is used for islanding detection has been reported in (Kim et al., 2011). The detection time using DFT based Goertzel algorithm (DFT–GA) is reported to be under 2 cycles.

1.5.2 Wavelet transform (WT) based methods

Wavelet transform, just like FT, is a technique used for the analysis of a signal. However, the difference lies in the fact that in wavelet analysis, the signal is characterized in terms of small waves, called wavelets, which are generated from a fixed function called mother wavelet. These wavelets are localized in both time and frequency, thus making wavelet transform a suitable candidate for the time–frequency analysis of signals (Polikar, 1999, Graps, 1995). Owing to the fact that wavelets have large windows at low frequencies and short windows for high frequencies, it can depict the dynamic behavior, transients, and discontinuities. This can be effectively used for islanding

detection. Also, wavelet transform can be used for non-stationary signals. WT can be classified as continuous (CWT) or discrete (DWT). In (Zhu et al., 2008) CWT and Mallat decomposition are used to detect islanding event and to filter the noise from signal, respectively. In order to reduce the computational burden arising from the numerous coefficients in CWT, alternate techniques, like DWT, have been investigated for islanding detection.

Daubechies mother wavelet based DWT is used for islanding detection by effectively capturing the changes in the signal at the DG terminals (Hsieh et al., 2008). Some of the reported advantages are, improved islanding detection capability and ease of programming.

A hybrid islanding detection method has been reported in (Pigazo et al., 2007, 2009) which monitors voltage and current at PCC. In addition to the passive method used, it also monitors the high-frequency components injected by the DG inverter and the associated filter and controller for islanding detection. DWT with Bi-orthogonal 1.5 mother wavelet has been used on the high-frequency components injected by the PV inverter at PCC as it offered good response times and time-frequency resolution. In addition to the above-mentioned advantages, this method requires a fewer number of sensors and has enhanced computational efficiency.

In (Samantaray et al., 2009), Daubechies db4 based DWT is applied for negative sequence components of current and voltage at the target DG terminals and the classification of islanding event is determined by the change in standard deviation and energy coefficients. In this method, the detection time for islanding event classification is reported as 1 cycle. The compactness and localization properties of Daubechies db4 are used to minimize the NDZ in (Hanif et al., 2010). Another feature of db4 is that it makes use of second level wavelet coefficients(d2) to identify the spectral changes in higher frequency components, where as db4 DWT and db5 DWT are used for islanding detection of wind turbine based DG and grid-connected PV DG, respectively (Karegar and Sobhani, 2012, Hanif et al., 2012). Dyadic DWT, a DWT technique based on Mallat's pyramid algorithm (Daubechies, 1990), has been used to detect islanding event because of its simplicity and non-redundancy (Sharma and Singh, 2012). DWT with Haar wavelet as a mother wavelet is used to detect islanding operation of a system with multiple DGs. Haar wavelet requires fewer decomposition levels, thus least detection time (Shariatinasab and Akbari, 2010). The detection time reported is 5.5 ms.

While CWT generates too many co-efficients and reduces the computational efficiency, DWT ends up mixing high frequencies, which results in loss of information. Wavelet Packet Transform(WPT) is proposed (Morsi et al., 2010) to overcome these challenges. In this method node rate of change of power index is defined based on WPT and ROCOP output at the DG terminals.

Wavelet transform based Multi-Resolution Analysis (MRA) is reported in (Ning and Wang, 2012) for islanding detection. WT based MRA extracts harmonic features by partitioning the entire harmonic spectrum into several frequency bands and the harmonic features for each band are generalized. In this technique WT based MRA is applied on voltage signals at the DG terminals to decompose them into different scales, wherein for each scale a series of wavelet coefficients are generated that correspond to a certain frequency bandwidth. Islanding is detected based on the change in the ratio of the wavelet coefficients. Wavelet Singular Entropy Index (WSEI) based islanding detection is proposed in (Samui and Samantaray, 2013). Wavelet Singular Entropy (WSE) encompasses the advantages of the WT, singular value decomposition, and Shannon entropy. To calculate WSEI, first WT is applied to the three-phase voltages at the DG terminals and a coefficient matrix is generated. Secondly, a singular value matrix is computed for the coefficient matrix, which is used to determine the WSE of individual phases. Lastly, WSE of all phases is added to calculate the WSEI which is used for islanding detection.

1.5.3 S-Transform (ST) based techniques

In order to overcome the limitations of WT, such as sensitivity to noise and consequently its inability to detect islanding events under a noisy environment, S-Transform (ST) has been proposed (Stockwell et al., 1996). ST consolidates the properties of STFT and WT and it is based on a moving and scalable Gaussian window (Ventosa et al., 2008, Dash et al., 2003a). ST constructs a time-frequency representation of a time series signal and offers frequency-dependent resolution and simultaneous localization of real and imaginary spectra. It also provides multi-resolution while keeping the phase of each frequency component unaffected, which comes in handy while detecting disturbances in a noisy environment.

Ray (Ray et al., 2012) proposed a method to detect islanding in a hybrid power system based on ST. In this method, ST is applied to the acquired voltage signal and

S-matrix is obtained. From the S-matrix energy, matrix and standard deviation (SD) are computed. An islanding event is positively detected when the energy and SD are above a fixed threshold value. In (Ray et al., 2010, 2011), negative sequence voltage is extracted for islanding event detection. Further, the performance of ST and WT based detection techniques are compared on the basis of simulation results and ST based method is reported to have detected islanding events even under noisy conditions. Another method that employs ST based cumulative sum detector (CUSUM) is reported in (Samantaray et al., 2010b). In this technique, ST is applied to the negative sequence voltage and current signals acquired from the target DG terminals and the spectral energy content of the same is computed. CUSUM is calculated from the spectral energy, which forms the basis for islanding detection.

In spite of its enhanced performance under a noisy environment, ST with Gaussian window fails to effectively localize the transient disturbances. To overcome this problem a modified version of ST, known as Hyperbolic S-Transform (HST), is proposed (Pinnegar and Mansinha, 2003b, Biswal et al., 2009, Huang et al., 2010). As opposed to ST, HST uses a pseudo-Gaussian hyperbolic window which has a frequency dependent shape in addition to height and width. The resulting asymmetry gives superior time time and frequency resolution both at high and low frequencies. An islanding detection method based on HST in a multi-DG system is presented in (Mohanty et al., 2012). In this technique negative sequence component of voltage retrieved from the PCC is considered for islanding detection. From the reported results, it is evident that HST performs better than WT and ST even under noisy conditions.

1.5.4 Time- Time (TT) Transform based techniques

Time-time transformation(TT-T) is a technique based on ST, which presents a one-dimensional time series data in a two – dimensional time-time series representation. TT-transform aids in providing an enhanced time localization of a signal through scaled windows (Pinnegar and Mansinha, 2003a).

An islanding event detection method based on TT-transform is proposed in (Khamis et al., 2012). It is shown that TT-transform method has the ability to detect islanding effectively based on the unique contour patterns of various disturbance signals. TT-transform technique has also been used in (Mohanty et al., 2012) to extract de-

sired features, which are further used for islanding detection. The performance is compared with WT and ST and it is found that TT-transform does a better job.

1.5.5 Hilbert Huang Transform (HHT) based techniques

The Hilbert–Huang Transform (HHT) is a signal processing technique used for processing non-stationary and non-linear signals. HHT is composed of two steps: In step one, the signal is decomposed into various components called as intrinsic mode functions(IMF). This is achieved by means of Empirical Mode Decomposition (EMD). In the second step, Hilbert transform is applied to the decomposed IMFs to obtain the Hilbert spectrum. This entire process is termed as HHT (Huang et al., 1998, Rilling et al., 2003). The merits of HHT over WT, STFT, and ST are discussed in the literature (Donnelly, 2006, Peng et al., 2005)

EMD based islanding detection method is proposed in (Niaki and Afsharnia, 2014). In this method EMD is applied to voltage at the PCC signal and the first IMF is used to detect the islanding condition. The reported detection time is under 2 cycles.

1.5.6 Mathematical Morphology based technique

Morphological filters are basically non-linear signal transformation tools (Maragos and Schafer, 1987). They are based on Mathematical Morphology(MM), a technique based on integral geometry and set theory and deals with the shape of a signal entirely in time domain . This technique is widely used in the field of image processing. The fundamental idea is to use a structural element (SE) as a probe to gather the data from the signal. Morphological transform decomposes a given signal into several parts which carry varied physical significance. Two basic morphological operators in MM are erosion and dilation, from which various compound morphological operators such as, opening, closing, Hit-Miss, and Top-Hat transform can be defined. Erosion is a shrinking transform where as dilation is an expanding process. New morphological operators such as, opening and closing operators are formed by conjugation of erosion and dilation operators (Gautam and Brahma, 2009, Li et al., 2005). In (Mohanty et al., 2015) difference in generalised opening and closing, open, close erosion and dilation are used for anomaly detection in a signal. MM based islanding detection is reported in (Farhan and Swarup, 2016), where MM operators like dilate erode difference filter(DEDf) are applied to the voltage and current signals acquired from

the target DG location. Further, these values are fed as an input to new operator defined as average of difference between maximum and minimum value of DEDF. In the next step a new operator called Mathematical Morphology Ratio Index(MM RI) is defined, which is used for islanding detection.

1.6 Intelligent techniques

From the foregoing review of various IDMs, it can be clearly noted that passive IDMs have the potential to achieve high detection speed, enhanced accuracy, and effectiveness in multiple DG environment when coupled with signal processing techniques. However, as the DG system complexity increases, it becomes evident that adding intelligence to DGs will greatly enhance the robustness of the system. Since intelligence based techniques can handle multiple parameters simultaneously, it is possible to train the DG for various islanding cases and enhance the accuracy of detection. While using intelligent techniques, signal processing technique will extract features from the acquired signal, which, in the next step will be used as an input to the intelligent technique in the form a feature vector as depicted in Fig.1.7. Various intelligent techniques are reviewed and further summarized in Table. 1.6, Table. 1.7, Table. 1.8, Table. 1.9, and Table. 1.10.

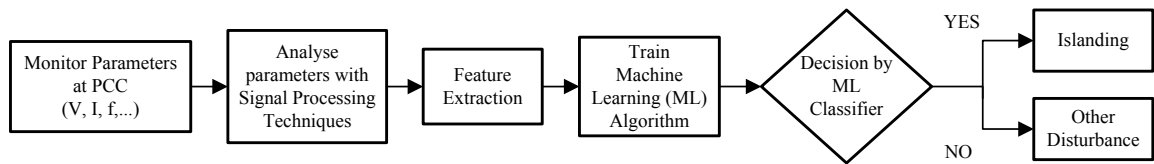


Figure 1.7: Block diagram of machine learning based islanding detection method

Table 1.4: Summary of various signal processing based islanding detection techniques

Reference	SP method	Tested system	Detection time	Efficiency/Accuracy	Sensitivity to noise
FT (Kim, 2012)	DFT	PV system	Around 1ms	-	-
(Kim et al., 2011)	DFT-GA	1-ph 2 stage PV	< 2 cycles	-	-
WT (Zhu et al., 2008)	CWT	Grid tied DG	0.6 s	-	-
(Hsieh et al., 2008)	DWT	DG at petroleum company	0.05-1 s	-	-
(Pigazo et al., 2007, 2009)	DWT	PV(Low power)	0.5 to 30 cycles	-	ΔP 5%, ΔQ 5%
(Samantaray et al., 2009)	DWT	Wind farm(DFIG)	1 cycle	-	ΔP 50%
(Hanif et al., 2010)	DWT	Grid tied PV	2.5 cycles	-	ΔP 0 - 20%
(Karegar and Sobhani, 2012)	DWT	Wind turbine (IG)	< 0.2 s	-	ΔP 0 - 25%
(Hamif et al., 2012)	DWT	PV system	0.05 s	-	ΔP 0 - \pm 20%
(Sharma and Singh, 2012)	DWT	Grid tied PV	> 1 cycle	-	-
(Shariatinasab and Akbari, 2010)	DWT	Synchronous DG	5.5 ms	-	ΔP 0%
(Morsi et al., 2010)	WPT	Wind farm	0.06 s	-	-
(Ning and Wang, 2012)	WT(MRA)	Inverter based DG	-	-	ΔP -37.3% - +21%
(Samui and Samantaray, 2013)	WSE	3 wind farms & Gen. Set	10 ms	-	ΔP 0 - 80%

Table 1.5: Summary of various signal processing based islanding detection techniques - Continued

Reference	SP method	Tested system	Detection time	Efficiency/Accuracy	Sensitivity to noise
ST (Ray et al., 2010, 2011)	ST	PV, Fuel cell & Wind	26-28 ms	-	20dB
(Samantaray et al., 2010b)	ST (CUSUM)	Wind farm(DFIG)	25 ms	100% at DG-1 92.3% at DG-4	-
(Mohanty et al., 2012)	HST	PV, Fuel cell & Wind	-	-	20dB
TT-T (Mohanty et al., 2012)	TT-T	PV, Fuel cell & Wind	-	-	20dB
(Khamis et al., 2012)	TT-T	1200V dc DG	-	-	-
HHT (Niaki and Afsharnia, 2014)	HHT	Inverter based DG	< 2 cycles	ΔP 0% - 80% ΔQ 0% - $\pm 20\%$	-
MM (Mohanty et al., 2015)	MM	PV & Wind (IEEE-30 bus)	22 ms	98.4% at DG-1 99% at DG-2 97.4% at DG-3 100% at DG-4	20dB
(Farhan and Swarup, 2016)	MM RI	Wind & Diesel Generator	≤ 20 ms	100% at DG-1 92.85% at DG-2 100% at DG-3	- ΔP 0% - 40% ΔP 0% - 20%

1.6.1 Neural Network based techniques

A biological neural network is a system with large number of highly interconnected processing units, known as neurons, that work together to solve a given problem. An artificial neural network (ANN), or more generally referred to as neural networks(NN), are defined as processing devices, either algorithms or actual hardware, that are designed based on the neuronal structure of the brain but on much smaller scales (Caudill, 1987). Neural networks have the ability to learn from data and recognize the patterns by means of a function that transforms the data and forwards them as activation functions to the neurons in the next layer. This process continues until the neuron in the output layer is activated, which means the ANN has successfully recognized the given data set. Based on its abilities, ANN is used as a classifier to classify islanding event by means of transient voltage signals produced at the instant of islanding(Fayyad and Osman, 2010). DWT is used for extracting features which are used for training the ANN classifier. In (Darabi et al., 2010) a self-organized map neural networks(SOM NN) with seven neurons has been used to classify islanding events. This method uses the input signal to the droop of the governor, which carries the frequency deviation information. Training of SOM NN is carried out in two stages with learning rates η_1 and η_2 set as 0.9 and 0.02 respectively with Gaussian neighborhood function. A multi-layer perceptron(MLP) type ANN has been employed for islanding detection in (Merlin et al., 2016). MLP has been selected owing to its ability to detect voltage and frequency variations. Also, this method uses only voltage at the DG terminals, sampled at 64 and 128 samples per second, as an input feature vector. NN based islanding detection is used for comparing the performance of other classifiers in (Faqhrudin et al., 2014). In this method out of 21 extracted features only 4 are used as a input vector. The selection of features is done by implementing forward sequential feature selection (FSFS) and backward sequential feature selection (BSFS).

Probabilistic Neural Networks (PNN)

In spite of the fact that ANN based islanding does a decent job of detecting islanding events it suffers from certain shortcomings, such as, longer computational times for training and vulnerability to false minima due to the incremental adaptation approach of back-propagation method. These can be overcome by using PNNs. A PNN is formed when the sigmoid activation function is replaced by an exponential activation function in a neural network (Specht, 1990). PNN basically has four layers,

namely, input layer, pattern layer, summation layer, and output layer. A method that employs transient signals generated during an islanding event along with PNN as a classifier is reported in (Lidula et al., 2009), which is tested on a system with an induction generator(IG) and synchronous generator(SG). In (Khamis et al., 2015), PNN in conjunction with phase–space technique for feature extraction has been used to classify islanding events.

1.6.2 Fuzzy logic based techniques

Fuzzy logic(FL) is a computational methodology that employs rule based approach to solve problems rather than mathematical modeling approach. These rule based fuzzy logic models are called as fuzzy inference systems(FIS). Contrary to the standard conditional logic, which is either 1 or 0, FL interprets truth in various degrees. In (Samantaray et al., 2010a, Kumarswamy et al., 2013), a fuzzy-rule based classifier is used for detecting an islanding event. A decision tree(DT) has been used to find the initial classification boundaries, based on which the membership functions and the corresponding rule base is developed. An active islanding detection scheme based on fuzzy inference rules is proposed in (Aguilar et al., 2013). The proposed method uses positive feed back in dq–synchronous reference frame. Voltage at the target DG and the frequency of the PLL (ω_{PLL}) as used as input features. Another active method based on d-axis injection method for inverter based synchronous DGs is presented in (Lin et al., 2012). When compared to the grid connected mode, in islanded mode of operation the disturbance signal will heighten the difference in frequency. This deviation in frequency is used to detect the islanding event. Further, a wavelet based fuzzy neural network based controller is used in place of a traditional PI controller to improve the performance of the proposed method.

1.6.3 Decision tree based techniques

A decision tree(DT) is a hierarchical model which is used for classification problems. DT classifier adopts a top-down approach, starting from the root node, which contains the initial classification problem, by recursively splitting the classification problem into internal nodes that test for various parameters until a classification is achieved at the leaf node (Kantardzic, 2011). In (El-Arroudi et al., 2007) a DT based pattern recognition classifier has been used to classify islanding events. DT classifier

is trained by a large data set for the DG under test and 11 parameters are used for classifying the events. The system that is tested in (El-Arroudi et al., 2007) is made use of in (Thomas and Terang, 2010) to classify islanding events by employing DT classifier. The difference, however, is that in (Thomas and Terang, 2010) the selection of parameters to classify islanding state is based on the ease of measurement. Accordingly, current(I), voltage(V), active power(P), reactive power(q), power factor(pf) and frequency(f) are selected. Ref. (Vatani et al., 2015) proposes an islanding detection algorithm based on two indices, namely, harmonic content of the reactance seen at the target DG and maximum rate of change of frequency(ROCOF), i.e., $\max \frac{df}{dt}$. A DT classifier employs these indices to classify islanding states. The performance of the DT based algorithm is further compared with ANN and SVM based techniques and it is reported that DT classifier performs better. A DT classifier with DWT for feature extraction has been used in (Heidari et al., 2013) to propose an optimum relay for islanding detection. This algorithm makes use of energy coefficients of transient voltage signal extracted from the target DG. Transient signals generated during the isolation of DG from the rest of the system are used for classifying the islanding events by a DT classifier in (Lidula et al., 2009). A 4-fold cross-validation is carried out to obtain better performance. A universal islanding detection algorithm is proposed in (Faqhrudin et al., 2014), in which, various classification techniques, including DT, were used for detecting islanding events.

1.6.4 Naive Bayesian classifier

Naive Bayes(NB) classifier is a classification technique that is based on Bayes' theorem. NB classifier assumes that the presence of a particular feature in a set is independent of the presence of any other variable in that set. Despite the fact that feature independence is a poor assumption in most cases, NB classifier often performs on par with other established classifiers (Rish, 2001). NB technique works particularly well with large data sets. An islanding detection technique is proposed in (Faqhrudin et al., 2012) which employs NB classifier for classification of islanding events where as validation is done by using support vector machine(SVM) and k-fold cross validation techniques. NB classifier with four-fold cross validation is proposed in (Faqhrudin et al., 2014). A total of 21 features were extracted from the PCC out of which 4 best features were selected using forward feature selection(FFS) and

backward feature selection(BFS). The proposed technique has been tested on three different cases: a)Inverter based DG, b)Synchronous based DG, and c)Multiple DGs. In case of inverter DG, NB classifier is reported to have a classification accuracy of 82% and 52% with all the 21 extracted features and four best features, respectively. Nevertheless, NB classifier performed extremely well with SG based DG and multiple DGs with a reported accuracy of almost 100%.

1.6.5 Support vector machine classifier

Support vector machine(SVM) is supervised learning algorithm, meaning it requires a set of data to train the algorithm. Once trained, the SVM will use kernel techniques to project the input space to a higher-dimensional feature space and identify the optimal hyperplane that classifies the data with minimum error and maximum distance between the hyperplane and nearest vector (Kantardzic, 2011). SVM classifiers or simply called as support vector classifiers(SVC) are unaffected by the sample dimensions. A SVM classifier for islanding detection is proposed in (Matic-Cuka and Kezunovic, 2014). Auto-regressive signal modeling is applied to the voltage and current signals at the PCC to extract a total of 62 features, which are used as an input feature vector for the SVM classifier with radial basis function as a kernel. In Ref. (Alam et al., 2014) SVM classifier is proposed for islanding event classification, especially for the cases where vector surge relay fails to operate positively. A five-fold cross-validation method is used to establish the SVM regularization parameter(C), bandwidth of radial basis function(RBF) kernel(σ), and degree of the polynomial kernel(p). Further, the proposed method is tested with linear, Gaussian RBF, and polynomial kernels. SVM classifier is also used in (Faqhrudin et al., 2014, Lidula et al., 2009, Faqhrudin et al., 2012) as one of the one of the classifiers.

1.6.6 Random forest classifier

Random Forest Classifier(RFC) is an ensemble learning technique that constructs decision trees(DTs) during the training phase, where each DT is constructed by using random subset of the actual data. And then these DTs are used to classify any input data set. An islanding detection scheme based on RFC is reported in (Faqhrudin et al., 2014). In this technique C4.5 DTs are constructed based on the entropy and Infogain, which are further used to classify islanding events. The performance of RFC

is compared with other classifiers and it is reported that RFC has better performance compared to other classifiers in terms of average accuracy, NDZ, and detection time. Another RFC based islanding detection scheme is presented in (Adari and Bhalja, 2016). This method uses the extracted sequence components from the voltage signal that is acquired at the PCC to classify islanding and non-islanding states.

Table 1.6: Summary of intelligent-based islanding techniques – I

Reference	Input features	Tested system	Detection time	Detection Efficiency/Accuracy	Sensitivity to noise	
ANN						
(Fayyad and Osman, 2010)	7 wavelet levels of V	3-ph PV Inverters	–	97.22% (DG 1), 97.77% (DG 2)	$\Delta P, \Delta Q$ Zero	–
(Darabi et al., 2010)	240 input vectors	SG	200ms	97.9%	ΔP 30%	–
(Merlin et al., 2016)	V at DG terminals 64 & 128 samples/sec	SG	2.75s(64)	99.28%	ΔP 0.1 - 1pu	–
(Faqhruldin et al., 2014)	V, f, Z_1 , and ϕ	SG & Inverter	0.2s (SG) 0.3s (inverter)	100% (SG) 97% (inverter)	$\Delta P \pm 30\%$ $\Delta Q \pm 5\%$	–
			0.26s (Both DGs)	100% (both DGs)		–

Table 1.7: Summary of intelligent-based islanding techniques – II

Reference	Input features	Tested system	Detection time	Detection Efficiency / Accuracy	Sensitivity to noise
PNN					
(Lidula et al., 2009)	Signal energy extracted by WT	IG & SG	0.032s+Processing time	85% (Avg.)	–
(Khamis et al., 2015)	5 phase – space features of DG V	4 SGs	0.24 s	100%	–
Fuzzy Logic					
(Samantaray et al., 2010a)	$\frac{\Delta P}{\Delta t}$, $\frac{\Delta f}{\Delta t}$, and Δf	2 SGs	–	100%	ΔP 40% 20dB and 30dB
(Kumarswamy et al., 2013)	$\frac{\Delta P}{\Delta t}$, $\frac{\Delta f}{\Delta t}$, and Δf	2 SGs	–	100%	20dB
(Aguar et al., 2013)	V_d and ω_{PLL}	1-ph inverter	–	97.9%	ΔP 0%
(Lin et al., 2012)	$Q - Q_{inv}$	Inverter	0.68 s	–	ΔP 0%

Table 1.8: Summary of intelligent-based islanding techniques – III

Reference	Input features	Tested DG	Detection time	Detection Efficiency / Accuracy	Sensitivity to noise
Decision Tree					
(El-Arroudi et al., 2007)	11 indices	SG	40–45 ms	100%	ΔP 5%
(Thomas and Terang, 2010)	Changes in I, V, P, Q, pf, f	SG	–	–	ΔP 40%
(Vatani et al., 2015)	HC_{odd}/HC_{even} & $\max.(df/dt)$	SG	300 ms	100%	ΔP 0–25%
(Heidari et al., 2013)	Energy coeffs of V (DWT)	IG & SG	0.01 s	98% (both DGs)	ΔP 0 %
(Lidula et al., 2009)	Signal energy extracted by WT	IG & SG	0.032 s + Processing time	90% (Avg.)	–
(Faqhruldim et al., 2014)	V, f, Z_1 , and ϕ	SG & Inverter both DGs	–	97%	$\Delta P \pm 30\%$
				95%	$\Delta Q \pm 5\%$
				96%	–

Table 1.9: Summary of intelligent-based islanding techniques – IV

Reference	Input features	Tested DG	Detection time	Detection Efficiency / Accuracy	Sensitivity to noise
SVM					
(Matic-Cuka and Kezunovic, 2014)	62 features from V & I	1-ph inverter PV	50 ms	98.94%	$\Delta P \pm 40\%$
(Alam et al., 2014)	$V, \theta, f, \frac{df}{dt}, \& \frac{dV}{dt}$	Three SGs	–	97.3% (Gaussian, RBF)	$\Delta Q \pm 5\%$ $\Delta P \ 0 - 100\%$
(Faqhruldin et al., 2014)	$V, f, Z_1,$ and ϕ	SG	–	98.3% (Polynomial)	$\Delta Q \ 0 - 50\%$
		Inverter	–	100%	$\Delta P \pm 40\%$
		both DGs	–	94%	$\Delta Q \pm 5\%$
		IG & SG	0.032 s	74% (Avg.)	–
(Lidula et al., 2009)	Signal energy extracted by WT		+Processing time		–
(Faqhruldin et al., 2012)	21 features extracted at PCC	Inverter	–	88.33%	$\Delta P \pm 30\%$
					$\Delta Q \pm 5\%$

Table 1.10: Summary of intelligent-based islanding techniques – V

Reference	Input features	Tested DG	Detection time	Detection Efficiency / Accuracy	Sensitivity to noise
RFC					
(Faqhruldin et al., 2014)	V, f, Z_1, ϕ	SG	0.18 s	100%	$\Delta P \pm 30\%$
		Inverter	0.18 s	98%	$\Delta Q \pm 5\%$
		both DGs	0.18 s	100%	–
(Adari and Bhalja, 2016)	Sequence components	SG, PV, & Wind DG	–	98.81%	$\Delta P 0\%$
NB					
(Faqhruldin et al., 2012)	21 features extracted at PCC	Inverter	120 ms	96.66%	$\Delta P \pm 30\%$, $\Delta Q \pm 5\%$
(Faqhruldin et al., 2014)	V, f, Z_1 , and ϕ	SG	–	100%	$\Delta P \pm 30\%$
		Inverter	–	56%	$\Delta Q \pm 5\%$
		both DGs	–	100%	–

This chapter explains the significance of islanding detection and various islanding detection methods are classified as classical, signal processing based, and intelligent techniques. Merits, and demerits of classical islanding methods are discussed briefly. Signal processing techniques as a means to improve the efficiency and accuracy of passive techniques is presented. The evolution of various signal processing methods employed for islanding detection along with their strengths and shortcomings are discussed. This is followed by the discussion of intelligent techniques and they, together with feature extraction by means of signal processing techniques, can play a role in adding robustness to the passive techniques and make them indispensable in a complex hybrid DG network with high density of DGs. This robustness is due to the fact that intelligent techniques can handle multiple parameters which is very essential in detecting islanding events during critical situation such as, at near zero power mismatch, in a multiple DG environment, or in a high density complex DG system.

The following is a summary of the discussions on IDMs along with some quantitative results.

- Passive IDMs have fastest detection times in the order of 4ms, and do not pose any threat to the power quality of the system. However, passive IDMs possess NDZ which is a drawback under certain conditions.
- Active IDMs overcome the disadvantage of NDZ and have reported detection times in the range of 13ms - 0.95s with a very good detection accuracy. The downside of active IDMs is that, they affect the power quality of the system.
- Hybrid IDMs inherit the advantages of both passive and active IDMs by employing them together. Hybrid IDMs have detection times in the order of 0.21s.
- Remote IDMs use communication as a means to detect islanding and hence it does not have any NDZ. However, they tend to be more expensive to implement. Reported detection times for remote IDMs are in the range of 200ms.
- Signal processing methods are a great tool to extract hidden features from the PCC signals and thereby enhance the detection capabilities of passive IDMs by reducing NDZ. SP based IDMs have a detection times in the order of 1ms - 28ms depending on the SP method.
- Intelligent IDMs overcome the need for setting a threshold value, which is imminent for all the above methods. Also, as the system becomes more complex

intelligent methods have a great advantage compared to traditional methods. Detection times of intelligent IDMs are reported in the range of 10ms - 300ms

1.7 Motivation

From the foregoing discussion it is evident that islanding detection has evolved over the years to improve the performance of IDMs in the context of NDZ, influence on power quality of the system, cost, detection accuracy, and detection time. However, given the proliferation of renewable energy sources at the distribution end of the system and modernization of the grid system, it is imperative that IDMs have to be embedded with intelligence to meet the requirements of the future smart grids. These intelligent IDMs should not only be efficient in terms of detection accuracy and have minimal to no NDZ but also should be able to handle voluminous amounts of data and be immune to noisy conditions. Furthermore, a feature to detect an islanding event even before its occurrence by monitoring the causes that lead to islanding can enhance islanding detection method. Based on the above observations the following research contributions are made in this work.

1.8 Contributions of this research work

In the proposed research work islanding detection based on image classification techniques is developed which has very good detection accuracy and has immunity to noisy conditions. The image classification based approach is enabled by converting time-series data to scalogram images. Feature extraction from the images together with machine learning classifier is used for islanding detection. Another method based on convolution neural networks for classifying islanding and non islanding events is also developed. The following contributions have been made in the proposed research work.

1. Development of an islanding detection method based on Histogram of Oriented Gradient(HOG) feature extraction from images and multiple support vector machine(SVM) classifiers.
 - Implementation of early islanding detection by monitoring the faults.
 - Testing the effectiveness of the IDM with noisy data.

2. Development of an islanding detection method using transfer learning on images and pre-trained convolution neural network (CNN) classifiers - AlexNet and VGG16.
 - Implementation of early islanding detection by monitoring the faults.
 - Testing the effectiveness of the IDM with noisy data.
 - Comparison of the performance under noisy conditions with feature extraction based method.
3. Development of an islanding detection method using image classification with custom designed convolution neural network (CNN) classifiers.
 - Implementation of early islanding detection by monitoring the faults.
 - Testing the effectiveness of the IDM with noisy data.
 - Comparison of the performance under noisy conditions with feature extraction based method and transfer learning based method.

1.9 Thesis organization

The whole thesis is organized into six chapters in the following manner and shown in Fig.1.9.

Chapter 1: A brief introduction to the concept of islanding, its definition and significance, need for islanding detection, international standards for islanding detection, and state-of-the-art literature related to islanding detection methods along with their evolution is discussed in this chapter.

Chapter 2: Dataset generation for supervised learning algorithms, process of converting time-series data to image, details of the system used for generating the dataset, various parameters used for islanding detection, and different events considered in the dataset are detailed in this chapter.

Chapter 3: The image dataset generated is used for islanding event classification. The first approach used for image classification is by means of extracting engineered features from the image and training a machine learning

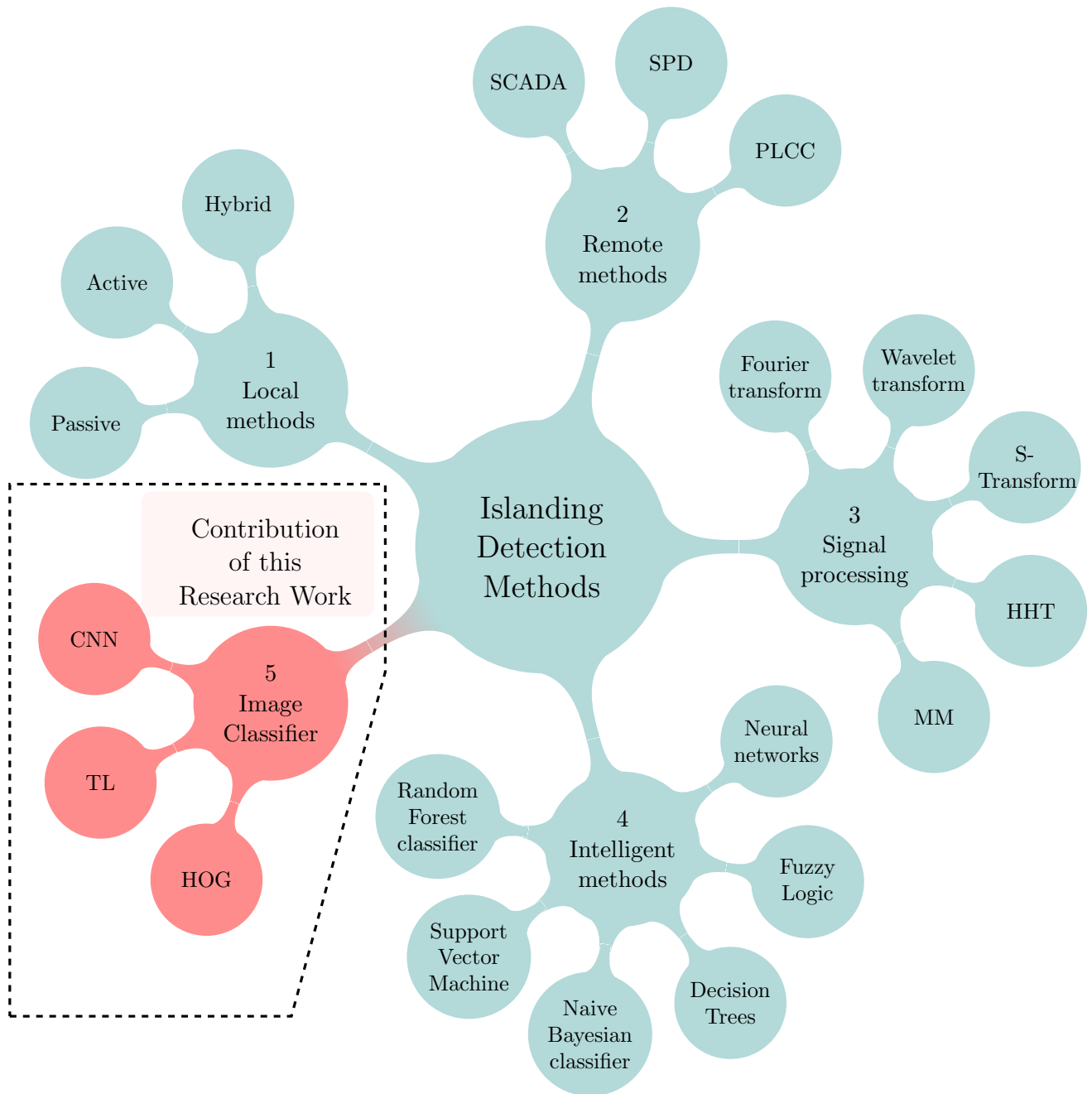


Figure 1.8: Classification of islanding detection methods - Contribution of this thesis work indicated

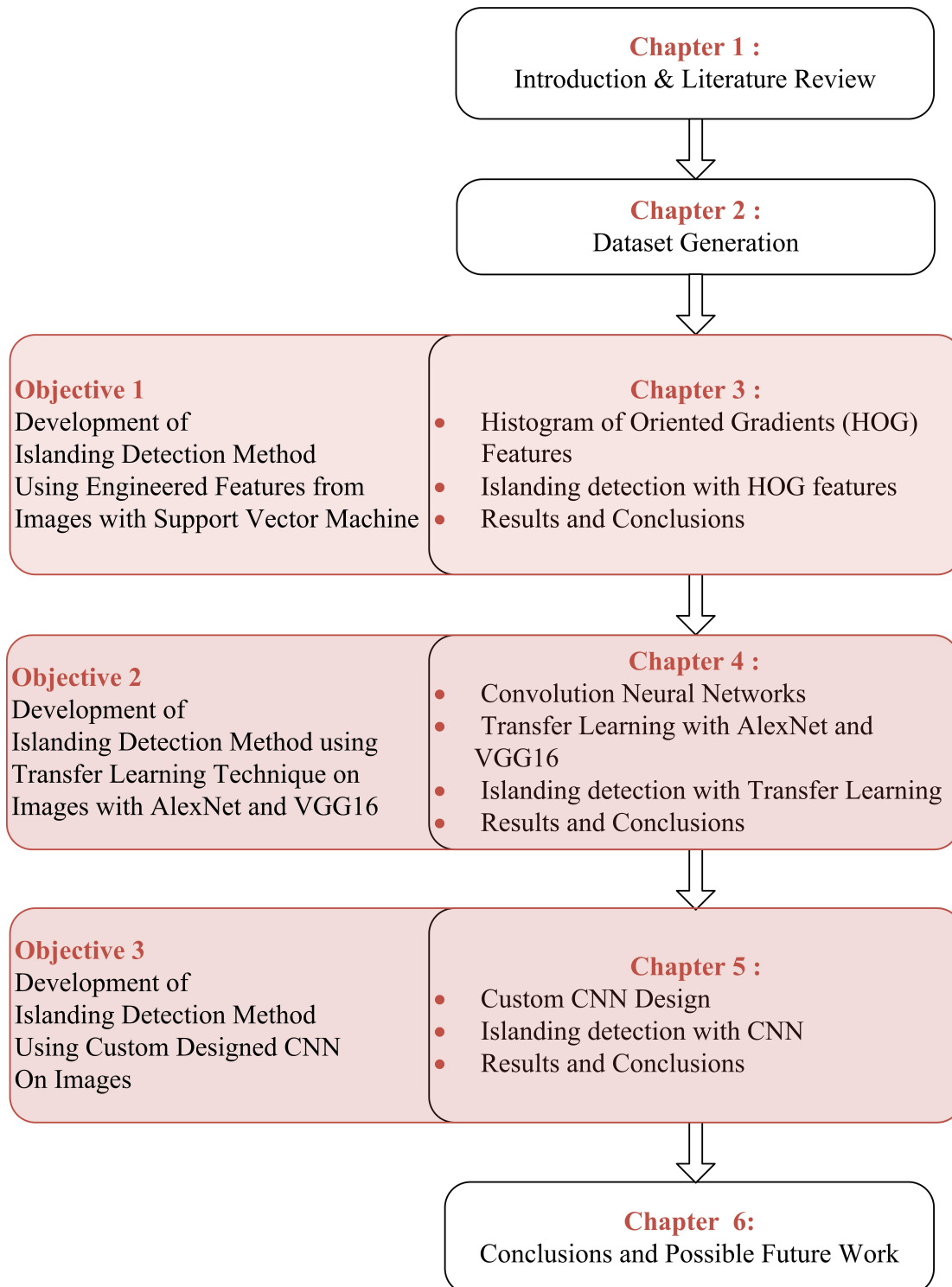


Figure 1.9: Organization of thesis

classifier. The engineered features employed are Histogram of Oriented Gradients (HOG) features and the classifier used is a Support Vector Machine (SVM) classifier. HOG feature extraction from images and effect of different parameters on accuracy is described in this chapter. The training and testing of SVM classifier on the dataset is also detailed in this chapter. The performance of HOG feature and SVM classifier based islanding detection method is discussed. The need for other feature extraction methods is established.

Chapter 4: In order to extract best features for classification a Convolution Neural Network (CNN) is chosen. CNN identifies best features during the training and testing phase. Some basics of CNN and its building blocks are first presented in this chapter. The definition and need for transfer learning are presented. Two popular CNN architectures, namely, AlexNet and VGG16 are used for transfer learning based islanding detection. The results of this approach are presented and discussed. The results of islanding detection using transfer learning are compared with HOG and SVM based method. Lastly, the need for designing a custom CNN for islanding detection is established.

Chapter 5: The details of custom CNN designing for islanding detection are described in this chapter. The architecture that offers better performance is designed and presented. Performance of the custom CNN for islanding detection is detailed. The advantages of custom designed CNN over transfer learning based approach are detailed. Lastly the performance of custom CNN based islanding detection is compared with transfer learning and HOG and SVM based methods are compared.

Chapter 6: This chapter concludes the contributions of the proposed research work and also discusses about scope for the possible future works.

Chapter 2

DATASET GENERATION

2.1 Introduction

Several intelligent IDMs have been presented and summarized in the literature in Chapter. 1. These intelligent techniques are also referred to as machine learning (ML) or deep learning (DL) or artificial intelligence (AI) techniques.

One definition of machine learning, as given by Thomas Mitchel, “A computer program is said to learn from experience E with respect to some class of tasks T and performance measure P , if its performance at tasks in T , as measured by P , improves with experience E ” (Mitchell, 1997). The tasks can be as varied as a spam mail detection problem to learning to drive an autonomous vehicle. The performance is a measure of how well a task is performed. And the experience would be the actual learning by watching us perform the task.

There are different varieties of learning algorithms, such as unsupervised and supervised. Unsupervised learning algorithms learn to perform the task by itself, whereas in supervised learning we will teach how to perform a task. In this work the task at hand is islanding detection. This is done by teaching an algorithm to learn and improve the performance, i.e., the islanding detection accuracy.

2.2 Supervised learning

Supervised learning refers to the process of teaching or training an algorithm with correctly labeled data, meaning the input and the correct answer are provided. The

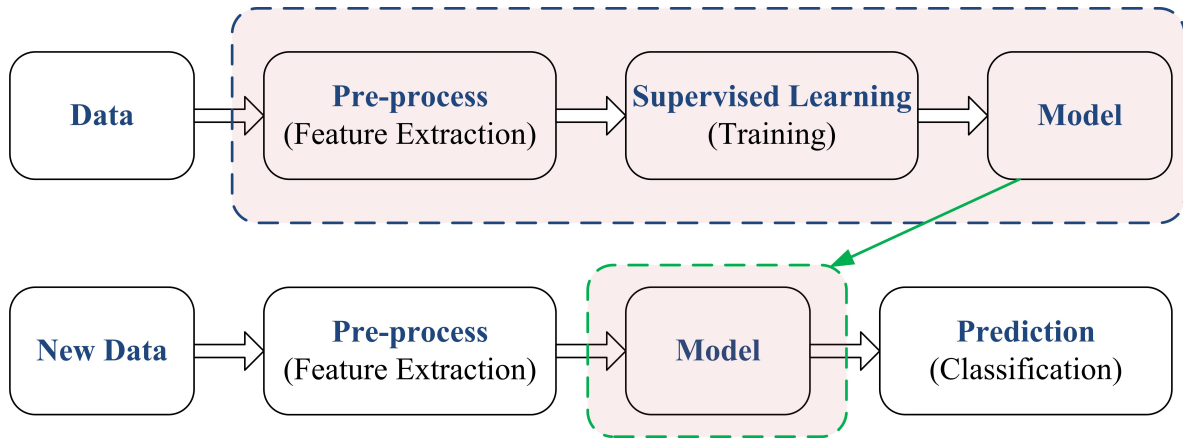


Figure 2.1: Supervised learning workflow

raw data is pre-processed to extract features that best represent the data. These features, along with the appropriate label, is used to train the algorithm. Once trained, the algorithm will generate a learned model. This learned model is then used to predict the outcome of any new inputs given to it as shown in Fig. 2.1. Therefore, for any supervised machine learning technique, appropriately labeled data is required for training and testing.

2.2.1 Need for image dataset

In this research we are presenting new islanding detection methods that employ image classification based techniques. Meaning, different image classification methods are used for classifying islanding and non-islanding events. This is done by using supervised learning algorithms. From the above discussions, it is known that for supervised learning techniques data with correct labels is a pre-requisite. Hence, image dataset pertaining to islanding and non-islanding cases have to be created.

The data that is acquired from the PCC is a time-series data. Therefore, to create an image dataset of islanding and non-islanding events, the first step is to convert the time-series data to images.

The next sections describe the process of converting time-series data to images, details of the system used to generate the dataset and also all the cases that have been simulated to create the image dataset.

2.3 Scalogram

The process of converting time-series data to images is presented here. An example time-series data that is generated by (2.1) is used to demonstrate the process. It is composed of two signals with frequencies $20Hz$ and $200Hz$ with amplitudes 10 and 20 respectively and the duration is taken as $1s$. These frequencies and magnitudes are arbitrarily chosen solely for the purpose of demonstration. This method involves taking wavelet transform of a signal.

$$x(t) = 10\sin(2\pi * 20 * t) + 20\sin(2\pi * 200 * t) \quad (2.1)$$

Wavelet transform of a signal $x(t)$ is defined as:

$$X(u, s) = \int_{-\infty}^{+\infty} x(t) \frac{1}{\sqrt{s}} \psi^*\left(\frac{t-u}{s}\right) dt \quad (2.2)$$

In wavelet analysis, the time-frequency energy density representation obtained by the wavelet transform is called a scalogram. It is defined as the square of amplitude of the wavelet transform (Sejdic et al., 2008). Or in simple terms a scalogram can be defined as a visual representation of wavelet transform, in which x and y axes represent time and frequency where as z -axis represents magnitude displayed in terms of color gradient.

The scalogram image for the time-series data, generated from (2.1), obtained by applying Continuous Wavelet Transform (CWT) with Morse wavelet is shown in Fig. 2.2. It can be seen from the image that it contains two frequencies, $20Hz$ and $200Hz$, with magnitudes 10 and 20 respectively. By employing this method we can convert any time-series data into image.

2.4 Data set generation

A lot of appropriately labeled data is required for training and testing any supervised learning based algorithm. For image classification problems standard data sets, such as ImageNet (Deng et al., 2009) and MNIST (LeCun, 1998), are available. However, in case of islanding detection no such standard data set is available. The dataset is generated by simulating various cases in a system. The details of the system used for

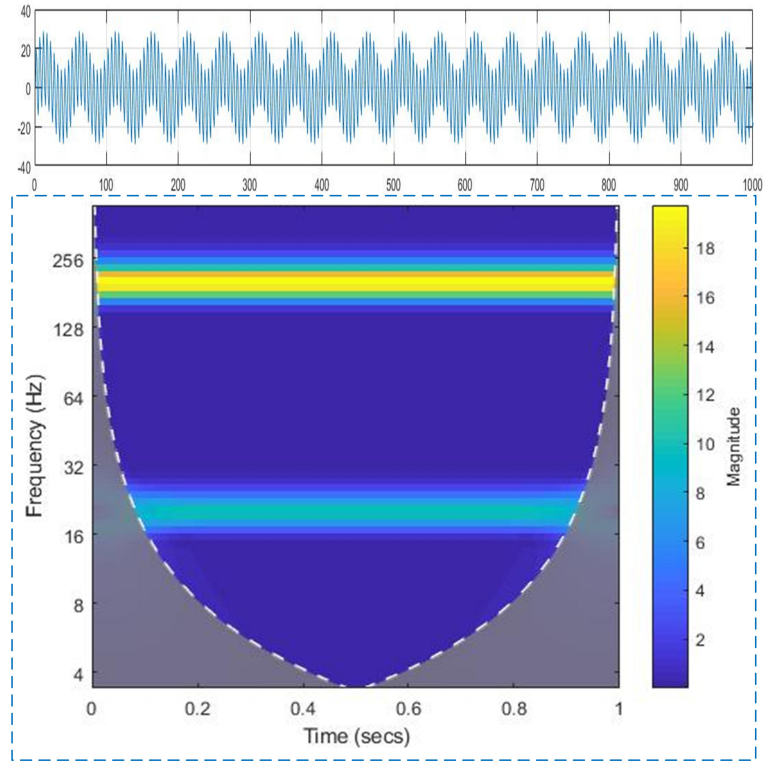


Figure 2.2: Scalogram image of the time-series data obtained from example equation

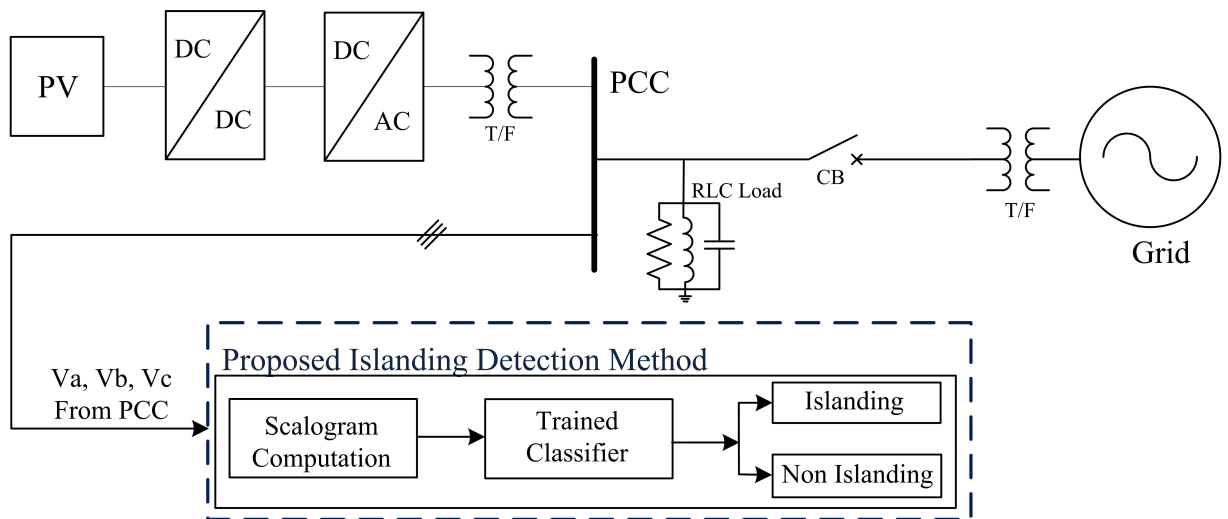


Figure 2.3: Schematic of the system used for generating data set

generating the dataset are presented here.

2.4.1 System description

A 100kW grid-connected PV system is considered for generating the image data set required for the proposed technique. The 100kW PV array is interfaced to the utility grid via a DC-DC boost converter with voltage rating of 500V, frequency 5kHz and a three-phase three level voltage source converter (VSC). The boost converter duty cycle is optimized by a maximum power point tracking algorithm to increase the PV array output voltage to 500V. The VSC converts the 500V DC link voltage to 260V AC voltage. This VSC employs two control loops, namely, external control loop and internal control loop. The external control loop regulates the voltage at DC link to $\pm 250V$ while the internal control loop regulates the I_d and I_q components of grid current. The output of external DC voltage controller is taken as I_{dref} while the I_{qref} is set to zero in order to maintain unity power factor. The V_d and V_q voltage outputs of the controller are used by the PWM generator after converting them to three modulating signals U_{abc} .

A schematic of the system is shown in Fig.2.3. The MATLAB/Simulink model of this system is based on (Giroux et al., 2012). This model has been adapted to meet the requirements of the proposed work.

To create the dataset an islanding event is created at a time instant of 0.4s and V_a, V_b, V_c from point of common coupling (PCC) are acquired for a total of 7 cycles at 1000 samples per second.

All simulations are carried out in MATLAB/Simulink.

2.4.2 Parameters used for islanding detection

Firstly, several islanding and non-islanding events are simulated and the three phase voltages, V_a, V_b and V_c from the PCC are acquired as a time-series data for each event. To generate the image data set for islanding and non-islanding cases the following parameters are computed from PCC voltages.

1. **Concatenated 3-ph voltages ($V_{[abc]}$)**

Concatenation, a process where an array of data is joined at the end of another array to form a single array, is used on the three phase voltages to represent

Table 2.1: Details of the system used for generating dataset

Component	Specifications
PV	100kW
330 SunPower modules (SPR-305E-WHT-D)	$V_{OC} = 64.2$ V $I_{SC} = 5.96$ A 66 strings of 5 series-connected modules
DC-DC boost converter	5kHz - 500V
VSC	3-ph 3-level 1980Hz 260V(AC), 60Hz
Filter	10-kvar capacitor bank
Transformer	3-ph,100-kVA, 260V/25kV, 60Hz
Utility grid	25-kV feeder and 120 kV line

the state of all three phases in a single array as $V_{[abc]}$. Let the voltages acquired from PCC, V_a, V_b, V_c be represented as:

$$V_a = [V_{a1}, V_{a2}, V_{a3}, \dots, V_{an}] \quad (2.3)$$

$$V_b = [V_{b1}, V_{b2}, V_{b3}, \dots, V_{bn}] \quad (2.4)$$

$$V_c = [V_{c1}, V_{c2}, V_{c3}, \dots, V_{cn}] \quad (2.5)$$

By concatenating the time series data of three voltages, we get $V_{[abc]}$.

$$V_{[abc]} = [V_{a1}, V_{a2}, V_{a3}, \dots, V_{an}, V_{b1}, V_{b2}, V_{b3}, \dots, V_{bn}, V_{c1}, V_{c2}, V_{c3}, \dots, V_{cn}] \quad (2.6)$$

This technique allows us to represent the state of all the three phases in a single image once the time series data is converted to a scalogram image.

2. Rate of change of voltages (ROCOV) ($\frac{dV_{[abc]}}{dt}$)

Similarly, ROCOV for all three phases is represented by concatenating $\frac{dV_a}{dt}$, $\frac{dV_b}{dt}$, and $\frac{dV_c}{dt}$, as given below.

$$\frac{dV_{[abc]}}{dt} = \left[\frac{dV_a}{dt}, \frac{dV_b}{dt}, \frac{dV_c}{dt} \right] \quad (2.7)$$

CWT is now applied for the time-series data in Equation.2.7 to generate scalogram images.

3. Rate of change of negative sequence voltage (ROCONSV) ($\frac{dV_{neg}}{dt}$) - for islanding and grid-connected cases

Sequence component voltages, positive sequence (V_1), negative sequence (V_2), and zero sequence (V_0), are computed from the PCC voltages using following equations:

$$V_1 = \frac{1}{3} (V_a + aV_b + a^2V_c) \quad (2.8)$$

$$V_2 = \frac{1}{3} (V_a + a^2V_b + aV_c) \quad (2.9)$$

$$V_0 = \frac{1}{3} (V_a + V_b + V_c) \quad (2.10)$$

Negative sequence component V_2 is computed from PCC voltages V_a, V_b, V_c using Eq.2.9, where a is a complex operator

$$a = 1\angle 120^\circ = e^{j2\pi/3}$$

Once the negative sequence component is computed, ROCONSV is given as

$$\frac{dV_{neg}}{dt} = \frac{dV_2}{dt} \quad (2.11)$$

4. Rate of change of negative sequence voltage (ROCONSV) ($\frac{dV_{neg}}{dt}$) - for early islanding detection

Early islanding detection refers to detecting an islanding event with reduced detection time or detecting islanding even before it has occurred by monitoring the

faults. This is based on the observation that most of the unintentional islanding events are a consequence of some kind of fault. Once a fault has occurred in the system, certain time is required for relay operation, breaker actuation, and circuit breaker contact separation as shown in the timing diagram (Kasztenny and Rostron, 2018). An islanding event occurs only after the contacts are separated. This is shown in the timing diagram in Fig. 2.4 as window for early islanding detection. The ROCONSV is monitored to check for fault conditions. ROCONSV is computed as shown in Eq.2.11.

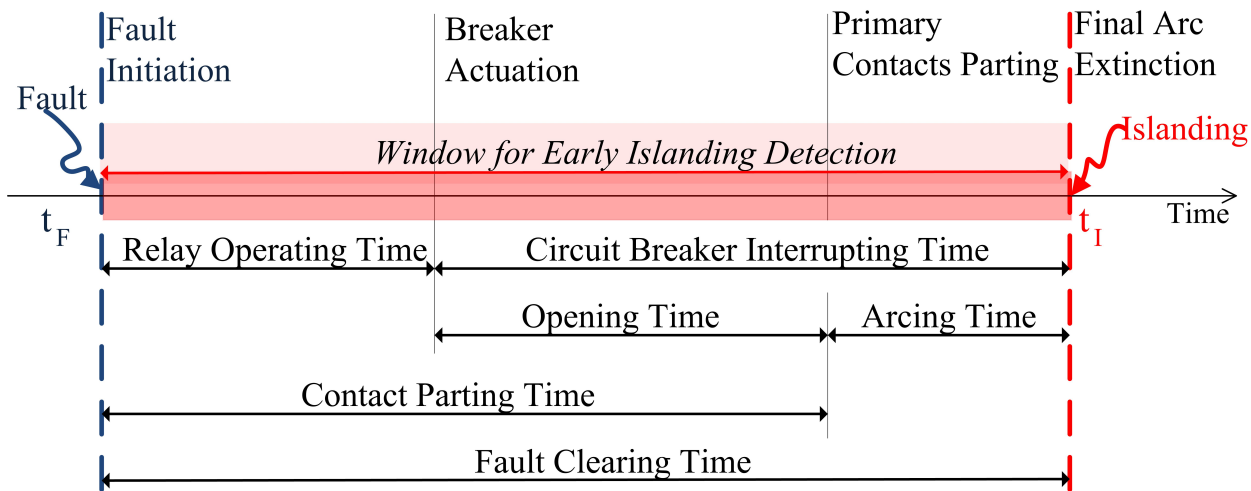


Figure 2.4: Time line of events after a fault

2.4.3 Test cases for islanding and non-islanding events

CWT is applied all the parameters - concatenated voltage $V_{[abc]}$, $\frac{dV_{[abc]}}{dt}$, $\frac{dV_{neg}}{dt}$ for islanding and early islanding detection - to generate a scalogram images. These images are then appropriately labeled as either an islanding or non-islanding case. The scalogram images of concatenated voltages $V_{[abc]}$ for grid-connected and islanded modes of operation are shown in Fig. 2.5. It is evident from these images that there is a clear distinction between islanded and non-islanded modes of operation, indicating the potential of image classification techniques for islanding detection.

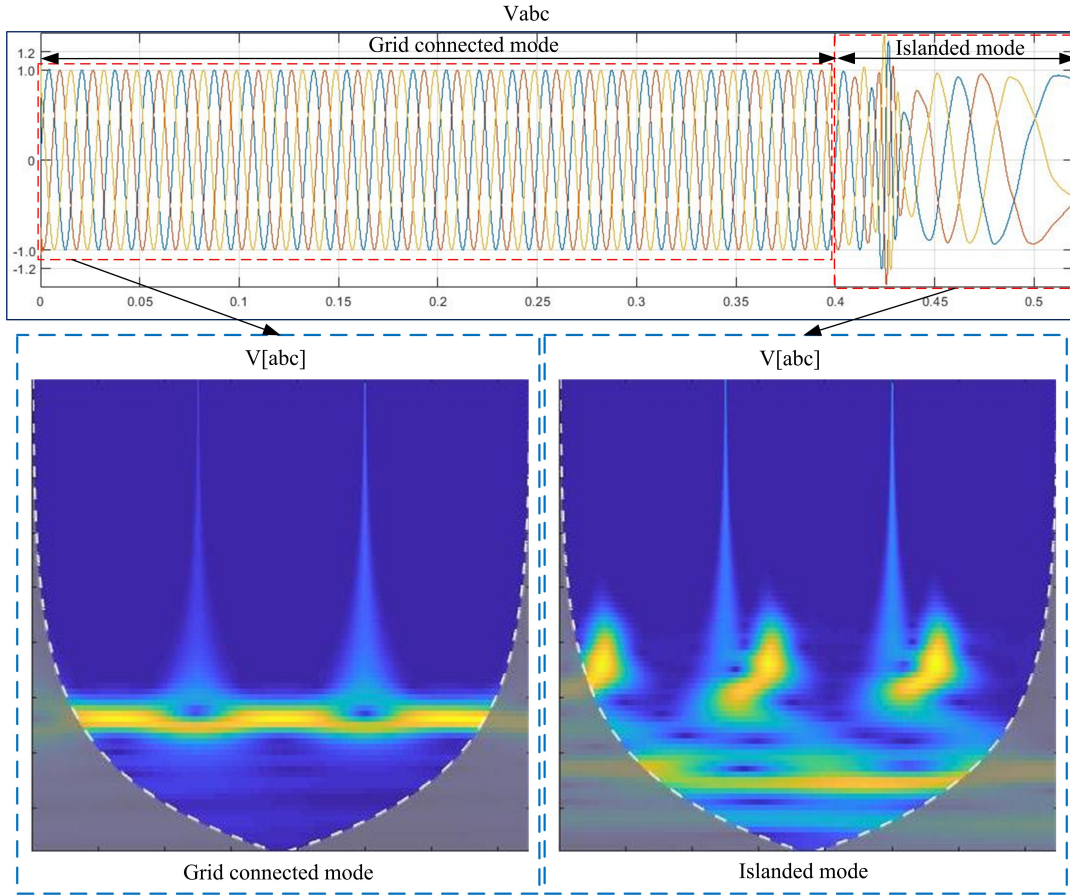


Figure 2.5: Scalogram images for concatenated voltages $V_{[abc]}$ for grid connected and islanded modes of operation

In case of most passive IDMs the detection of an islanding event is very difficult when the power mismatch between the DG source generation and the load is near zero or minimum. To take this aspect into account several cases at near zero power mismatch are considered in the data set. In case of non-islanded mode of operation, sudden switching (ON/OFF) of inductive (L) or capacitive (C) loads are often misclassified as islanding events. Hence, several cases of sudden switching of (L) and (C) loads are also included.

To create a dataset for training and testing, for each parameter a total of 400 events, 200 islanding and 200 grid-connected, are simulated. Detecting islanding events is complicated when the power mismatch between the DG power generation and the load power consumption is near zero. Therefore, these events are considered in the data set. Out of 200, from each class, 170 are used for training. However,

the testing dataset is augmented by creating 60 more events from the remaining 30. This is done by adding two types of noise to the images, namely, salt and pepper, and speckle. These are common type of noises that are added to images. By doing so, we can test the performance of the proposed IDM for noisy conditions and also augment the testing dataset to 90. The entire testing dataset is completely unseen by the classifier.

A separate dataset is created for early islanding detection. The fault events are simulated for different fault resistances. Therefore, several fault conditions are simulated and the ROCONSV (dV_{neg}/dt) is computed, which will further be converted into scalogram image. A total of 2080 cases are simulated to create the dataset for training and testing the islanding detection classifiers. The cases that are considered in the dataset are tabulated in Table. 2.2.

Some scalogram images for islanding and non-islanding cases are depicted in Fig. 2.6. Scalogram images of grid-connected and islanded modes of operation for $dV_{[abc]}/dt$ is depicted in Fig. 2.6.(a). Similarly, images of grid-connected and islanded modes of operation for dV_{neg}/dt for islanding detection case are shown in Fig. 2.6.(b). Scalogram images related to early islanding detection based on dV_{neg}/dt for normal and fault conditions are shown in Fig. 2.6.(c). All these images show a clear distinction between normal and abnormal cases.

Similarly for non-islanding cases certain events have a tendency to be misclassified as islanding events. These events are considered in the dataset. The scalogram images for sudden switching ON of inductive load is shown in Fig.2.7.(a), sudden switching OFF of inductive loads is depicted in Fig.2.7.(b), sudden switching ON of capacitive load is shown in Fig.2.7.(c) and sudden switching OFF of capacitive load is shown in Fig.2.7.(d). It can be seen from different scalogram images in Fig.2.7 that the variation in the magnitude of the voltage is only reflected as a change in color gradient. The patterns in the scalogram images are not affected by magnitude variations.

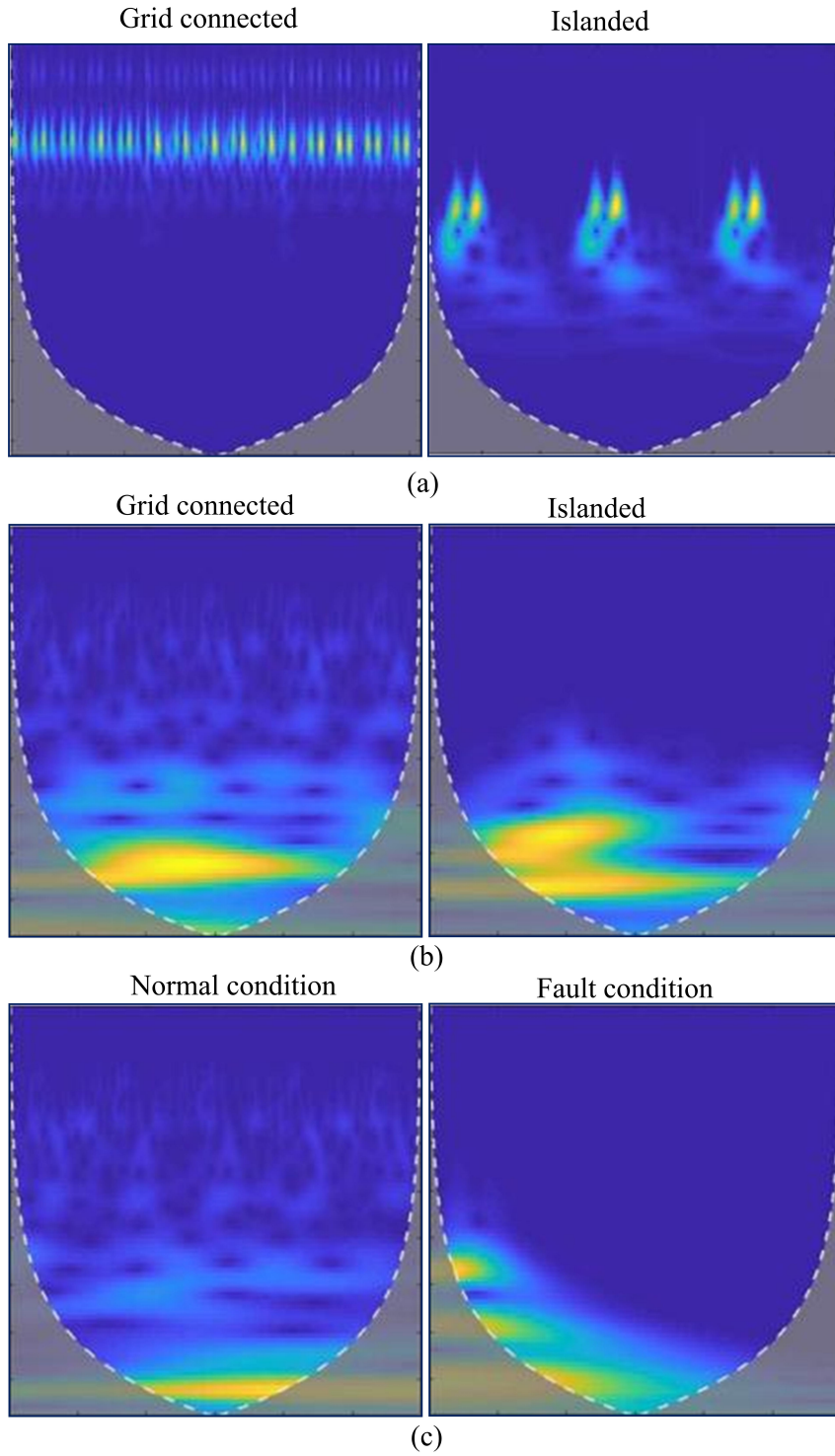


Figure 2.6: Scalogram images for different parameters (a) $dV_{[abc]}/dt$ for grid connected and islanded case (b) dV_{neg}/dt for grid connected and islanded case (c) dV_{neg}/dt for normal condition and fault condition (for early islanding detection)

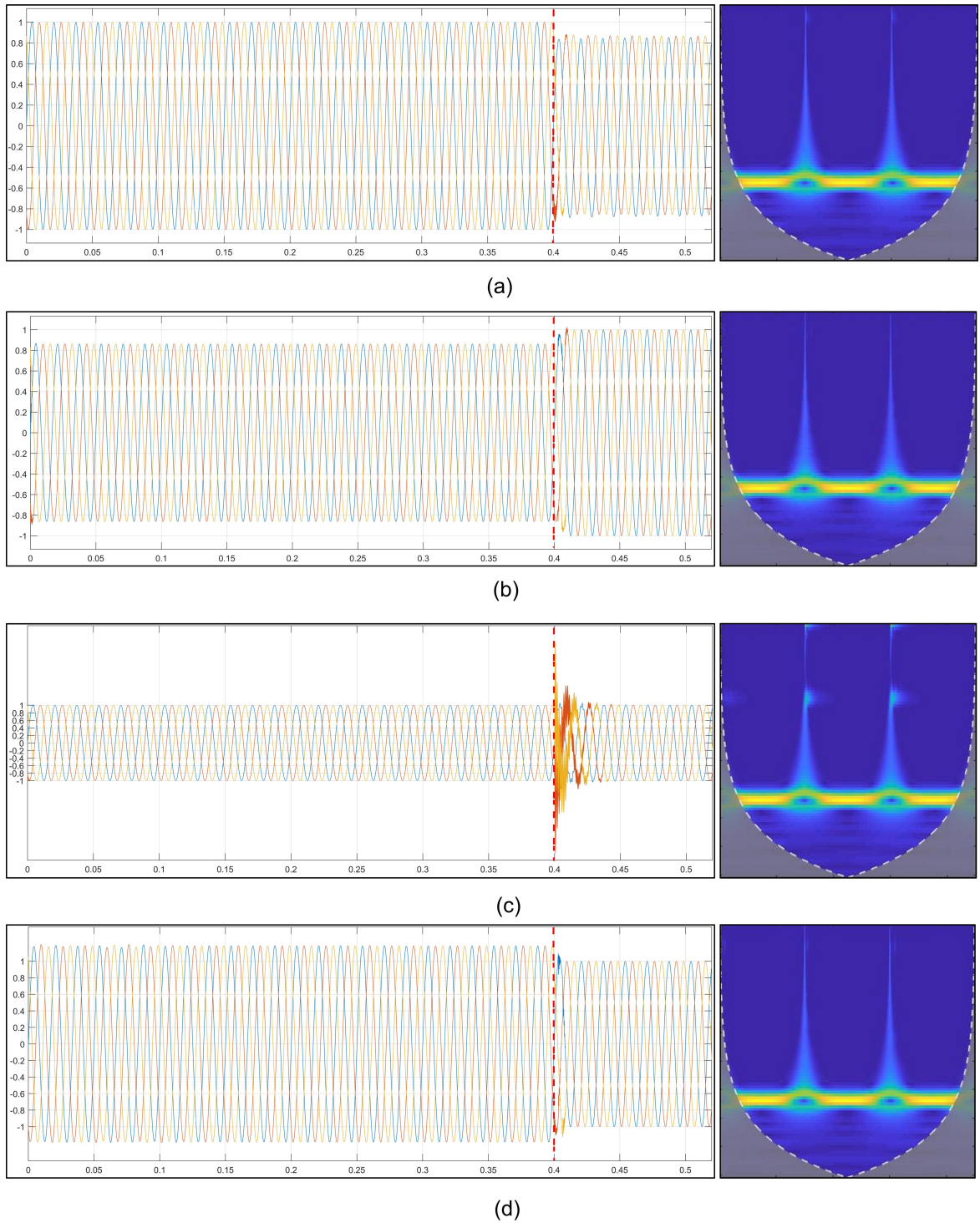


Figure 2.7: Scalogram images for various non-islanding cases: (a) Sudden switching ON of Inductive load/Induction motor load (b) Sudden switching OFF of Inductive load/Induction motor load (c) Sudden switching ON of Capacitive load (d) Sudden switching OFF of Capacitive load

Table 2.2: Various cases simulated to create data set

Parameter	Island	Grid	Island (Noise)		Grid (Noise)		Total
			Salt & Pepper	Speckle	Salt & Pepper	Speckle	
$V_{[abc]}$	200	200	30	30	30	30	520
$dV_{[abc]}/dt$	200	200	30	30	30	30	520
dV_{neg}/dt	200	200	30	30	30	30	520
Parameter	Fault	No Fault	Fault (Noise)		No fault (Noise)		
			Salt & Pepper	Speckle	Salt & Pepper	Speckle	
dV_{neg}/dt	200	200	30	30	30	30	520
							2080

Table 2.3: Training and testing data used for all islanding detection methods

Training Dataset		Testing Dataset							
Parameter	Island	Grid	Island (Noise)		Grid				
	No-Noise	Salt & Pepper	Speckle	No-Noise	Salt & Pepper	Speckle	No-Noise	Salt & Pepper	Speckle
$V_{[abc]}$	170	170	30	30	30	30	30	30	30
$dV_{[abc]}/dt$	170	170	30	30	30	30	30	30	30
dV_{neg}/dt	170	170	30	30	30	30	30	30	30
Parameter	Fault	No Fault	Fault (Noise)		No Fault		No fault (Noise)		
	No-Noise	Salt & Pepper	Speckle	No-Noise	Salt & Pepper	Speckle	No-Noise	Salt & Pepper	Speckle
dV_{neg}/dt	170	170	30	30	30	30	30	30	30

The dataset for islanding and grid-connected cases for different parameters is now used for training and testing the islanding detection methods. The dataset is divided into training and testing dataset as shown in Table. 2.3. For all parameters in each class, islanding/non-islanding or fault/normal, 170 images are used for training. All these 170 images are cases without any noise. For testing 90 images are used in each class. Out of 90 images, 30 images are with out any noise, 30 are images with salt & pepper noise and the remaining 30 are images with speckle noise. By splitting the dataset as described above, it enables us to test the performance of different IDMs for noisy conditions and how immune each IDM is to noisy conditions.

2.5 Summary

In this chapter the definition of supervised learning is first given. From this definition, the need for dataset to train and test the ML/DL/AI algorithms is presented. Since the proposed islanding detection method uses image classification based techniques an appropriately labeled image dataset of islanding and non-islanding cases is required. The process of converting time-series data to scalogram images is explained with an example equation with arbitrary frequencies and magnitudes. Further, different parameters that are considered for islanding detection and early islanding detection are explained in detail. The details regarding early islanding detection feature are also presented. Lastly, example scalogram images for different events are depicted along with the tabulated dataset details.

Chapter 3

HISTOGRAM OF ORIENTED GRADIENTS FEATURE BASED ISLANDING DETECTION

3.1 Introduction

As presented in Chapter. 2 Section.2.2, supervised learning requires training with appropriately labeled data. Features are extracted from the data to train an algorithm to generate a learned model. In machine learning parlance, feature is the input to an algorithm, both while training and testing. This is shown in Fig. 3.1. It depicts the importance of feature extraction. The purpose of feature extraction is to acquire the most pertinent information from the raw data and represent it in a reduced dimension. In simple terms, feature extraction is a process of transforming the input raw data and into a set of features that best represent the data.

3.2 Feature extraction from images

For classification, features should comprise necessary details to differentiate between given classes. The performance of any machine learning algorithm for classification relies to a great extent on the feature extraction. Therefore, extracting better features is an important aspect of classification problem. Best features are those that represent the inherent structures in the data and be insensitive to irrelevant information in the

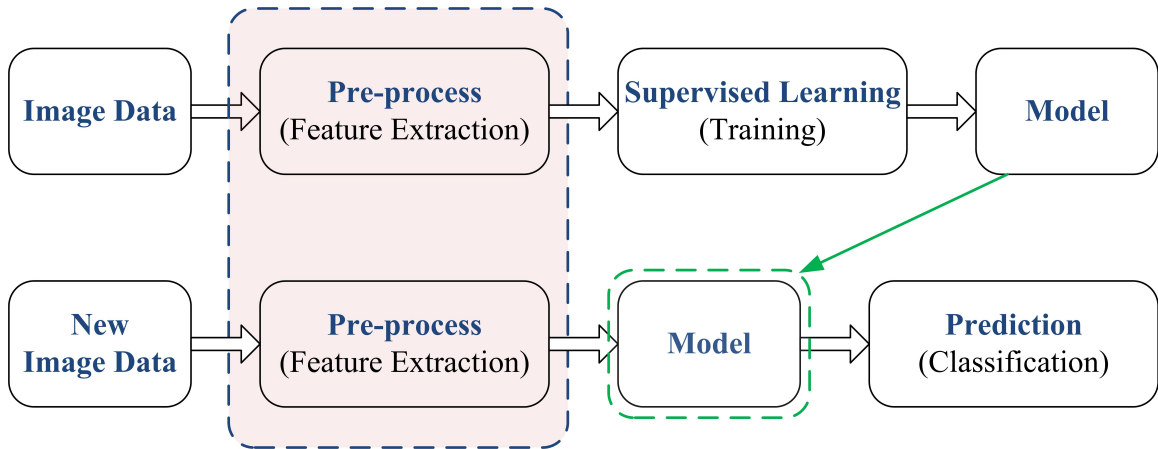


Figure 3.1: Feature extraction in supervised learning

raw data.

Identifying the best features is more often than not an iterative process that includes both features and model performance evaluation. Defining the type of features to be extracted from raw data is also referred to as feature engineering. There are several features that can be extracted from an image that are reported in the literature. In the proposed image classification based IDM, histogram of oriented (HOG) features are used.

3.2.1 Histogram of oriented gradient features

Histogram of Oriented Gradients, or simply known as HOG features or HOG descriptors, is an extremely popular technique used in the domain of image classification and computer vision. The concept of HOG descriptors was reported in (Dalal and Triggs, 2005). HOG descriptors were originally used for human detection with great success.

To serve as a quick reference, the steps for computing HOG features is described here. For simplicity, a 16x16 pixel image is considered for HOG descriptors computation as shown in Fig. 3.2. The image is in gray scale whose pixel values vary from 0, representing black, to 255, representing white. Arbitrary values are assumed for pixels around the pixel of interest (x, y) . To begin with, an image is segmented into cells and blocks. In this computation we assume the size of a cell to be 8x8 pixels. And the block size is assumed to be 2x2 cells as shown in Fig. 3.2. These values can be changed based on the requirements and applications.

With reference to an image, a gradient is a vector that points in the direction of

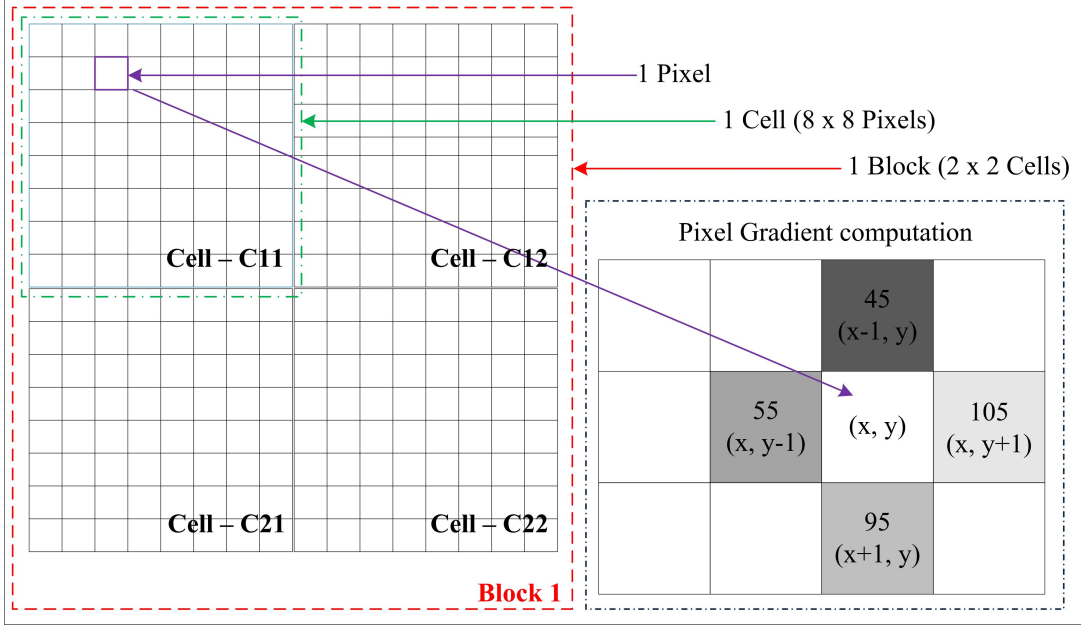


Figure 3.2: Gradient computation for a given pixel

most rapid increase in intensity. It is mathematically represented as (3.1)

$$\nabla f(x, y) = \begin{bmatrix} g_x \\ g_y \end{bmatrix} = \begin{bmatrix} \frac{\delta f(x, y)}{\delta x} \\ \frac{\delta f(x, y)}{\delta y} \end{bmatrix} \quad (3.1)$$

In the considered example, gradient vector is computed as shown in (3.2)

$$\nabla f(x, y) = \begin{bmatrix} f(x, y + 1) - f(x, y - 1) \\ f(x + 1, y) - f(x - 1, y) \end{bmatrix} \quad (3.2)$$

The two attributes of gradient vector are magnitude and direction. These are given by equations (3.3) and (3.4), respectively.

$$|\nabla f| = \sqrt{g_x^2 + g_y^2} \quad (3.3)$$

$$\theta = \tan^{-1} \left(\frac{g_y}{g_x} \right) \quad (3.4)$$

$$\nabla f(x, y) = \begin{bmatrix} f(x, y + 1) - f(x, y - 1) \\ f(x + 1, y) - f(x - 1, y) \end{bmatrix} = \begin{bmatrix} 105 - 55 \\ 95 - 45 \end{bmatrix}$$

$$\nabla f(x, y) = \begin{bmatrix} 50 \\ 50 \end{bmatrix}$$

$$|\nabla f| = \sqrt{50^2 + 50^2} = 70.71 \quad (3.5)$$

$$\theta = \tan^{-1} \left(\frac{50}{50} \right) = 45^\circ \quad (3.6)$$

Similarly, the magnitude and direction are calculated for all the pixels in a cell. In the next step, these values are assigned to bins to create a histogram of a particular cell. Bins represent direction values from 0 to 180. As a general rule of thumb, based on empirical observations, nine bins are considered. For every pixel in a cell, we now have two components, namely, magnitude and direction. This is shown in Fig. 3.3. The allocation of magnitude to a particular bin is based on the direction angle θ . In the considered example, θ is 45° . This falls between the bins centered around 30° and 50° . Magnitude will be allocated to both bins based on the proximity of actual θ to the center of the bin. Meaning, if θ is closer to center of a bin, then it receives more share of magnitude. Distance of 45° to the bins centered around 30° and 50° is 15 and 5, respectively. Therefore, bin centered around 50° gets $\frac{3}{4}^{th}$ and bin centered around 30° gets $\frac{1}{4}^{th}$ of magnitude as shown in Fig. 3.3. This allocation is carried out for all the 64 pixels in cell C_{11} . This forms a histogram of oriented gradients (HOG) block for cell C_{11} , represented as $H_{(C_{11})}$.

The key point to be noted is that now a total of 128 features from 8x8 pixels (64 magnitudes and 64 directions) are represented in a HOG block with just 9 features. For a total of 256 pixels in 16x16 area we get 512 features. All these 512 features can be represented in a HOG feature vector in 36 features as 4 HOG blocks each of size 9

This entire process is repeated for cells C_{12} , C_{21} and C_{22} . The final HOG feature vector for entire image is formed by concatenating all the HOG blocks, $H_{(C_{11})}$, $H_{(C_{21})}$, $H_{(C_{12})}$, $H_{(C_{22})}$, as shown in Fig. 3.4. This feature vector can now be used as an input to a machine learning classifier.

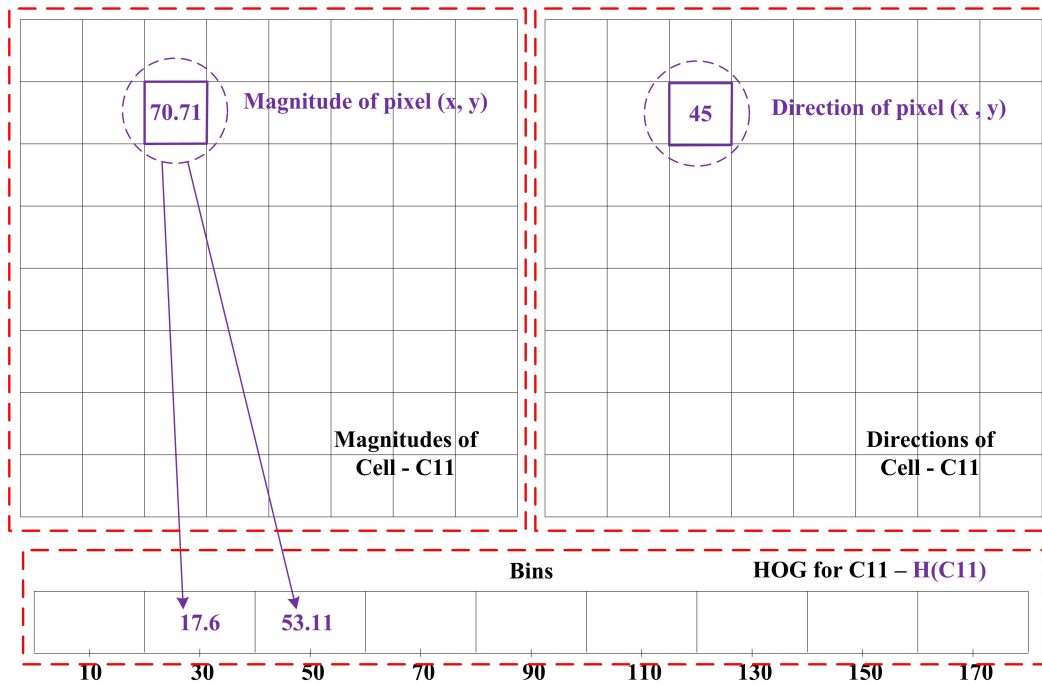


Figure 3.3: Magnitude allocation for bins based on direction

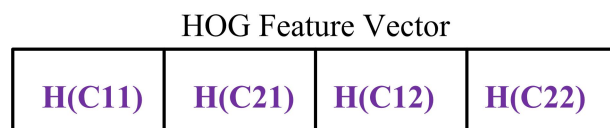


Figure 3.4: Final HOG feature vector for 16x16 pixel image

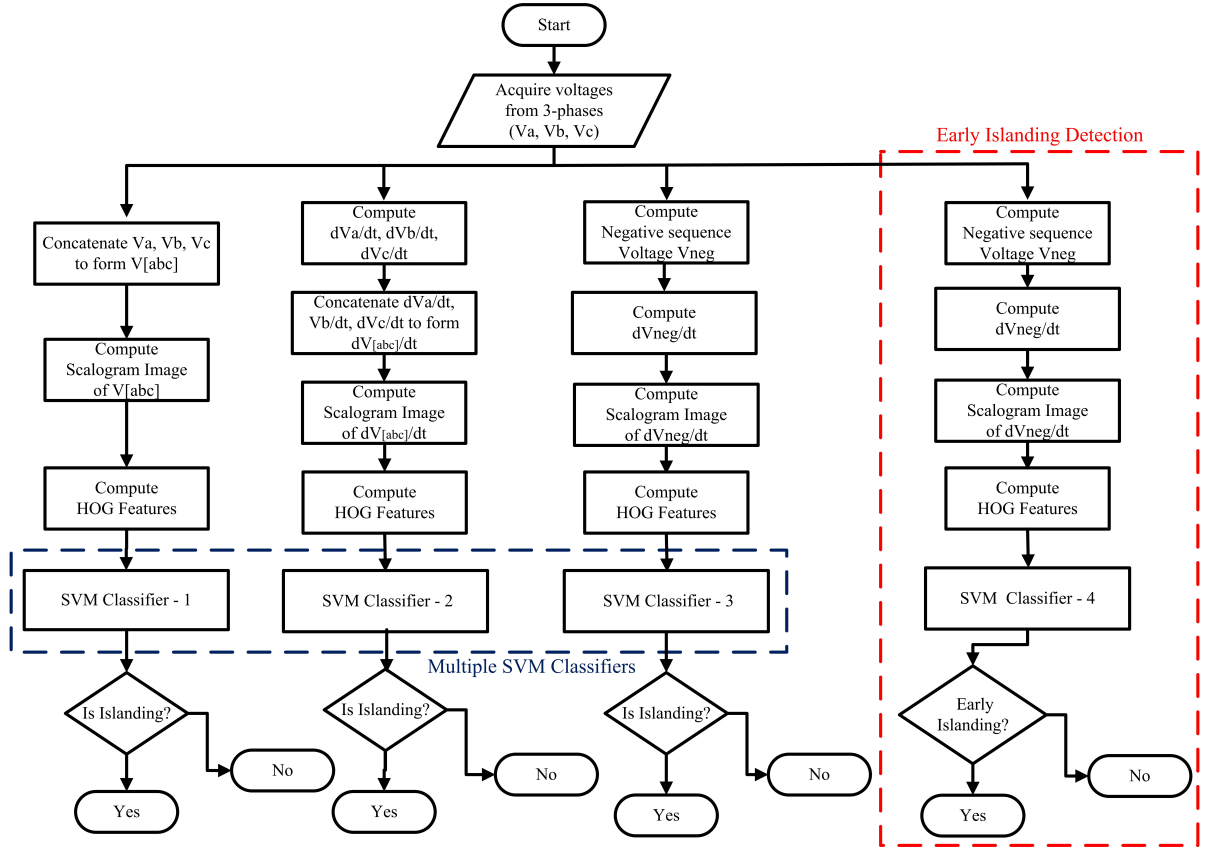


Figure 3.5: Flowchart of the proposed HOG feature based islanding detection method

3.3 Proposed method

The steps involved in the proposed image classification based IDM using multiple SVM classifiers are depicted as a flowchart in Fig.3.5.

The proposed method uses three parameters for islanding detection. Each parameter is computed from the acquired PCC voltages, V_a , V_b , and V_c . The first parameter is voltage. Once the three phase voltages are acquired from the PCC, they are concatenated to form single time-series data $V_{[abc]}$. This concatenated time-series data is then converted to a scalogram image by applying CWT on $V_{[abc]}$. Concatenation enables us to characterize the state of V_a , V_b , and V_c in one scalogram image. HOG features are extracted from the image and the HOG feature vector is then fed to a pre-trained SVM classifier for detecting an islanding event. The second parameter that is used in the proposed method is ROCOV dV/dt . The ROCOV is computed for each of the acquired voltages, V_a , V_b , and V_c . The computed values are then con-

catenated to form a single time series data $dV_{[abc]}/dt$. CWT is applied on $dV_{[abc]}/dt$ to convert the time-series data to image. HOG features are extracted from the image which is then fed to a pre-trained SVM classifier for islanding detection.

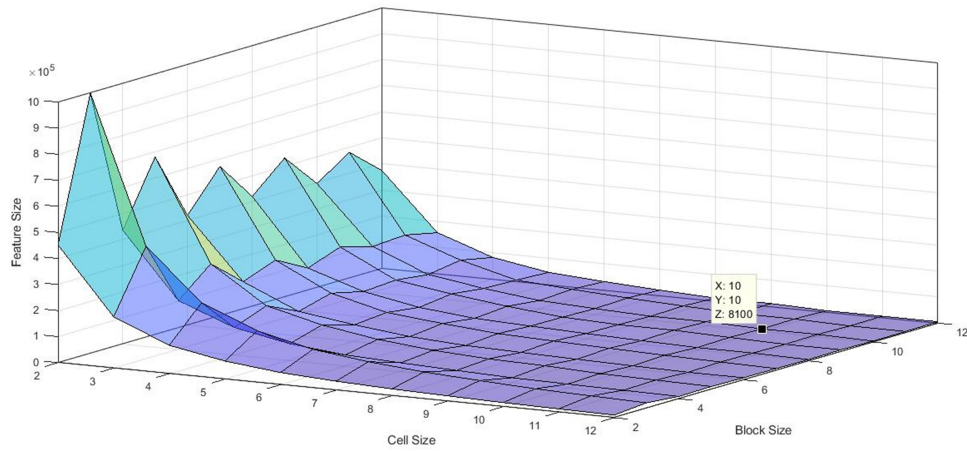
Similarly, the next parameter used for islanding detection is ROCONSV dV_{neg}/dt . The negative sequence component of voltage is first calculated from the acquired PCC voltages V_a , V_b , and V_c . In the next step the ROCONSV is computed. This time-series data of dV_{neg}/dt is converted to a scalogram image. HOG features are extracted from the image which is then given as an input to a pre-trained SVM classifier for detecting islanding event.

Support vector machine(SVM) is used as a classification tool. The choice of SVM as a classification tool stems from the fact that it is inherently a binary classifier (Cortes and Vapnik, 1995). This fits into the problem of islanding detection, requiring a YES or NO. SVM with different kernels, such as, linear kernel, Gaussian kernel, polynomial kernel, radial basis function (RBF) kernel are used for training and testing the proposed method. Multiple SVM classifiers are used for islanding detection based on different parameters.

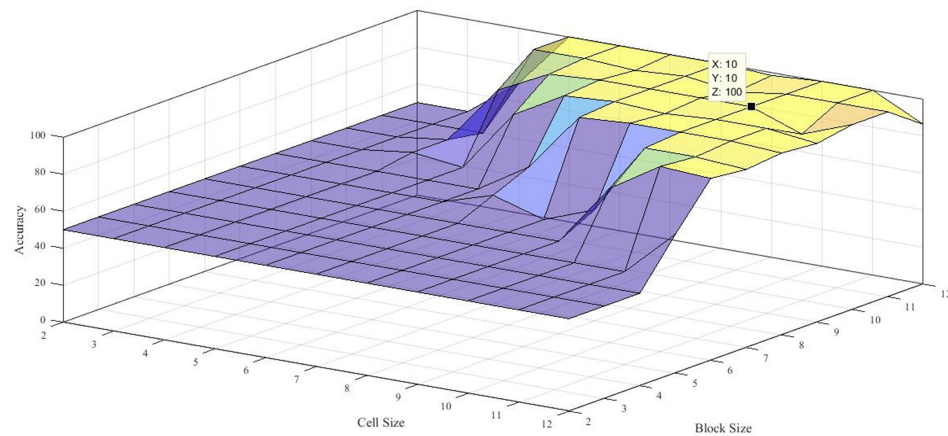
In addition to islanding detection, a early islanding detection using ROCONSV is also implemented. An unintentional islanding event is a result of opening of a circuit breaker (CB). One of the primary reasons for the opening of a CB is a fault in the system. Therefore, by detecting a fault we can detect an islanding event even before its occurrence. A separate dataset is created for various fault events and their corresponding changes in dV_{neg}/dt . An SVM is trained on HOG features extracted from images that represent fault cases and normal cases to enable early islanding detection.

3.4 Results and discussions

For computing HOG features cell size and block size must be chosen. By choosing smaller cell sizes a lot of finer details can be extracted, however this will lead to an increase in the number of computations, the feature vector size. On the other hand, a bigger cell size results in lesser number of computations and smaller feature vector size. Therefore, the first step is to determine these values. The variation of feature vector size with respect to cell size and different block sizes is shown in Fig.3.6.(a). It can be observed that for any given block size the feature size reduces dramatically



(a)



(b)

Figure 3.6: (a) Size of HOG feature vector for different block and cell sizes (b) Plot of accuracy for optimizing cell size and block size

with increase in the cell size. To choose a proper cell size another factor that must be taken into consideration is the detection accuracy. The effect of cell size and block size on accuracy of detection is depicted in Fig.3.6.(b). It can be noticed that the accuracy has stagnated for smaller cell sizes and consistently reaches 100% for cell size 10 and corresponding block size of 8, 9, 10, 11, and 12. Based on these results the cell size and block size are chosen as 10 and 10, respectively. These values have been used for feature extraction. Once the HOG features are extracted, the next step is to train the SVM classifiers. The dataset that is presented in Table.2.2 is used for training and testing. 170 images from each class are used for training and remaining 90 images are used for testing.

SVM with different kernels, such as, linear kernel, Gaussian kernel, polynomial

kernel, radial basis function (RBF) kernel are tested along with a 5-fold cross validation. The following are the tuned values for the SVM classifiers - C is 0.0019, kernel scale parameter is 1.4 , and the order of the polynomial kernel is 2. The results for data without noise are presented in Table.3.1. The detection accuracy for data without noise is 100% for all parameters with all kernels. The classification accuracy of HOG-Scalogram technique with SVM classifier is better when compared to the method proposed in (Faqhrudin et al., 2014) for inverter based system. However, noise sensitivity analysis has not been reported in (Faqhrudin et al., 2014). Further, the proposed method has explicitly considered several non-islanding cases which are often misclassified as islanding events as described in Chapter. 2.

Table 3.1: Classification results for HOG based IDM - for all kernels

Islanding detection		
Parameter	No. of cases: No-Noise	Accuracy
$V_{[abc]}$	60	100%
$dV_{[abc]}/dt$	60	100%
dV_{neg}/dt	60	100%
Early islanding detection		
Parameter	No. of cases: No-Noise	Accuracy
dV_{neg}/dt	60	100%

Table 3.2: Classification results for HOG based IDM - for different kernels

Islanding detection		Accuracy			
Parameter	No. of cases: Noise	Linear	Gaussian	RBF	Ploynomial
$V_{[abc]}$	180	82.77%	66.66%	66.66%	66.66%
$dV_{[abc]}/dt$	180	83.33%	83.33%	66.66%	66.66%
dV_{neg}/dt	180	66.66%	66.66%	66.66%	66.66%
Early islanding detection		Accuracy			
Parameter	No. of cases: Noise	Linear	Gaussian	RBF	Ploynomial
dV_{neg}/dt	180	66.66%	66.66%	66.66%	66.66%

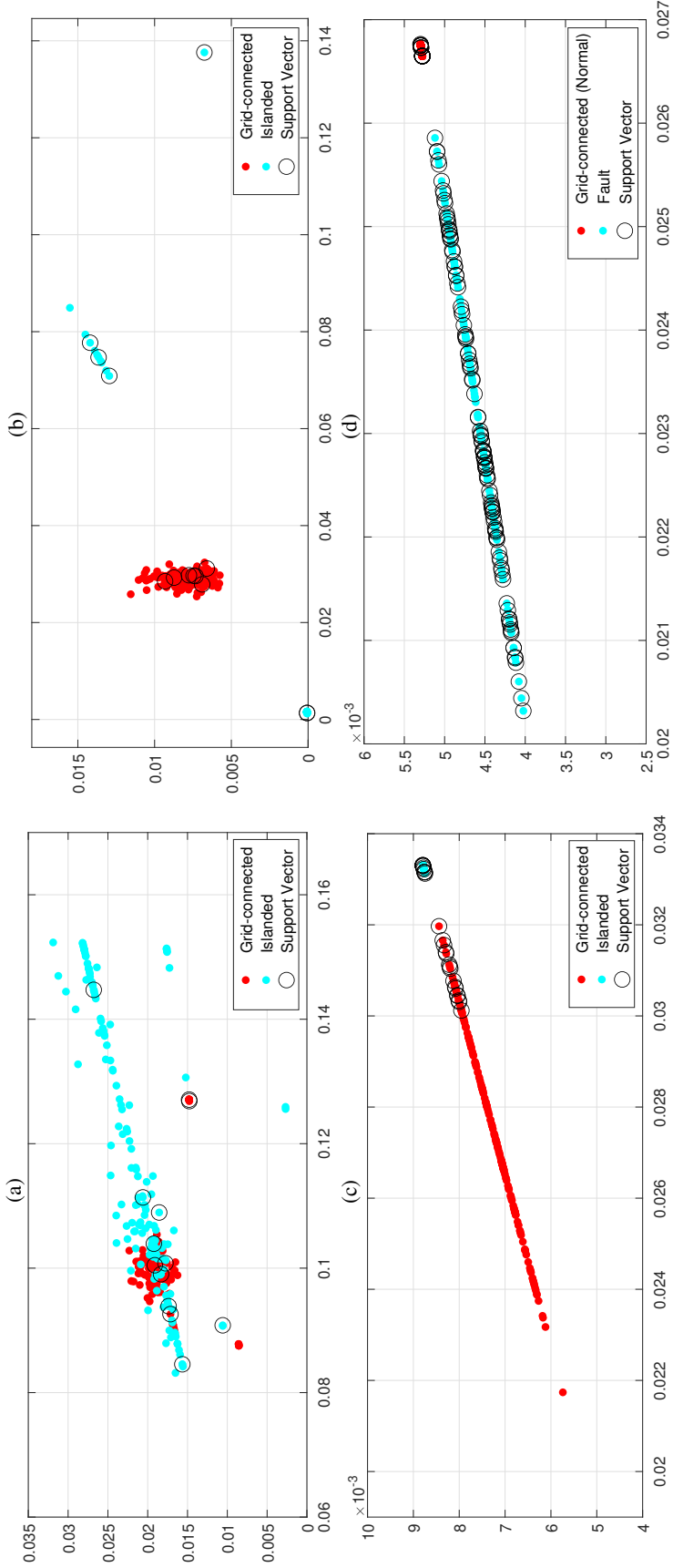


Figure 3.7: (a) V_{abc} (b) V_{abc} (c) $|V_{abc}|$ - Islanding detection (d) $\frac{dV_{neg}}{dt}$ - Early islanding detection (Fault)

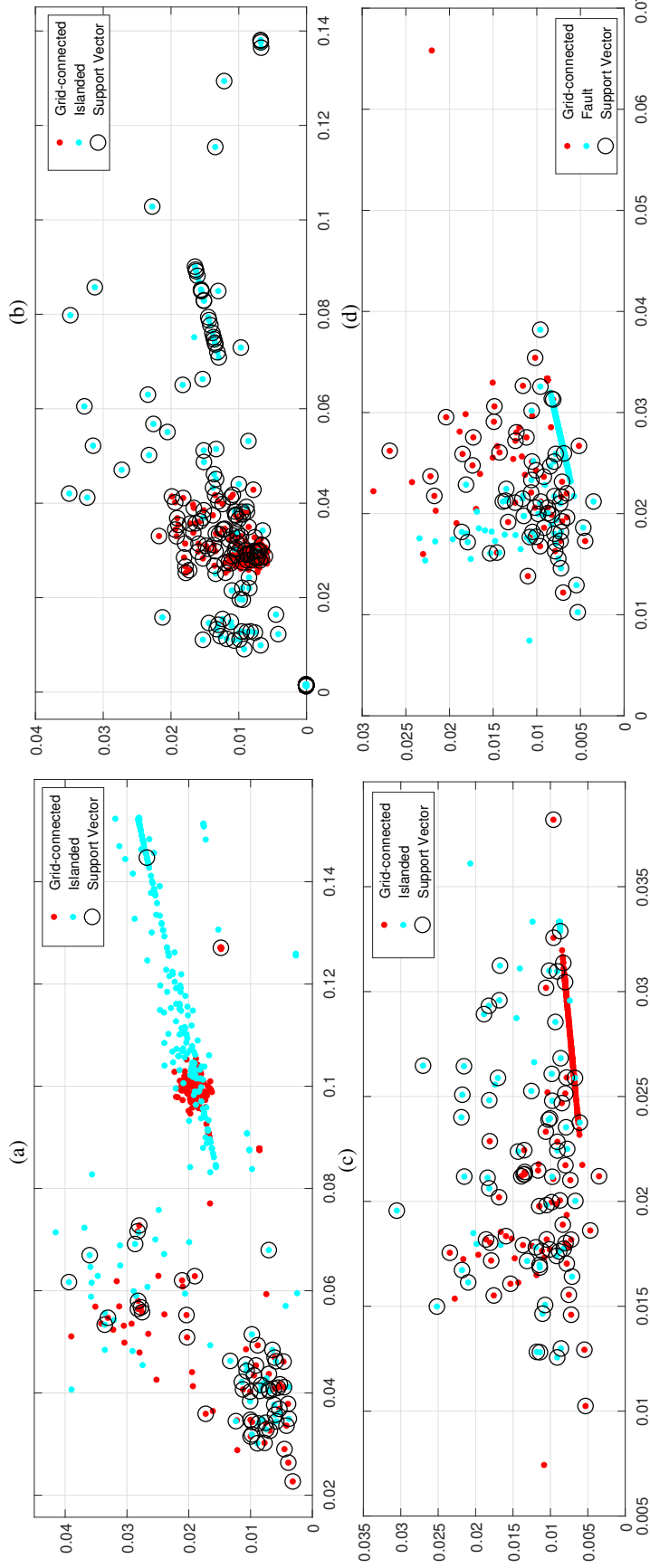


Figure 3.8: (a) $V_{[abc]}$ (b) $V_{[abc]}$ vs $\frac{dV_{[neg]}}{dt}$ (c) $V_{[neg]}$ vs $\frac{dV_{[abc]}}{dt}$ (d) $V_{[neg]}$ vs $\frac{dV_{[neg]}}{dt}$ - Early islanding detection (Fault)

The results for noise dataset is presented in Table.3.2. The islanding detection accuracy for noise dataset is poor compared to the no noise dataset for all kernels.

The reason for the decline in the islanding detection accuracy for noisy dataset can be understood by looking at the features and the support vectors for both datasets. The support vector plot for data without noise and with noise is shown in Fig.3.7 and Fig.3.8, respectively. The plots shown in Fig.3.7.(a), Fig.3.7.(b), Fig.3.7.(c), Fig.3.7.(d) represent support vector plots for $V_{[abc]}$, $\frac{dV_{[abc]}}{dt}$, $\frac{dV_{[neg]}}{dt}$ - Islanding detection, and $\frac{dV_{[neg]}}{dt}$ - Early islanding detection(Fault), respectively. It can be seen that the HOG features are affected by the noise addition. The parameters which had good separability in Fig.3.7 have been affected by the addition of noise, which is evident in Fig.3.8. This can be attributed to the fact that HOG features are dependent on the intensity of the pixels, which is affected by the noise. Also, for some parameters, such as, ROCONSV for islanding detection the scalogram images have complex patterns which can be easily affected by the noise. Therefore, for better classification accuracies features that are independent of intensity are required.

Since feature selection can affect the classification accuracy, it is an ideal choice to opt for convolution neural networks that perform feature extraction, without explicitly specifying the nature of features. This is a contrasting approach from the HOG descriptors which are engineered features.

3.5 Summary

In this chapter, HOG feature based islanding detection method with different parameters is presented. The process of HOG feature extraction is explained. The methodology for HOG feature based islanding detection with SVM classifiers is detailed. The parameters for HOG feature extraction, such as, cell size and block size, are selected by investigating their influence on the feature size and detection accuracy. SVM classifiers are trained and tested with different kernels along with a 5-fold cross-validation. The islanding detection accuracy has been found to be very good for dataset with no noise. However, the performance of HOG feature based islanding detection with SVM classifier is found to be sensitive to the noisy dataset. The reason for the decline in the detection accuracy has been explained with support vector plot for both datasets. This problem can be addressed by choosing features that are not affected by noise.

Chapter 4

TRANSFER LEARNING BASED ISLANDING DETECTION

4.1 Introduction

From Chapter 3, it is observed that HOG features are sensitive to noise and hence the islanding detection accuracy is affected. To overcome this problem, features that are not affected by noise must be chosen. Several image classification techniques have been reported in the literature. Some of these techniques employ engineered features, such as HOG features, where the features are explicitly designed. However, the recent developments in the domain of image classification have reportedly used neural network based architectures.

4.2 Need for better features

Since HOG features are affected by the intensity of noise, it is important to use features that are immune to noise. Also, HOG features are engineered features, meaning they are explicitly defined. Engineered feature may sometimes not give the features that represent the image in its entirety. The performance of such features may not be suited for all applications, especially if the application is in a completely new domain.

4.2.1 Neural networks for image classification

Neural networks have been used in the field of AI/ML for a long time. Neural networks or Artificial Neural Networks (ANNs) are artificially simulated models of biologically inspired neurons in the brain. ANNs are made up of basic building blocks called neurons connected in layers. These layers are generally an input layer, which receives the input, an output layer giving the responses to the inputs. In between these two layers there are hidden layers. There can be one or more number of hidden layers depending on the application. The interconnection between each unit is represented by a weight. Most of the ANNs are usually fully connected, meaning all the units in one layer are connected to all the units in the hidden layer as shown in Fig. 4.1.

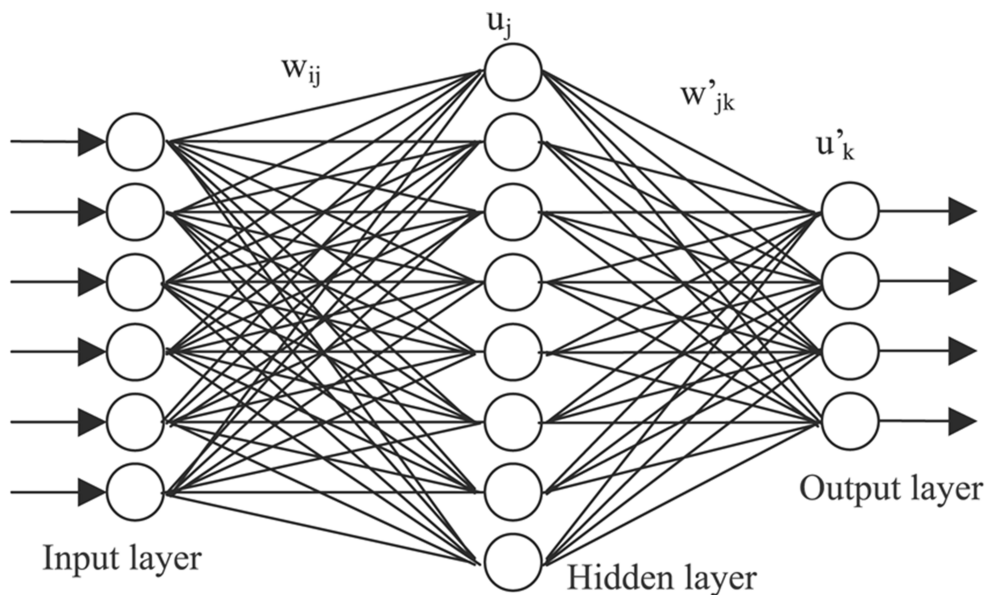


Figure 4.1: General architecture of ANN

The problem with ANNs is that they become very complex when dealing with larger datasets because of their fully connected architecture. This problem has been solved by a convolution neural networks, a type of neural networks.

A CNN has a lot of similarities to a neural network (NN). Both NN and CNNs have neurons as basic building blocks, with biases and learnable weights. Each neuron receives inputs and a dot product is performed. At the end, the entire network of NN or CNN, has a single differentiable score as output. However, the major difference is that CNNs or ConvNets have at least one convolution layer. Most of the layers

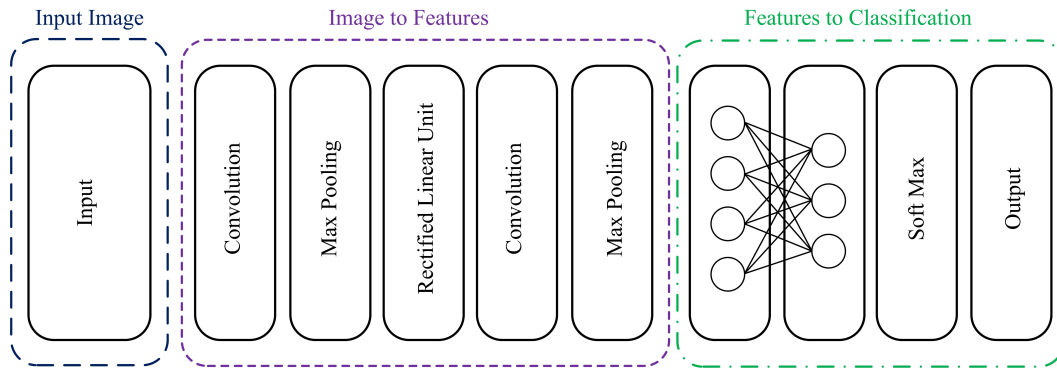


Figure 4.2: General architecture of a CNN

in CNN convert an input image to features. Only the last few layers are used for classification. CNNs have been popularly used in image classification and computer vision applications.

In supervised learning based techniques feature extraction is a crucial step during training and testing phases. These features must be chosen properly to assure good classification accuracy. Contrary to this, in deep learning a CNN can perform end to end learning, meaning, the classifier learns both the features and classification directly from the images. This is also known as data driven approach. Therefore, by using CNNs the features are learned from the data as opposed to HOG descriptors which are engineered features.

4.2.2 Convolution neural networks

A CNN is generally made of different types of layers such as:

- Convolution
- Activation
- Pooling
- Softmax
- Fully connected layer

A General architecture of CNN is shown in Fig. 4.2.

1. Convolution layer A convolution layer is the core of a CNN. It comprises of a set of learnable filters (also known as kernels). The spatial extension the filter is confined to the size of the filter. A convolution operation in this case is basically an element wise multiplication and sum of filter and image. If the image has multiple channels (RGB), then the same filter is applied for each channel. This convolution computes the dot product of entries of the filter and the image space that it occupies. For a filter $f[x; y]$ and image $g[x; y]$, convolution operation is given as Eq.4.1.

$$f[x, y] * g[x, y] = \sum_{n_1=-\infty}^{\infty} \sum_{n_2=-\infty}^{\infty} f[n_1, n_2].g[x - n_1, y - n_2] \quad (4.1)$$

An example image of 6x6 size and two filters of 3x3 size are shown in Fig. 4.3. The operation of different layers are explained with this example. Convolution is a mathematical operation where a dot product is performed between the filter and the image. Simply put, an element wise multiplication and addition for the entire image. The filter slides over the image pixel by pixel to achieve this. The step size of slide is known as stride. Here, we choose stride as 1.

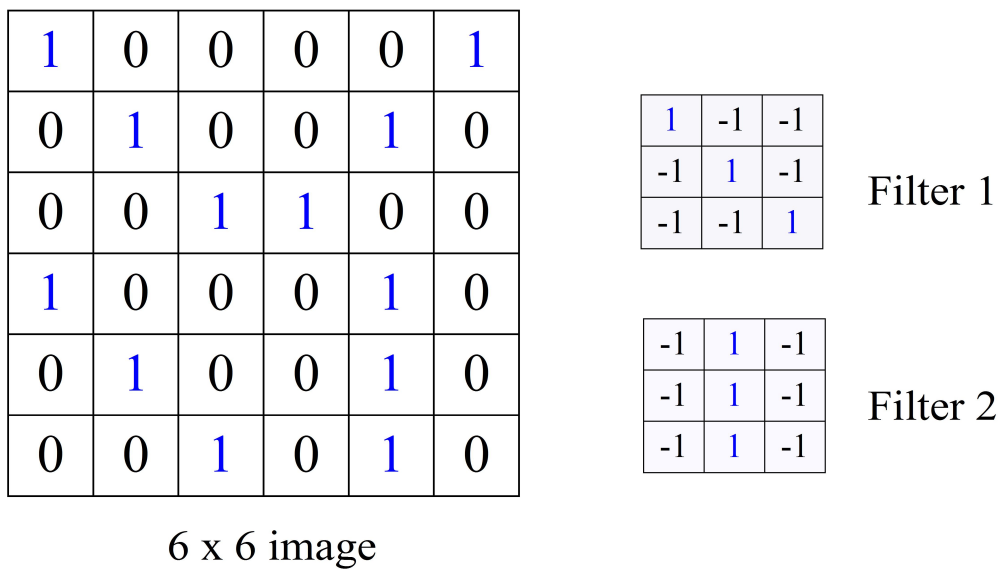


Figure 4.3: Example image and filters for convolution operation

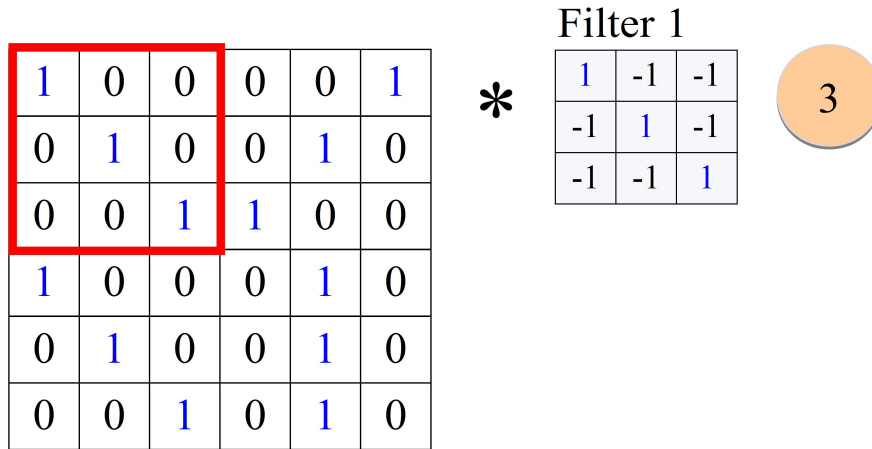


Figure 4.4: Convolution operation in a CNN with Filter 1

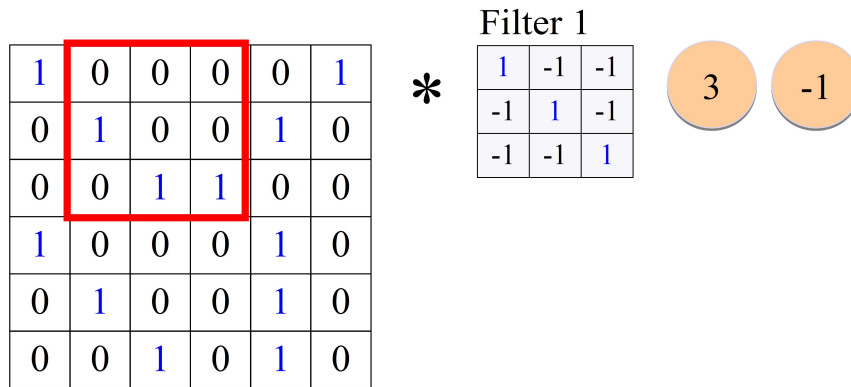


Figure 4.5: Convolution operation in a CNN with Filter 1

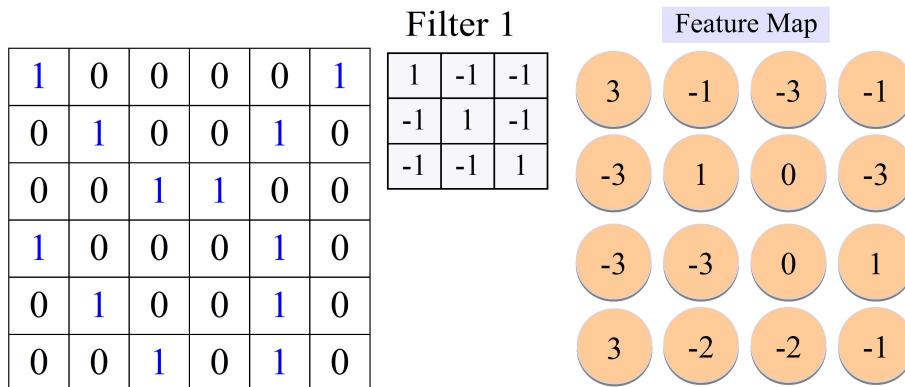


Figure 4.6: Feature map for Filter 1 after convolution operation on entire image

As shown in Fig. 4.4, the element wise multiplication and addition will give us a value of 3. Now the filter slides over the image with stride 1. The next position is shown in Fig.4.5. Now for this position, element wise multiplication and addition gives a value of -1. Similarly, the filter -1 is moved over the entire image, and the all the resulting values form a feature map. The feature map generated by filter-1 is shown in Fig. 4.6.

In a similar way, a feature map for filter-2 is also generated and shown in Fig.4.7. The number of feature maps depend on the number of filters used. The size of the filter and number of filters used in a CNN is a design choice. They are carefully chosen to give best performance.

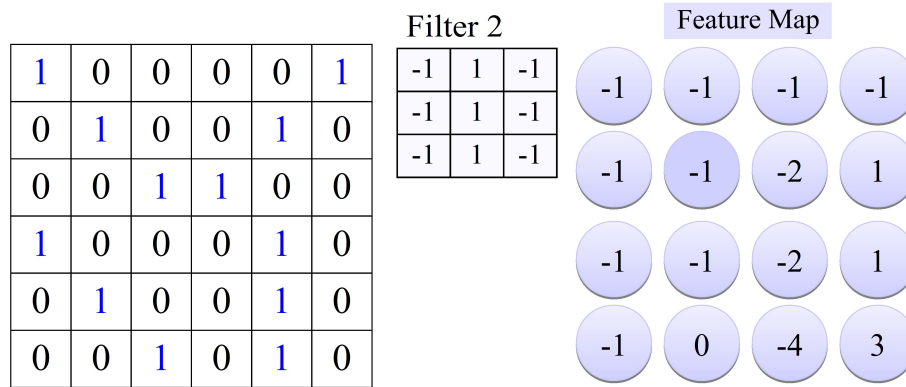


Figure 4.7: Feature map for Filter 2 after convolution operation on entire image

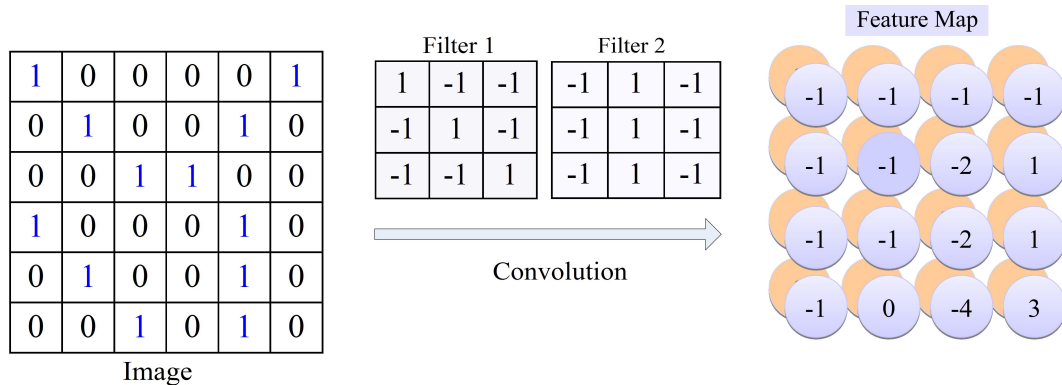


Figure 4.8: Feature maps for Filter 1 and Filter 2 after convolution operation on entire image

2. Activation layer

Consider a single layer NN

$$z = W^T x + b \quad (\text{Linear Transformation})$$

$$a = f(z) \quad (\text{Non-linear Transformation})$$

where:

W is the weight parameter to be learned

x is the output from the first layer

a is the activation parameter

f is a non-linear function

The activations at the output of a convolution layer are linear in nature. These activations are passed through a non-linear function to achieve non-linear transformation. There are different activation functions available.

- Sigmoid

$$f(x) = \frac{1}{1 + e^{-x}} \quad (4.2)$$

- $\tanh(x)$

$$\frac{e^x - e^{-x}}{e^x + e^{-x}} \quad (4.3)$$

- Rectified Linear Unit (ReLU)

$$f(x) = \begin{cases} x, & x \geq 0 \\ 0, & x < 0 \end{cases} \quad (4.4)$$

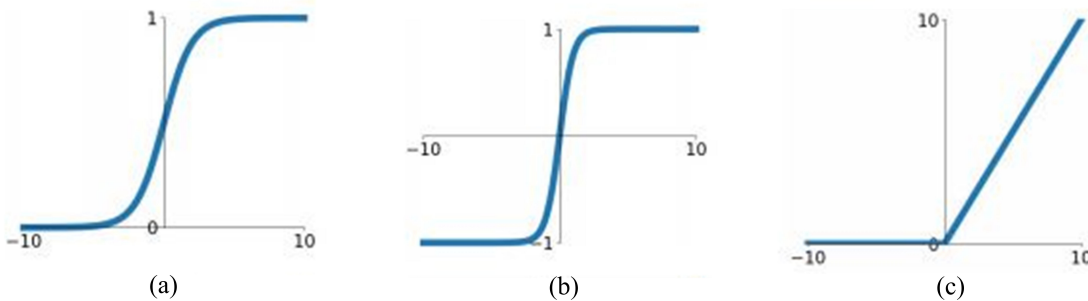


Figure 4.9: Activation functions (a) Sigmoid function (b) tanh function (c) Rectified linear unit (ReLU) function

Rectified Linear Unit (ReLU) layer is mostly used as an activation function to the output of previous layers. This layer returns zero if the input is negative or the same number for positive values. The output feature map will be as shown in Fig.4.10.

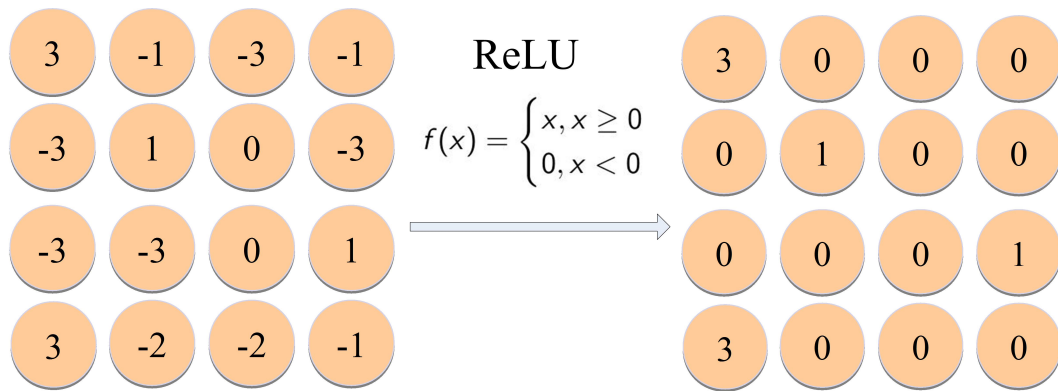


Figure 4.10: Feature map transformation after applying ReLU activation

3. Max pooling layer

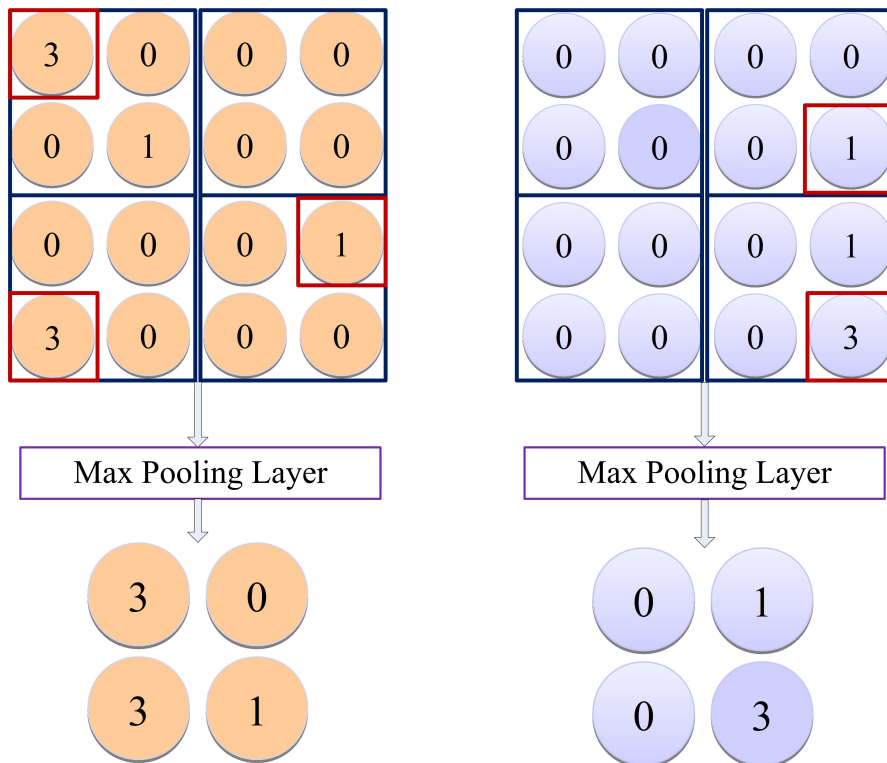


Figure 4.11: Feature map transformation after applying max pooling

Pooling layer performs down sampling of the features that are extracted in convolution layer, i.e., the feature maps. Pooling layer operates on each feature map independently. Most commonly used approach is max pooling. The output of the pooling layer is shown in Fig.4.11.

4. Softmax layer

A softmax layer takes an n-dimensional input vector of real numbers and converts them into probabilities for each class. These probabilities are later used for determining the target class for a given input. Softmax function is given as Eq.4.5. An important aspect of softmax function is that the calculated probabilities are in the range of 0 to 1 and all these probabilities add up to 1.

$$x_i = \frac{e^{z_i}}{\sum_{j=1}^n e^{z_j}} \quad (4.5)$$

5. Fully connected layer

In a fully connected layer a list of features becomes a list of votes. In other words, this layer produces class scores from the activations that will be used for classification.

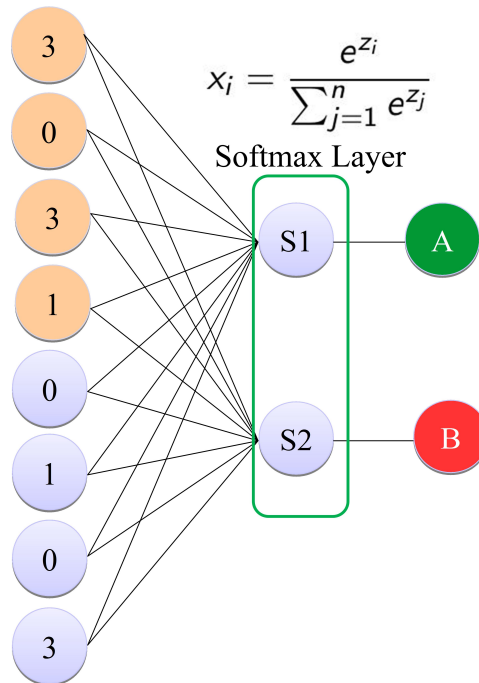


Figure 4.12: Fully connected layer with class outputs

A combination of all these layers is used to design a CNN. The combinations, number of layers and the order varies for different applications. In addition to the type and number of layers, the design of a CNN also includes the choice of other hyper-parameters such as, learning rate, momentum, solver, number of epochs and batch size. A significant aspect to be noted is that, two CNNs with the same exact architecture and same design parameters will exhibit a different behavior based on the data that is used to train them. The behavior of the network is learned from the data itself, leading to a data driven approach.

4.3 Transfer learning

Since designing a CNN is resource intensive and iterative process, it is a common practice to reuse the best architectures that have performed well. Transfer learning refers to the idea of reusing a CNN model that has demonstrated good performance for a certain application to solve a different but related problem. This approach enables us to save time and resources that are needed to train and optimize the CNN and also speed up the design process. However, some minor changes have to be made to the CNN to meet the requirements of the problem at hand. These changes generally are confined to the classification layer, where the number of classes are adjusted according to the problem and the training parameters, such as learning rate, batch size and so on.

4.4 Proposed islanding detection method

The details of the proposed transfer learning based islanding detection method are presented in this section. The steps involved in the proposed image classification based IDM using multiple CNNs is depicted as a flowchart in Fig. 4.13. As shown in Fig. 4.13, the proposed method uses three parameters, $V_{[abc]}$, $dV_{[abc]}/dt$, dV_{neg}/dt for islanding detection and dV_{neg}/dt for early islanding detection. All these parameters are converted to images and given as an input to the pre-trained CNN classifier. For applying transfer learning two CNNs have been used - AlexNet(Krizhevsky et al., 2012) and VGG16(Simonyan and Zisserman, 2014). Both these architectures have performed very well in the ImageNet challenge. ImageNet is an image dataset that has over ten million images in over a thousand classes. This dataset is used for image

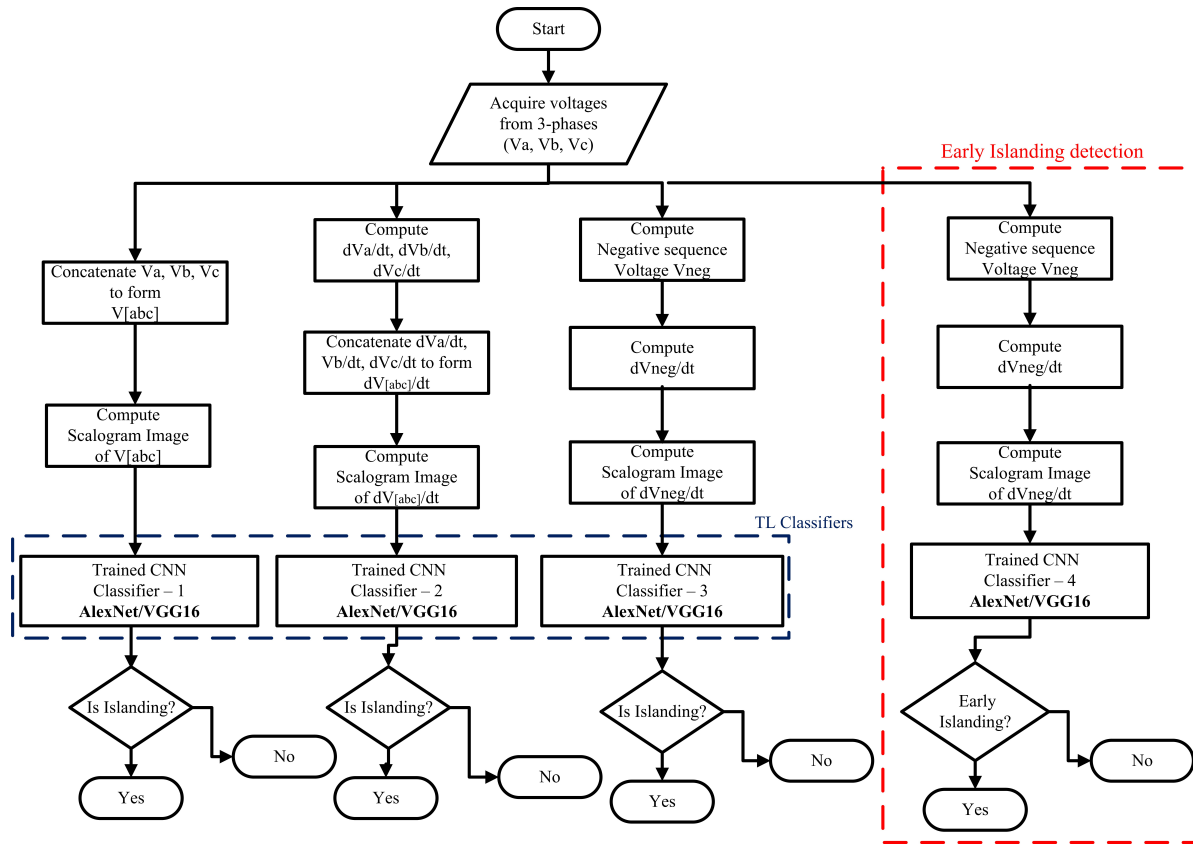


Figure 4.13: Islanding detection method using transfer learning classifiers

classification contest ImageNet Large Scale Visual Recognition Challenge(ILSVRC).

4.4.1 AlexNet

AlexNet is a CNN that was designed to classify images in ImageNet dataset in a thousand different classes. It has won the ILSVRC contest in 2012 with a top-5 error of 15.3%. AlexNet’s architecture was much deeper and larger than the previous nets. It has over 60 million parameters in five convolution layers and 3 fully connected layers. Another important feature in AlexNet was the usage of ReLu non-linearity. It showed that by using ReLu deep networks can be trained more efficiently, as opposed to *tanh* or *sigmoid*. It accepts input images of size 227x227. The architecture of AlexNet is shown in Fig.4.14 (Krizhevsky et al., 2012) and the details are summarized here in Table. 4.1.

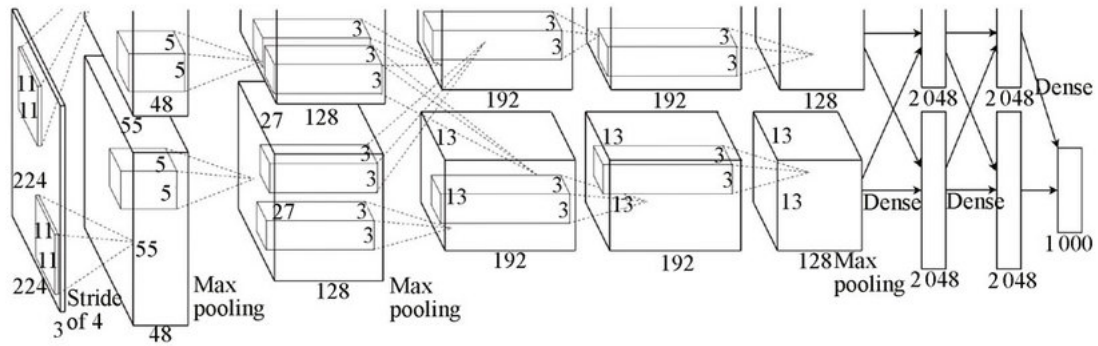


Figure 4.14: AlexNet architecture

Table 4.1: Alexnet architectural details

Layer	Filter size	No. of filters	Stride	Padding
Conv 1_1	11x11x3	96	1	1
MAX POOL1 3x3 filters at stride 2				
Normalization Layer				
Conv 2_1	5x5x3	256	1	2
MAX POOL2 3x3 filters at stride 2				
Normalization Layer				
Conv 3_1	3x3x3	384	1	1
Conv 3_1	3x3x3	384	1	1
Conv 3_1	3x3x3	256	1	1
MAX POOL3 3x3 filters at stride 2				
Fully Connected Layer - 1				
Fully Connected Layer - 2				
Fully Connected Layer - 3				



Figure 4.15: VGG16 architecture

4.4.2 VGG16

VGG16 is a CNN that was designed by Visual Geometry Group at Oxford university to classify images in ImageNet dataset. It was runner up in ILSVRC 2014 with a top-5 error of 7.3%. VGG16 networks architecture was much deeper compared to AlexNet. It has over 138 million parameters in thirteen convolution layers and three fully connected layers. Key outcomes from VGG16 architecture is that a deep network has better visual representation. Also, VGG16 network has used uniform filter sizes throughout the network and the number of filters are increased for each layer. It has also shown that normalization layer doesn't have much effect on the classification accuracy. It accepts input images of size 224x224. The architecture of VGG16 is shown in Fig.4.15 and the details are summarized here in Table.4.2.

Table 4.2: VGG16 architectural details

Layer	Filter size	No. of filters	Stride	Padding
Conv 1_1	3x3x3	64	1	1
Conv 1_1	3x3x3	64	1	1
MAX POOL1 2x2 filters at stride 2				
Conv 2_1	3x3x3	128	1	1
Conv 2_2	3x3x3	128	1	1
MAX POOL2 2x2 filters at stride 2				
Conv 3_1	3x3x3	256	1	1
Conv 3_1	3x3x3	256	1	1
Conv 3_1	3x3x3	256	1	1
MAX POOL3 2x2 filters at stride 2				
Conv 4_1	3x3x3	512	1	1
Conv 4_1	3x3x3	512	1	1
Conv 4_1	3x3x3	512	1	1
MAX POOL4 2x2 filters at stride 2				
Conv 4_1	3x3x3	512	1	1
Conv 4_1	3x3x3	512	1	1
Conv 4_1	3x3x3	512	1	1
MAX POOL5 2x2 filters at stride 2				
Fully Connected Layer - 1				
Fully Connected Layer - 2				
Fully Connected Layer - 3				

4.5 Results and discussion

Both AlexNet and VGG16 nets are first trained with the islanding dataset detailed in Table. 2.2. One instance of each net is used for the parameters considered - $V_{[abc]}$, $V_{[abc]}/dt$, $dV_{[neg]}/dt$ for islanding, and $dV_{[neg]}/dt$ for early islanding detection. The optimized learning rate and momentum values used for training are 0.001 and 0.2 respectively. The training plots of accuracy for all the parameters for both AlexNet and VGG16 are plotted in Fig. 4.16. It can be seen from the plots that the training accuracy for all the parameters has reached the maximum value after 250 iterations.

Once training process is finished the next step is to test both networks with the testing dataset. The testing results are tabulated in Table.4.3.

The results show that AlexNet has good classification accuracy for $V_{[abc]}$, $V_{[abc]}/dt$, and early islanding detection based on $dV_{[neg]}/dt$ with 1, 0, and 15 misclassifications respectively.

The performance was poor for $dV_{[neg]}/dt$ for islanding with 40 misclassifications.

On the other hand VGG16 has shown good performance for $V_{[abc]}$, $V_{[abc]}/dt$, and islanding detection based on $dV_{[neg]}/dt$ with 7, 0, and 4 misclassifications respectively.

The performance for early islanding detection based on $dV_{[neg]}/dt$ was poor with 43 misclassifications.

The performance of transfer learning based IDM is seen to be better than the HOG feature based IDM. This shows that transfer learning based IDM is immune to noisy conditions. However, the performance of TL based IDM still needs to be improved for two parameters. For islanding detection based on $dV_{[neg]}/dt$ the VGG16 architecture has better classification accuracy. But on the other hand, the classification accuracy is low for early islanding detection based on $dV_{[neg]}/dt$.

Similarly, the classification accuracy for islanding detection based on $dV_{[neg]}/dt$ for Alexnet is low, where as accuracy for early islanding detection based on $dV_{[neg]}/dt$ is better.

From the results we can observe that certain architectural features, such as, size of the filters and the depth of the network have influence on the classification accuracy. This is evident from the $dV_{[neg]}/dt$ for islanding and $dV_{[neg]}/dt$ for early islanding detection parameters.

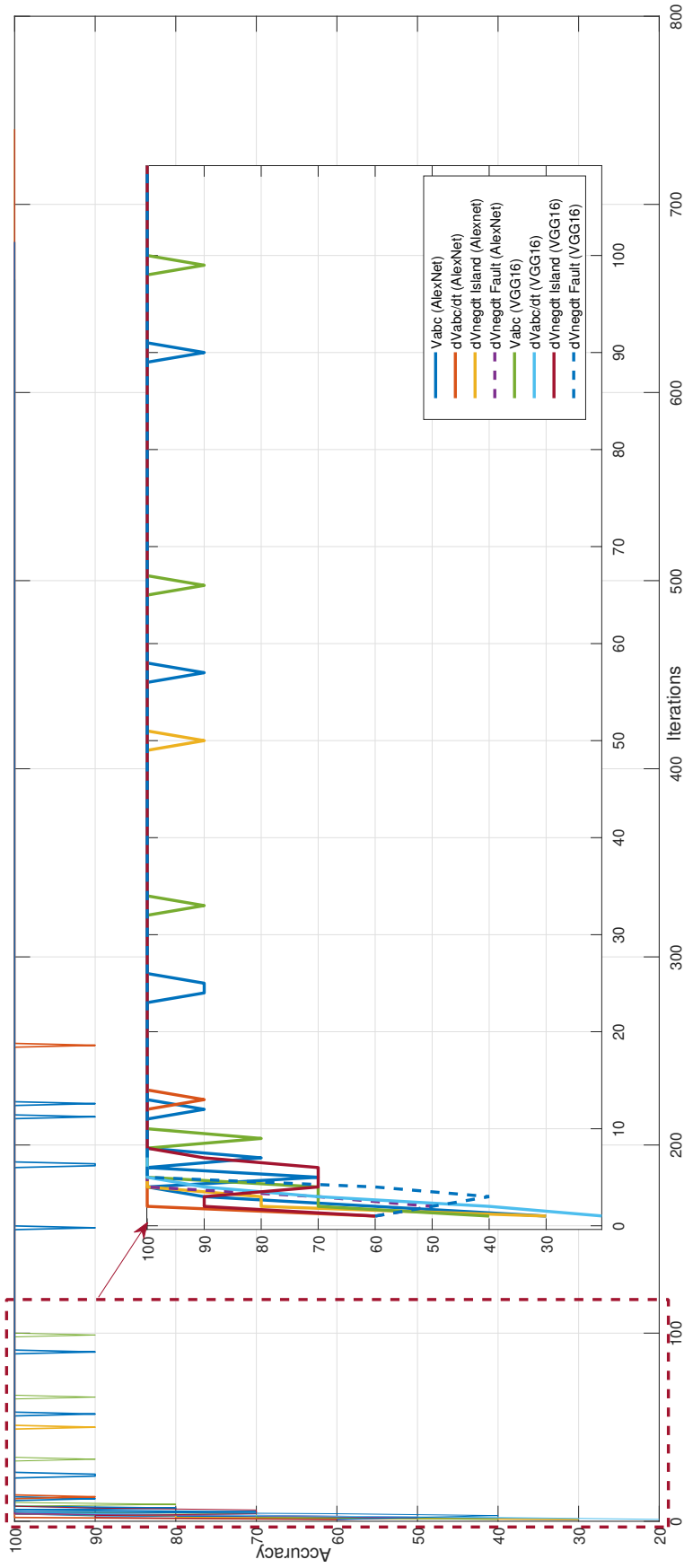


Figure 4.16: Training plots of AlexNet and VGG16 for $V_{[abc]}$, $dV_{[abc]}/dt$, dV_{neg}/dt , and early islanding detection based on dV_{neg}/dt for fault conditions

Table 4.3: Classification results for Transfer Learning

Islanding detection			
Parameter	No. of cases	Accuracy (AlexNet)	Accuracy (VGG16)
$V_{[abc]}$	180	99.44%	96.11 %
$dV_{[abc]}/dt$	180	100% %	100%
dV_{neg}/dt	180	77.77%	97.77%
Early islanding detection			
Parameter	No. of cases	Accuracy (AlexNet)	Accuracy (VGG16)
dV_{neg}/dt	180	91.66%	76.11%

4.6 Summary

An islanding detection method based on transfer learning based technique has been developed. General details of CNN, different layers and their function is briefly presented in this chapter. The definition of transfer learning and the need for transfer learning is discussed. Two pre-trained CNN architectures, AlexNet and VGG16, that have performed well in ILSVRC on ImageNet dataset are chosen for islanding event classification. These two nets are trained on the islanding dataset. The results show that AlexNet has good performance for $V_{[abc]}$, $dV_{[abc]}/dt$, and dV_{neg}/dt for early islanding detection. VGG16 on the other hand has shown better performance for $V_{[abc]}$, $dV_{[abc]}/dt$, and dV_{neg}/dt for islanding detection.

Chapter 5

CUSTOM CONVOLUTION NEURAL NETWORK BASED ISLANDING DETECTION

5.1 Introduction

The results of transfer learning based islanding detection using AlexNet and VGG16 from Chapter.4 show that transfer learning can be used as a potential technique for islanding detection. The performance of TL based IDM was better than HOG feature based IDM. TL based IDM has also shown that it is immune to noisy data.

However, the performance for certain parameters need to be improved. Also, for wider implementation of this method the complexity of the architecture must also be reduced to enhance time, memory and computation efficiency of the CNN. This can be achieved by designing a custom CNN for performing islanding detection. In this chapter the need for custom CNN design and the details of islanding detection method using custom CNN will be presented.

5.2 Proposed CNN based islanding detection method

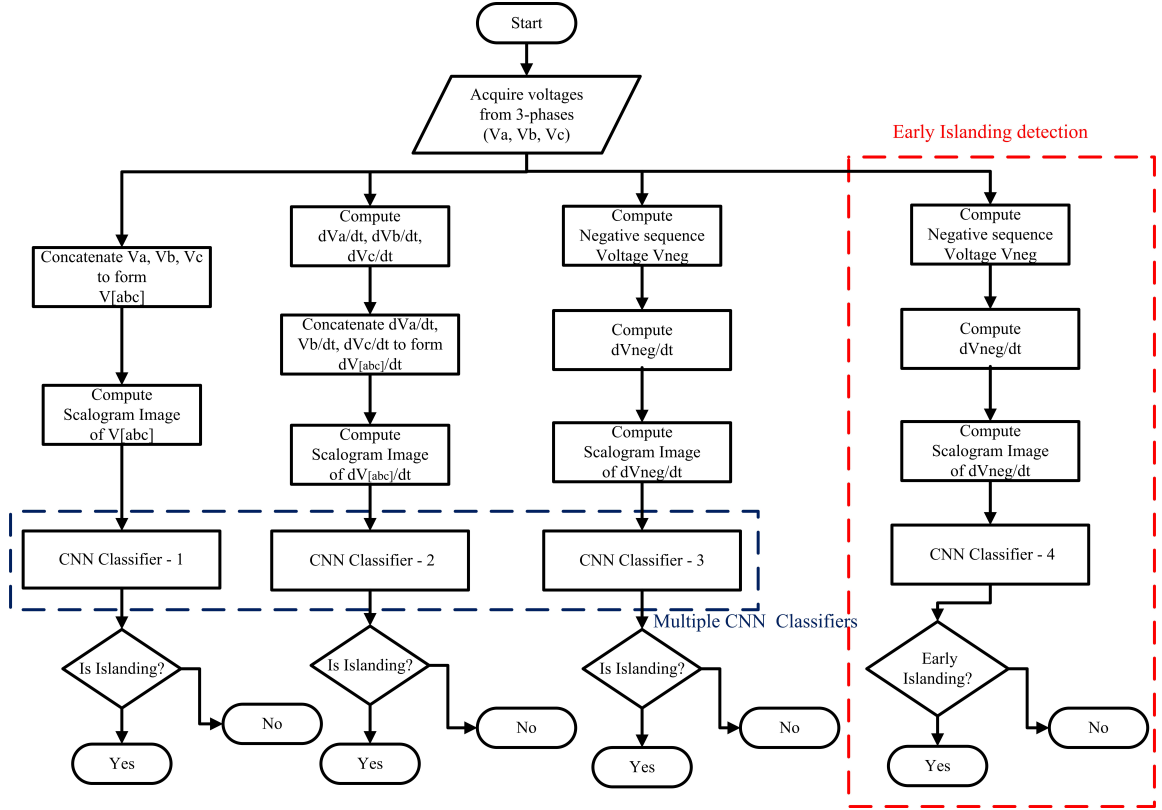


Figure 5.1: Proposed islanding detection method with multiple CNN classifiers

The details of the proposed IDM methodology are presented in this section. The steps involved in the proposed image classification based IDM using multiple CNNs are depicted as a flowchart in Fig. 5.1. The proposed method uses three parameters for islanding detection. Each parameter is computed from the acquired PCC voltages, V_a , V_b , and V_c . The first parameter is voltage. Here once the three phase voltages are acquired from the PCC, they are concatenated to form single time-series data $V_{[abc]}$. This concatenated time-series data is then converted to a scalogram image by applying CWT on $V_{[abc]}$. Concatenation enables us to represent the state of all three phases in one scalogram image. This image is then fed to a trained CNN classifier for detecting an islanding event.

The second parameter that is used in the proposed method is ROCOV dV/dt . The ROCOV is computed for each of the acquired voltages, V_a , V_b , and V_c . The computed values are then concatenated to form a single time series data $dV_{[abc]}/dt$. CWT is

applied on $dV_{[abc]}/dt$ to convert the time-series data to image, which is then fed to a trained CNN classifier for islanding detection.

The third parameter used for islanding detection is ROCONSV dV_{neg}/dt . The negative sequence component of voltage is first calculated from the acquired PCC voltages V_a , V_b , and V_c . In the next step the ROCONSV is computed. This time-series data of dV_{neg}/dt is converted to a scalogram image, which is then given as an input to a trained CNN classifier for detecting islanding event.

In addition to islanding detection, a feature for early islanding detection using ROCONSV is also proposed in this research. An unintentional islanding event is a result of opening of a circuit breaker. One of the primary reasons for the opening of a circuit breaker is a fault in the system. Therefore, by detecting a fault we can detect an islanding event even before its occurrence. A separate data set is created for various fault events and their corresponding changes in dV_{neg}/dt . Also, a CNN is trained on images that represent fault cases and normal cases to enable early islanding detection.

5.3 Results and discussions

In this section the details of the custom designed CNNs for islanding detection, the design philosophy, and the design approach are presented. The details of the designed CNNs and their performance for islanding detection is also presented.

5.3.1 Design of CNN

The design of a CNN involves optimizing several parameters. These parameters include architecture hyperparameters and training hyperparameters. Architecture hyperparameters, such as, number of filters in each layer, number of layers, filter sizes, selection and combination of different layers determine the architecture and layout of various layers. Training hyperparameters include, learning rate, type of solver, momentum, loss function and so on. The input to the CNN is an RGB image of 227x227 size. The design approach followed in the proposed method is discussed as follows.

The architecture of the CNN, meaning, number of layers and the filter size required for achieving good performance is first designed. This is done by fixing all training hyperparameters and test the CNN by increasing the number of layers, starting from

a single layer. Each layer consists of a convolution layer, a rectified linear unit, and a max pooling layer. Final layer is a fully connected layer with two class output combined with a softmax layer. The final layer is decided based on the number of classes that the data set is divided into. In this case the data is divided into two classes, namely, islanded and grid connected. This process is repeated for different filter sizes.

The design philosophy followed to determine the optimal architecture for the CNN is derived from the design principles of VGG16 network(Simonyan and Zisserman, 2014). Therefore the size of the filters have been kept small and uniform throughout the CNN layers. As evident from the results shown in Fig. 5.2.(a), the number of layers is fixed at three, since it is shown to give better performance for all the filter sizes.

In the next step, the training hyperparameters, learning rate and momentum are optimized by fixing the number of layers. The results from the plots in Fig. 5.2.(a) and Fig. 5.2.(b) indicate that the filter size of 3x3 gives better performance.

From Fig.5.3.(a) and Fig.5.3.(b) it can be seen that the performance of the CNN is better for learning rate value of 0.001 and momentum value of 0.2. Stochastic gradient descent with momentum(sgdm) solver has been used in the training process.

The final design values for architecture of CNN-I and training hyperparameters are tabulated in Table 5.1 and Table 5.2, respectively. This architecture is used for $V_{[abc]}$, $dV_{[abc]}/dt$, and for early detection based on dV_{neg}/dt .

For islanding detection using dV_{neg}/dt , the design approach of CNN-I, which is based on VGG16 design philosophy was resulting in a very deep architecture similar to VGG16. This was resulting in a large network and huge number of parameters. To reduce the complexity of the network another CNN is designed with a different design approach. The design philosophy of CNN-II for islanding detection based on dV_{neg}/dt is to use multiple convolution layers with gradually increasing filter sizes. The number of filters is also increased as we progress into the network. The final design values of architecture of CNN-II and training hyperparameters are tabulated in Table 5.3 and Table 5.4, respectively.

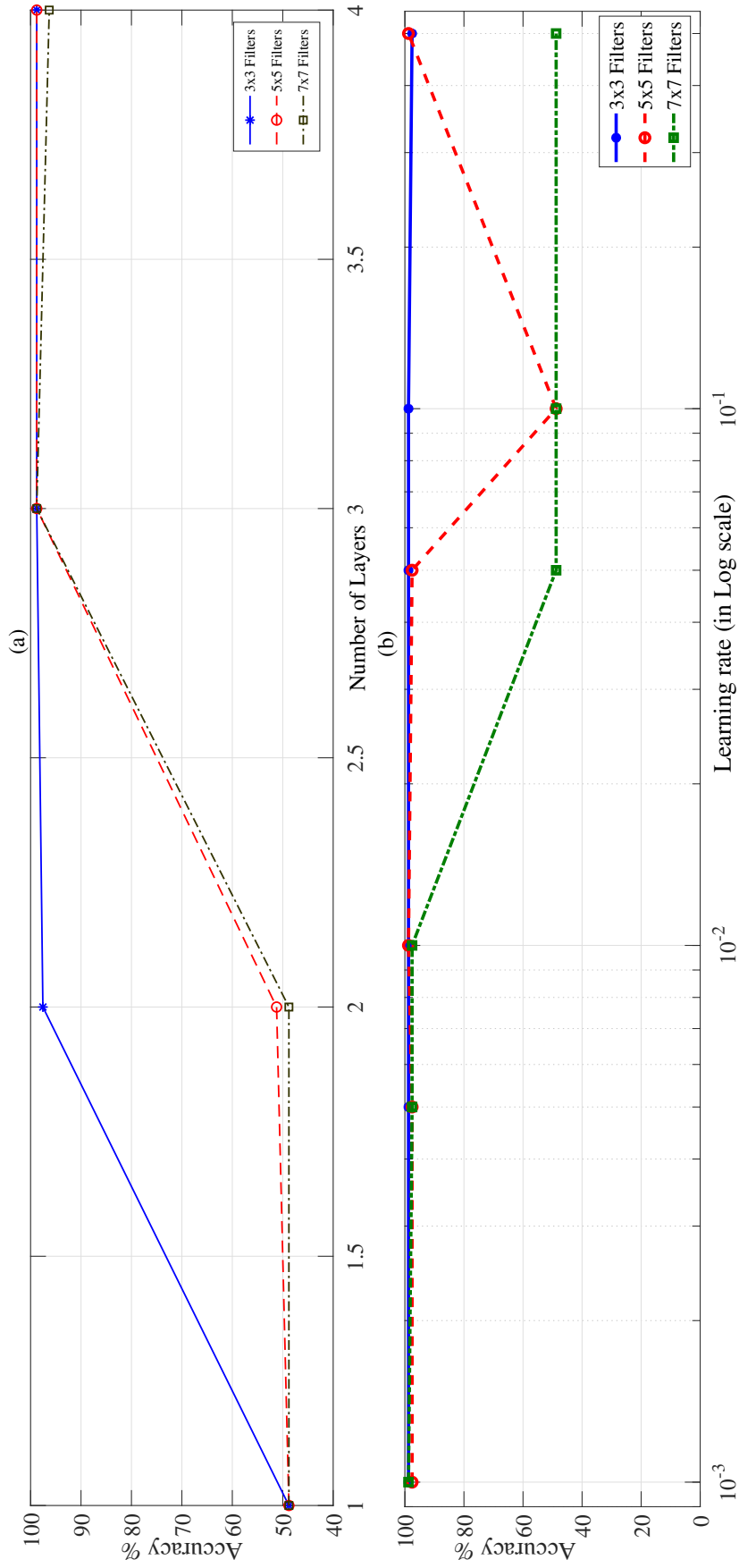


Figure 5.2: Results for CNN training (a) Plots of training accuracy for all CNNs (b) Plots of training loss for all CNNs

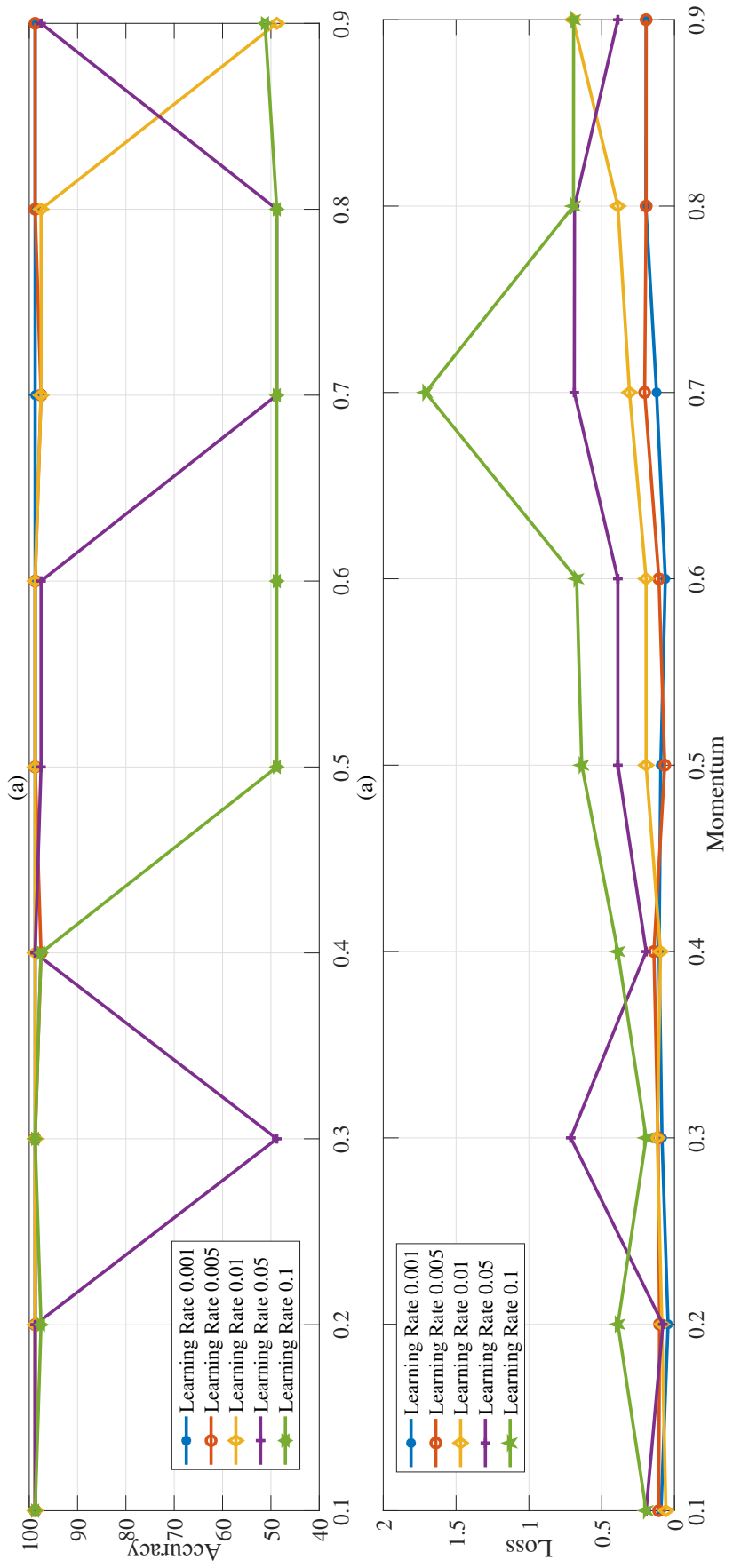


Figure 5.3: Results for CNN training (a) Plots of training accuracy for all CNNs (b) Plots of training loss for all CNNs

Table 5.1: Custom designed CNN-I architectural details

Layer	Filter size	No. of filters	Stride	Padding
Conv 1_1	3x3x3	8	1	1
ReLU Layer				
MAX POOL1 2x2 filters at stride 1				
Conv 2_1	3x3x3	16	1	1
ReLU Layer				
MAX POOL1 2x2 filters at stride 1				
Conv 3_1	3x3x3	32	1	1
ReLU Layer				
MAX POOL1 2x2 filters at stride 1				
Fully Connected Layer – SoftMax				

Table 5.2: CNN-I training hyperparameter details

Training Hyperparameter	Design Value
Solver	Stochastic Gradient Descent with Momentum (sgdm)
Learning rate	0.001
Momentum	0.2
Mini-batch size	20
Maximum epochs	10
Weight initialization	random
Loss function	Cross entropy

Table 5.3: Custom designed CNN-II architectural details

Layer	Filter size	No. of filters	Stride	Padding
Conv 1_1	3x3x3	16	1	1
ReLU Layer				
MAX POOL1 2x2 filters at stride 2				
Conv 2_1	5x5x3	32	1	2
ReLU Layer				
MAX POOL1 2x2 filters at stride 2				
Conv 3_1	7x7x3	64	1	3
ReLU Layer				
MAX POOL1 2x2 filters at stride 2				
Fully Connected Layer – SoftMax				

Table 5.4: CNN-II training hyperparameter details

Training Hyperparameter	Design Value
Solver	Stochastic Gradient Descent with Momentum (sgdm)
Learning rate	0.001
Momentum	0.2
Mini-batch size	30
Maximum epochs	10
Weight initialization	random
Loss function	Cross entropy

5.3.2 Custom CNN based IDM results

Once the CNN is designed, the next step is to train the CNN to perform islanding detection. Training CNN is an iterative process until desired performance is achieved. Training process is monitored by looking at the training accuracy and training loss. We have a total of three parameters used for islanding detection and one parameter for early islanding detection. The CNN-I architecture is used for islanding detection using $V_{[abc]}$, $dV_{[abc]}/dt$, and for early detection based on dV_{neg}/dt . The CNN-II architecture is used for islanding detection based on dV_{neg}/dt . The training plots for these are depicted in Fig.5.4. (a) and Fig.5.4.(b). Training process is monitored by looking at the training accuracy and training loss. The significance of monitoring both these parameters can be seen from these plots where the training accuracy has reached maximum value, yet the training loss is not minimized. Once the loss is minimized the trained CNN is used for classifying islanding events. The islanding event classification results for CNN-I and CNN-II are tabulated in Table 5.5. The results show that the performance of custom designed CNNs have a performance that is better than HOG feature based islanding and transfer learning based islanding detection. For islanding detection based on $V_{[abc]}$, $dV_{[abc]}/dt$ and early islanding detection with dV_{neg}/dt , the classification accuracy on the testing dataset is 100%. For islanding detection based on dV_{neg}/dt the classification accuracy is 99.44%. The average detection time for the proposed islanding detection method is 218ms.

Table 5.5: Classification results for custom CNN based IDM

Islanding detection		
Parameter	No. of cases	Accuracy
$V_{[abc]}$	180	100% (CNN-I)
$dV_{[abc]}/dt$	180	100% (CNN-I)
dV_{neg}/dt	180	99.44% (CNN-II)
Early islanding detection		
Parameter	No. of cases	Accuracy
dV_{neg}/dt	180	100% (CNN-I)

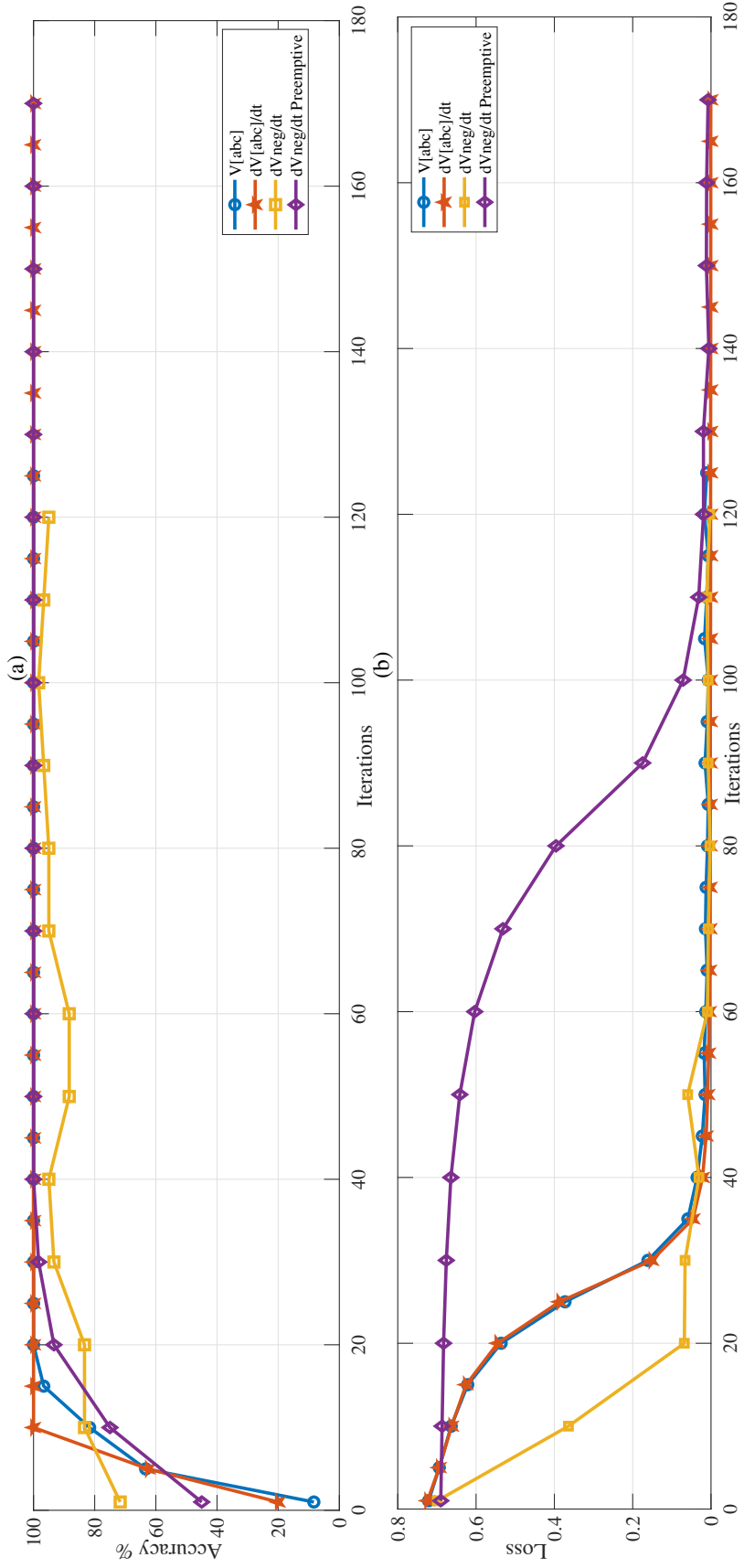


Figure 5.4: Results for CNN training (a) Plots of training accuracy for all CNNs (b) Plots of training loss for all CNNs

The advantage of having custom designed CNN for islanding event classification over transfer learning based method can be explained in terms of CNN complexity, number of parameters to be tuned, memory requirements and the time taken for training. The number of parameters and the memory requirements are computed and tabulated in Table 5.6 and Table 5.7.

These parameters can be calculated using the following equations. If the Conv layer accepts an input volume of width W_1 , height H_1 and depth D_1

$W_1 \times H_1 \times D_1$

and the hyperparameters are:

filter size: $F \times F$

number of filters: K

stride: S

padding: P

This produces an output volume of $W_2 \times H_2 \times D_2$, where

$$W_2 = (W_1 - F + 2P)/S + 1 \quad (5.1)$$

and

$$H_2 = (H_1 - F + 2P)/S + 1 \quad (5.2)$$

and

$$D_2 = K \quad (5.3)$$

The parameters for each Conv layer generated will be

$$Parameters = (F.F.D_1).K \quad (5.4)$$

and K biases.

These are computed for both CNN-I and CNN-II architectures and tabulated in Table 5.6 and Table 5.7, respectively.

The comparison of transfer learning based islanding event classification and custom CNN based islanding can now be made based on these computations. The parameters chosen for computation are number of layers, number of filters, parameters, classification accuracy, training time, number of filters, and the memory requirement for each of the nets. The comparison is made between AlexNet, VGG16, CNN-I and CNN-II architectures.

Table 5.6: Activation maps and parameters in CNN-I

Layer	Type	Activations	Parameters
Input: 227x227x3	Image input	227x227x3	–
Conv 1_1	Convolution		
FxF:3x3, K:8			Weights: 3x3x3x8
S=1, P=1		227x227x8	Bias: 1x1x8
ReLU 1_1	Re Lu	227x227x8	–
MAX POOL 1_1	Pooling		
2x2 with S=1		226x226x8	–
Conv 2_1	Convolution		
FxF:3x3, K:16			Weights: 3x3x8x16
S=1, P=1		226x226x16	Bias: 1x1x16
ReLU 2_1	Re Lu	226x226x16	–
MAX POOL 2_1	Pooling		
2x2 with S=1		225x225x16	–
Conv 3_1	Convolution		
FxF:3x3, K:32			Weights: 3x3x16x32
S=1, P=1		225x225x32	Bias: 1x1x32
ReLU 3_1	Re Lu	225x225x32	–
MAX POOL 3_1	Pooling		
2x2 with S=1		224x224x32	–
Fully Connected	FC	1x1x2	Weights:2x1605632 Bias:2x1
SoftMax		1x1x2	–

Table 5.7: Activation maps and parameters in CNN-II

Layer	Type	Activations	Parameters
Input: 227x227x3	Image input	227x227x3	–
Conv 1_1	Convolution		
FxF:3x3, K:16			Weights: 3x3x3x16
S=1, P=1		227x227x16	Bias: 1x1x16
ReLU 1_1	Re Lu	227x227x16	–
MAX POOL 1_1	Pooling		
2x2 with S=2		113x113x16	–
Conv 2_1	Convolution		
FxF:5x5, K:32			Weights: 5x5x16x32
S=1, P=2		113x113x32	Bias: 1x1x32
ReLU 2_1	Re Lu	113x113x32	–
MAX POOL 2_1	Pooling		
2x2 with S=2		56x56x32	–
Conv 3_1	Convolution		
FxF:7x7, K:64			Weights: 7x7x32x64
S=1, P=3		56x56x64	Bias: 1x1x64
ReLU 3_1	Re Lu	56x56x64	–
MAX POOL 3_1	Pooling		
2x2 with S=2		28x28x64	–
Fully Connected	FC	1x1x2	Weights:2x50176 Bias:2x1
SoftMax		1x1x2	–

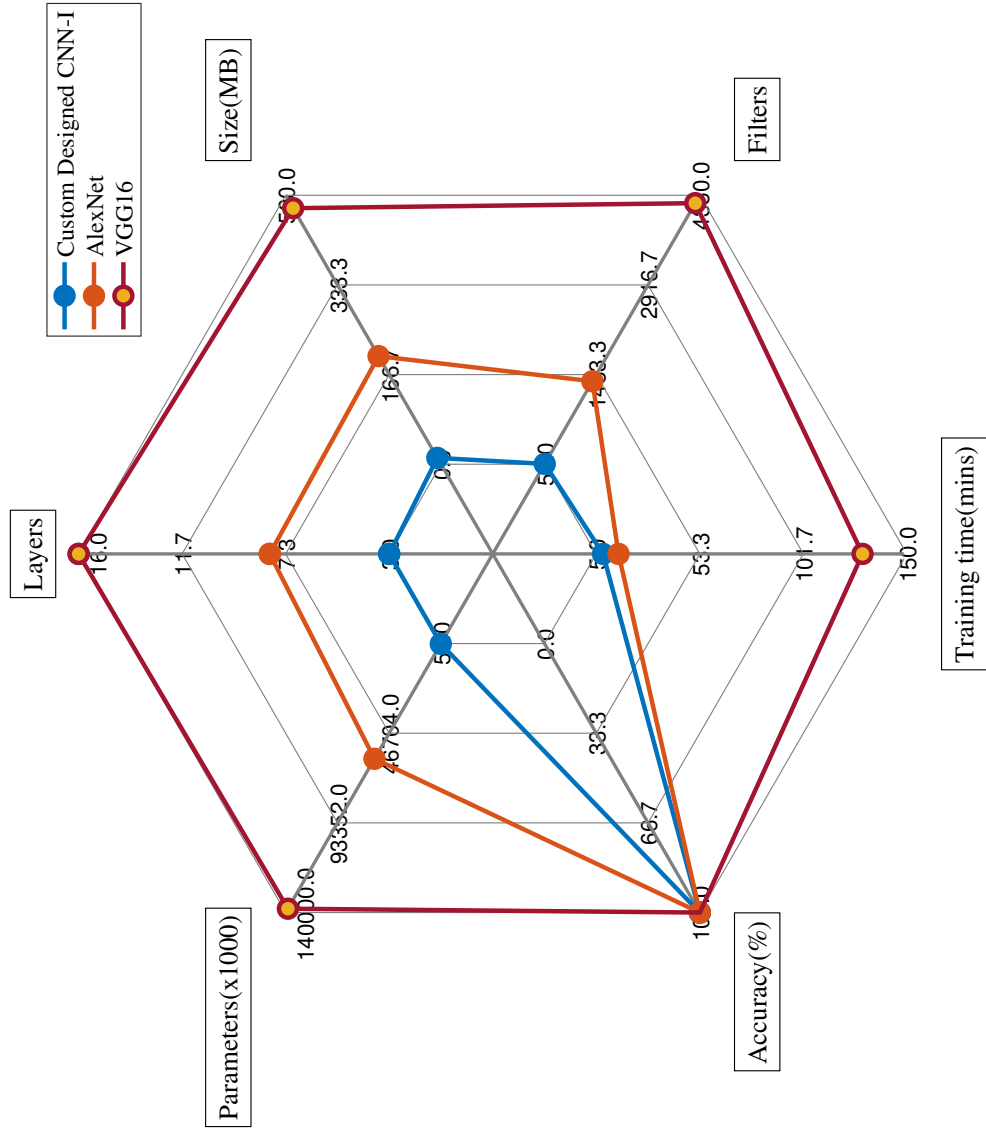


Figure 5.5: Plots comparing different aspects of AlexNet, VGG16 and custom designed architecture CNN-I

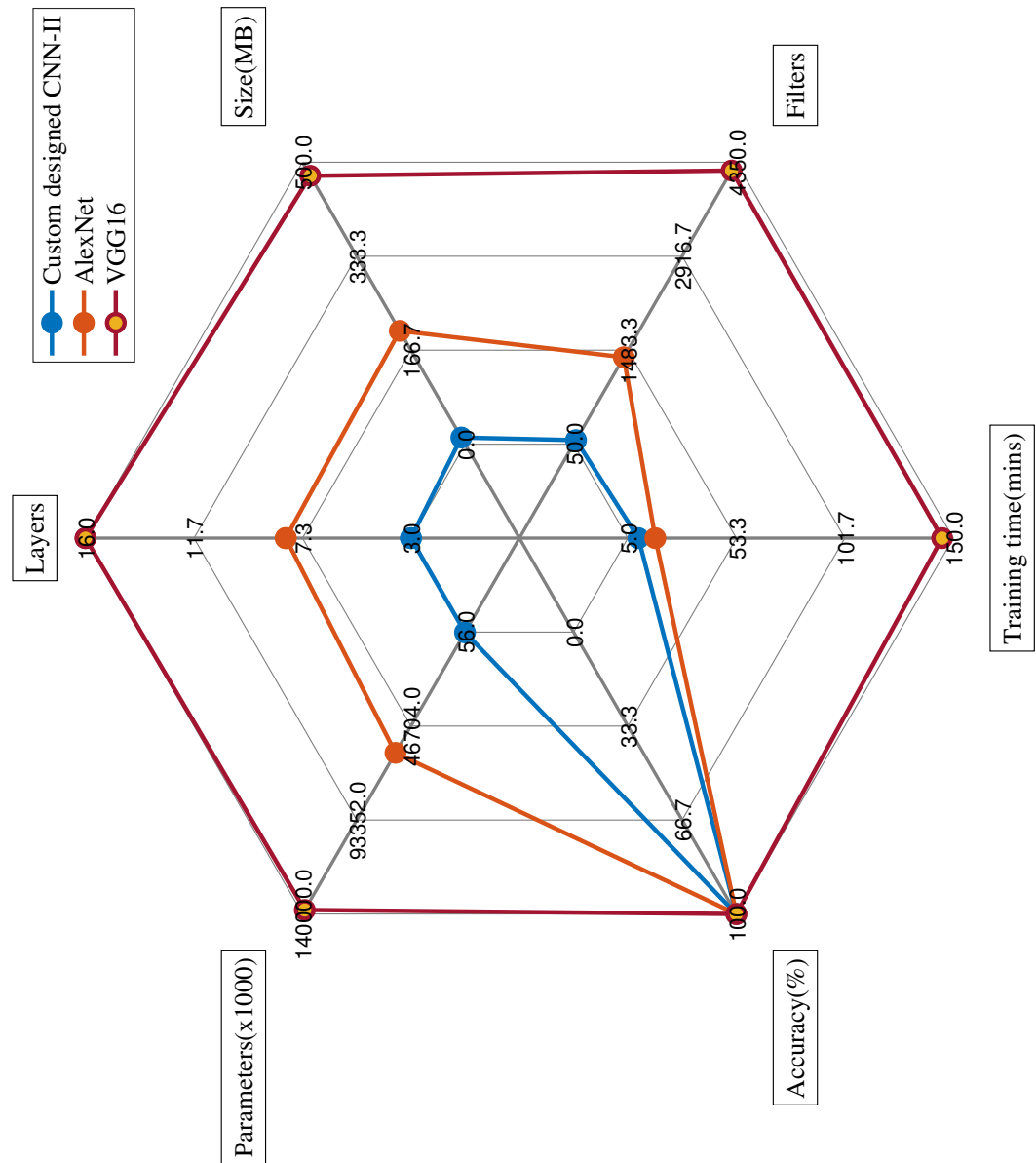


Figure 5.6: Plots comparing different aspects of AlexNet, VGG16 and custom designed architecture CNN-II

The number of parameters in AlexNet (Krizhevsky et al., 2012) and VGG16 (Simonyan and Zisserman, 2014) is 60 and 140 million parameters, respectively. AlexNet has five convolution layers and three fully connected layers where are VGG16 has thirteen convolution layers and three fully connected layers. Total number of filters in AlexNet is 1376 and VGG16 is 4224. The average training time taken for these networks on islanding dataset is 17.24 minutes and 145.03 minutes respectively.

On the other hand, CNN-I and CNN-II architecture has 3.2 million parameters and 214×10^3 parameters. This is a considerable reduction in the number of parameters. In terms of number of filters, CNN-I has 56 filters and CNN-II has 112 filters. Both CNN-I and CNN-II have three convolution layers and one fully connected layer. The average training time for CNN-I and CNN-II are 9.7 minutes and 8.16 minutes, respectively.

The comparison of AlexNet, VGG16, and CNN-I architectures is shown in Fig. 5.5, and the comparison of AlexNet, VGG16, and CNN-II architectures is shown in Fig.5.6. It can be seen that custom designed CNN architectures have reduced complexity when compared to transfer learning models.

5.4 Summary

In this chapter the need for custom designed CNN architectures as opposed to transfer leaning based models is first explained. In order to reduce the complexity of the network two custom CNN architectures are designed. The design approach followed is detailed. Two CNN architectures, CNN-I and CNN-II are designed. It is observed that CNN-I architecture has good performance for $V_{[abc]}$, $dV_{[abc]}/dt$ and early islanding detection with dV_{neg}/dt . However, the complexity of the network was increasing significantly for islanding detection based on dV_{neg}/dt . To overcome this CNN-II architecture is proposed. The classification results of custom CNN based IDM are better than HOG feature based IDM and comparable with transfer learning based IDM at nearo zero power mismatch ans also noisy conditions. Contrary to transfer learning based IDM it has been shown that the complexity of the network has greatly reduced in custom CNNs in terms of number of layers, number of filters, parameters, memory occupied on the system, and training time. This shows that custom CNN based IDM has better performance in terms of classification accuracy, immunity to noise, and has reduced network complexity.

Chapter 6

CONCLUSIONS AND FUTURE SCOPE

6.1 Conclusions

For effective islanding detection at near zero power mismatch and noisy conditions three islanding detection methods are developed using image classification based methods with SVM classifier and CNN classifier. Furthermore, in this thesis, an early islanding detection feature based on monitoring the rate of change of negative sequence voltage under fault and normal conditions is also developed. The conclusive remarks of the contributions in this thesis are presented below.

Chapter 1 presents the background of the thesis, islanding phenomenon in a microgrid and the need for detecting islanding events. Various international standards for islanding detection are summarized. The state-of-the-art literature related islanding detection methods along with the evolution of IDMs is discussed in detail. The need for intelligent IDMs that can perform better detection at near zero power mismatch and noisy conditions are highlighted. The contributions of the thesis are also outlined.

Chapter 2 presents the need for dataset in supervised learning methods. The process of converting any time-series data to images is first presented. The details of the system used for dataset generation, different parameters used for detecting islanding, and various events that are considered for generating the dataset are presented. Also, a feature for early islanding detection by monitoring the fault and normal conditions

is also presented.

In chapter 3, an islanding detection method based on feature extraction from images and SVM classifier is presented. The importance of feature extraction from the images is detailed. Histogram of oriented gradients features are explained. The optimal parameters for HOG feature extraction, training and testing of SVM classifier on islanding image dataset is presented. The performance of HOG based IDM and the need for other feature extraction methods is discussed.

In chapter 4, improved feature extraction by using CNNs is presented. In this chapter brief introduction about the workings of a CNN are discussed. To minimize the design and testing time, pre-trained CNNs are used for islanding detection by applying transfer learning technique. Two CNN architectures that have performed well in ImageNet challenge are used for transfer learning. The performance of AlexNet and VGG16 for islanding dataset is discussed and compared with HOG based IDM. Lastly, the need for designing custom CNN is presented.

Chapter 5 presents a custom CNN based islanding detection method. The design approach for two CNN architectures is detailed. The architectures of two CNNs is discussed along with the training and testing. The final architectures of two CNNs are presented as CNN-I and CNN-II. The performance of CNN based IDM is compared with transfer learning based IDM. Further, it is also discussed how custom CNN based IDM has reduced the network complexity in terms of layers, number of filters, parameters, size occupied on the system, and the training time. Lastly, it has been concluded that in comparison to HOG based IDM and transfer learning based IDM, custom CNN based IDM has better performance at near zero power mismatch and noisy conditions with respect to HOG based IDM and has reduced complexity with respect to transfer learning based IDM.

6.2 Future scope

Based on the research carried out in this thesis, the recommendations for future research are presented.

1. Image classification based islanding detection can be further improved by monitoring other parameters. By monitoring more parameters, the effectiveness of the islanding detection method may be improved.

2. More studies on early islanding detection by monitoring fault and normal conditions can be carried out. Statistical methods can be applied to come up with better indices that can be used for early islanding detection with enhanced effectiveness.
3. For any machine learning or deep learning model a larger dataset can result in better learning of the features and better classification accuracies. Therefore, a larger dataset with more number of parameters can be created.

Also, there is no standard dataset or a standard system for testing islanding detection methods. This can be used as an opportunity to create a standard system or a standard dataset in the lines of ImageNet for image classification research.

4. For enhanced classification accuracy ensemble machine learning/deep learning models can be used.
5. In addition to islanding detection, image classification based approach can be applied to other applications such as power quality event classification and power system fault classification.

Appendix A

Image noise

In the process of data augmentation, two types of noises have been added to the image dataset.

- **Salt and pepper noise**

Salt and pepper noise manifests itself as sparsely occurring black and white pixels. In this type of noise, we can control the density of noise. Meaning, we can specify the percentage of pixels that will be affected. Noise density used for augmenting the dataset is 5%.

- **Speckle noise**

Speckle noise is a multiplicative noise which is represented by the equation

$$J = I + n * I$$

Here,

' I ' represents pixels of the image and

' n ' is a uniformly distributed random noise with zero mean and a variance of 0.05.

The variance can be changed as per the requirement.

Bibliography

- 1547.2-2008 (2008). IEEE standard for interconnecting distributed resources with electric power systems. *IEEE*, 1547.2:2008–2009.
- Adari, S. and Bhalja, B. R. (2016). Islanding detection of distributed generation using random forest technique. In *Power Systems (ICPS), 2016 IEEE 6th International Conference on*, pages 1–6. IEEE.
- Aguiar, C. R., Bastos, R. F., Neves, R. V. A., Reis, G. B., and Machado, R. Q. (2013). Fuzzy positive feedback for islanding mode detection in distributed generation. In *2013 IEEE Power Energy Society General Meeting*, pages 1–5.
- Ahmad, K. N. E. K., Selvaraj, J., and Rahim, N. A. (2013). A review of the islanding detection methods in grid-connected pv inverters. *Renewable and Sustainable Energy Reviews*, 21:756–766.
- Alam, M. R., Muttaqi, K. M., and Bouzerdoum, A. (2014). A multifeature-based approach for islanding detection of dg in the subcritical region of vector surge relays. *IEEE Transactions on Power Delivery*, 29(5):2349–2358.
- Balamurugan, K., Srinivasan, D., and Reindl, T. (2012). Impact of distributed generation on power distribution systems. *Energy Procedia*, 25:93 – 100. PV Asia Pacific Conference 2011.
- Biswal, B., Dash, P. K., and Panigrahi, B. K. (2009). Non-stationary power signal processing for pattern recognition using hs-transform. *Applied Soft Computing*, 9(1):107–117.
- Caudill, M. (1987). Neural networks primer, part I. *AI expert*, 2(12):46–52.

- Chang, W.-Y. (2010). A hybrid islanding detection method for distributed synchronous generators. In *Power Electronics Conference (IPEC), 2010 International*, pages 1326–1330. IEEE.
- Chiang, W.-J., Jou, H.-L., and Wu, J.-C. (2012). Active islanding detection method for inverter-based distribution generation power system. *International Journal of Electrical Power & Energy Systems*, 42(1):158–166.
- Cortes, C. and Vapnik, V. (1995). Support-vector networks. *Machine learning*, 20(3):273–297.
- Dalal, N. and Triggs, B. (2005). Histograms of oriented gradients for human detection.
- Darabi, A., Moeini, A., and Karimi, M. (2010). Distributed generation intelligent islanding detection using governor signal clustering. In *Power Engineering and Optimization Conference (PEOCO), 2010 4th International*, pages 345–351. IEEE.
- Dash, P., Panigrahi, B., and Panda, G. (2003a). Power quality analysis using S-transform. *IEEE transactions on power delivery*, 18(2):406–411.
- Dash, P. K., Panigrahi, B. K., Sahoo, D. K., and Panda, G. (2003b). Power quality disturbance data compression, detection, and classification using integrated spline wavelet and S-transform. *IEEE Transactions on Power Delivery*, 18(2):595–600.
- Daubechies, I. (1990). The wavelet transform, time-frequency localization and signal analysis. *IEEE Transactions on Information Theory*, 36(5):961–1005.
- De Mango, F., Liserre, M., Dell’Aquila, A., and Pigazo, A. (2006). Overview of anti-islanding algorithms for pv systems. part i: Passive methods. In *Power Electronics and Motion Control Conference, 2006. EPE-PEMC 2006. 12th International*, pages 1878–1883. IEEE.
- Deng, J., Dong, W., Socher, R., Li, L.-J., Li, K., and Fei-Fei, L. (2009). Imagenet: A large-scale hierarchical image database. In *2009 IEEE conference on computer vision and pattern recognition*, pages 248–255. Ieee.
- Donnelly, D. (2006). The fast fourier and Hilbert-Huang transforms: a comparison. In *Computational Engineering in Systems Applications, IMACS Multiconference on*, volume 1, pages 84–88. IEEE.

- El-Arroudi, K., Joos, G., Kamwa, I., and McGillis, D. T. (2007). Intelligent-based approach to islanding detection in distributed generation. *IEEE transactions on power delivery*, 22(2):828–835.
- Faqhrudin, O. N., El-Saadany, E., and Zeineldin, H. (2012). Naïve bayesian islanding detection technique for distributed generation in modern distribution system. In *Electrical Power and Energy Conference (EPEC), 2012 IEEE*, pages 69–74. IEEE.
- Faqhrudin, O. N., El-Saadany, E. F., and Zeineldin, H. H. (2014). A universal islanding detection technique for distributed generation using pattern recognition. *IEEE Transactions on Smart Grid*, 5(4):1985–1992.
- Farhan, M. A. and Swarup, K. S. (2016). Mathematical morphology-based islanding detection for distributed generation. *IET Generation, Transmission & Distribution*, 10(2):518–525.
- Fayyad, Y. and Osman, A. (2010). Neuro-wavelet based islanding detection technique. In *Electric Power and Energy Conference (EPEC), 2010 IEEE*, pages 1–6. IEEE.
- Freitas, W., Xu, W., Affonso, C. M., and Huang, Z. (2005). Comparative analysis between rocof and vector surge relays for distributed generation applications. *IEEE Transactions on power delivery*, 20(2):1315–1324.
- Gautam, S. and Brahma, S. M. (2009). Overview of mathematical morphology in power systems—A tutorial approach. In *2009 IEEE Power & Energy Society General Meeting*, pages 1–7. IEEE.
- Giroux, P., Sybille, G., Osorio, C., and Chandrachood, S. (2012). 100-kw grid-connected pv array demo detailed model. *MathWorks File Exchange*.
- Graps, A. (1995). An introduction to wavelets. *IEEE computational science and engineering*, 2(2):50–61.
- Gu, Y. H. and Bollen, M. H. (2000). Time-frequency and time-scale domain analysis of voltage disturbances. *IEEE Transactions on Power Delivery*, 15(4):1279–1284.
- Hanif, M., Basu, M., and Gaughan, K. (2012). Development of EN50438 compliant wavelet-based islanding detection technique for three-phase static distributed generation systems. *IET renewable power generation*, 6(4):289–301.

- Hanif, M., Dwivedi, U., Basu, M., and Gaughan, K. (2010). Wavelet based islanding detection of DC-AC inverter interfaced DG systems. In *Universities Power Engineering Conference (UPEC), 2010 45th International*, pages 1–5. IEEE.
- Heidari, M., Seifossadat, G., and Razaz, M. (2013). Application of decision tree and discrete wavelet transform for an optimized intelligent-based islanding detection method in distributed systems with distributed generations. *Renewable and Sustainable Energy Reviews*, 27:525–532.
- Hsieh, C.-T., Lin, J.-M., and Huang, S.-J. (2008). Enhancement of islanding-detection of distributed generation systems via wavelet transform-based approaches. *International Journal of Electrical Power & Energy Systems*, 30(10):575–580.
- Huang, N., Xu, D., and Liu, X. (2010). Power quality disturbances recognition based on HS-transform. In *Pervasive Computing Signal Processing and Applications (PCSPA), 2010 First International Conference on*, pages 311–314. IEEE.
- Huang, N. E., Shen, Z., Long, S. R., Wu, M. C., Shih, H. H., Zheng, Q., Yen, N.-C., Tung, C. C., and Liu, H. H. (1998). The empirical mode decomposition and the Hilbert spectrum for nonlinear and non-stationary time series analysis. In *Proceedings of the Royal Society of London A: Mathematical, Physical and Engineering Sciences*, volume 454, pages 903–995. The Royal Society.
- Jang, S.-I. and Kim, K.-H. (2004). An islanding detection method for distributed generations using voltage unbalance and total harmonic distortion of current. *IEEE transactions on power delivery*, 19(2):745–752.
- Jou, H.-L., Chiang, W.-J., and Wu, J.-C. (2007). Virtual inductor-based islanding detection method for grid-connected power inverter of distributed power generation system. *IET Renewable Power Generation*, 1(3):175–181.
- Kantardzic, M. (2011). *Data mining: concepts, models, methods, and algorithms*. John Wiley & Sons.
- Karegar, H. K. and Sobhani, B. (2012). Wavelet transform method for islanding detection of wind turbines. *Renewable Energy*, 38(1):94–106.

- Karimi, H., Yazdani, A., and Iravani, R. (2008). Negative-sequence current injection for fast islanding detection of a distributed resource unit. *IEEE Transactions on power electronics*, 23(1):298–307.
- Karimi, M., Mokhtari, H., and Iravani, M. R. (2000). Wavelet based on-line disturbance detection for power quality applications. *IEEE Transactions on Power Delivery*, 15(4):1212–1220.
- Kasztenny, B. and Rostron, J. (2018). Circuit breaker ratings—a primer for protection engineers. In *2018 71st Annual Conference for Protective Relay Engineers (CPRE)*, pages 1–13. IEEE.
- Khamis, A., Shareef, H., and Mohamed, A. (2015). Islanding detection and load shedding scheme for radial distribution systems integrated with dispersed generations. *IET Generation, Transmission & Distribution*, 9(15):2261–2275.
- Khamis, A., Shareef, H., and Wanik, M. (2012). Pattern recognition of islanding detection using TT-transform. *Journal of Asian Scientific Research*, 2(11):607–13.
- Kim, I.-S. (2012). Islanding detection technique using grid-harmonic parameters in the photovoltaic system. *Energy Procedia*, 14:137–141.
- Kim, J.-H., Kim, J.-G., Ji, Y.-H., Jung, Y.-C., and Won, C.-Y. (2011). An islanding detection method for a grid-connected system based on the goertzel algorithm. *IEEE Transactions on Power Electronics*, 26(4):1049–1055.
- Krizhevsky, A., Sutskever, I., and Hinton, G. E. (2012). Imagenet classification with deep convolutional neural networks. In *Advances in neural information processing systems*, pages 1097–1105.
- Kumarswamy, I., Sandipamu, T. K., and Prasanth, V. (2013). Analysis of islanding detection in distributed generation using fuzzy logic technique. In *2013 7th Asia Modelling Symposium*, pages 3–7.
- Kunte, R. S. and Gao, W. (2008). Comparison and review of islanding detection techniques for distributed energy resources. In *2008 40th North American Power Symposium*, pages 1–8.

- LeCun, Y. (1998). The mnist database of handwritten digits. <http://yann.lecun.com/exdb/mnist/>.
- Lee, L. and Girgis, A. (1988). Application of DFT and FFT algorithms to spectral analysis of power system load variation. In *System Theory, 1988., Proceedings of the Twentieth Southeastern Symposium on*, pages 26–29. IEEE.
- Li, C., Cao, C., Cao, Y., Kuang, Y., Zeng, L., and Fang, B. (2014). A review of islanding detection methods for microgrid. *Renewable and Sustainable Energy Reviews*, 35:211–220.
- Li, G., Zhou, M., Luo, Y., and Ni, Y. (2005). Power quality disturbance detection based on mathematical morphology and fractal technique. In *2005 IEEE/PES Transmission & Distribution Conference & Exposition: Asia and Pacific*, pages 1–6. IEEE.
- Lidula, N., Perera, N., and Rajapakse, A. (2009). Investigation of a fast islanding detection methodology using transient signals. In *Power & Energy Society General Meeting, 2009. PES'09. IEEE*, pages 1–6. IEEE.
- Lidula, N. W. A. and Rajapakse, A. D. (2011). Microgrids research: A review of experimental microgrids and test systems. *Renewable and Sustainable Energy Reviews*, 15(1):186–202.
- Lin, F.-J., Tan, K.-H., and Chiu, J.-H. (2012). Active islanding detection method using wavelet fuzzy neural network. In *Fuzzy Systems (FUZZ-IEEE), 2012 IEEE International Conference on*, pages 1–8. IEEE.
- Liu, F., Kang, Y., Zhang, Y., Duan, S., and Lin, X. (2010). Improved sms islanding detection method for grid-connected converters. *IET renewable power generation*, 4(1):36–42.
- Lopes, L. A. and Sun, H. (2006). Performance assessment of active frequency drifting islanding detection methods. *IEEE Transactions on Energy Conversion*, 21(1):171–180.
- Mahat, P., Chen, Z., and Bak-Jensen, B. (2009). A hybrid islanding detection technique using average rate of voltage change and real power shift. *IEEE Transactions on Power delivery*, 24(2):764–771.

- Mango, F. D., Liserre, M., and Dell'Aquila, A. (2006). Overview of anti-islanding algorithms for pv systems. part ii: Activemethods. In *2006 12th International Power Electronics and Motion Control Conference*, pages 1884–1889.
- Maragos, P. and Schafer, R. (1987). Morphological filters—Part I: Their set-theoretic analysis and relations to linear shift-invariant filters. *IEEE Transactions on Acoustics, Speech, and Signal Processing*, 35(8):1153–1169.
- Matic-Cuka, B. and Kezunovic, M. (2014). Islanding detection for inverter-based distributed generation using support vector machine method. *IEEE Transactions on Smart Grid*, 5(6):2676–2686.
- Menon, V. and Nehrir, M. H. (2007). A hybrid islanding detection technique using voltage unbalance and frequency set point. *IEEE Transactions on Power Systems*, 22(1):442–448.
- Merlin, V., Santos, R., Grilo, A., Vieira, J., Coury, D., and Oleskovicz, M. (2016). A new artificial neural network based method for islanding detection of distributed generators. *International Journal of Electrical Power & Energy Systems*, 75:139–151.
- Mitchell, T. M. (1997). *Machine Learning*. McGraw-Hill, Inc., New York, NY, USA, 1 edition.
- Mohanty, S. R., Kishor, N., Ray, P. K., and Catalão, J. P. (2012). Islanding detection in a distributed generation based hybrid system using intelligent pattern recognition techniques. In *2012 3rd IEEE PES Innovative Smart Grid Technologies Europe (ISGT Europe)*, pages 1–5. IEEE.
- Mohanty, S. R., Kishor, N., Ray, P. K., and Catalo, J. P. (2015). Comparative study of advanced signal processing techniques for islanding detection in a hybrid distributed generation system. *IEEE Transactions on Sustainable Energy*, 6(1):122–131.
- Morsi, W. G., Diduch, C., and Chang, L. (2010). A new islanding detection approach using wavelet packet transform for wind-based distributed generation. In *The 2nd International Symposium on Power Electronics for Distributed Generation Systems*, pages 495–500. IEEE.

- Niaki, A. M. and Afsharnia, S. (2014). A new passive islanding detection method and its performance evaluation for multi-DG systems. *Electric Power Systems Research*, 110:180–187.
- Ning, J. and Wang, C. (2012). Feature extraction for islanding detection using wavelet transform-based multi-resolution analysis. In *2012 IEEE Power and Energy Society General Meeting*, pages 1–6. IEEE.
- O’kane, P. and Fox, B. (1997). Loss of mains detection for embedded generation by system impedance monitoring.
- Pai, F.-S. and Huang, S.-J. (2001). A detection algorithm for islanding-prevention of dispersed consumer-owned storage and generating units. *IEEE Transactions on Energy Conversion*, 16(4):346–351.
- Peng, Z., Peter, W. T., and Chu, F. (2005). A comparison study of improved Hilbert–Huang transform and wavelet transform: application to fault diagnosis for rolling bearing. *Mechanical systems and signal processing*, 19(5):974–988.
- Pigazo, A., Liserre, M., Mastromauro, R. A., Moreno, V. M., and Dell’Aquila, A. (2009). Wavelet-based islanding detection in grid-connected pv systems. *IEEE Transactions on Industrial Electronics*, 56(11):4445–4455.
- Pigazo, A., Moreno, V. M., Liserre, M., and Dell’Aquila, A. (2007). Wavelet-based islanding detection algorithm for single-phase photovoltaic PV distributed generation systems. In *2007 IEEE International Symposium on Industrial Electronics*, pages 2409–2413. IEEE.
- Pinnegar, C. R. and Mansinha, L. (2003a). A method of time–time analysis: The TT-transform. *Digital Signal Processing*, 13(4):588–603.
- Pinnegar, C. R. and Mansinha, L. (2003b). The S-transform with windows of arbitrary and varying shape. *Geophysics*, 68(1):381–385.
- Polikar, R. (1999). The story of wavelets. *Physics and Modern Topics in Mechanical and Electrical Engineering*, pages 192–197.
- PVPS, I. (2002). Evaluation of islanding detection methods for photovoltaic utility-interactive power systems. *Report IEA PVPS T5-09*.

- Ray, P. K., Kishor, N., and Mohanty, S. R. (2010). S-transform based islanding detection in grid-connected distributed generation based power system. In *Energy Conference and Exhibition (EnergyCon), 2010 IEEE International*, pages 612–617. IEEE.
- Ray, P. K., Kishor, N., and Mohanty, S. R. (2012). Islanding and power quality disturbance detection in grid-connected hybrid power system using wavelet and S-transform. *IEEE Transactions on Smart Grid*, 3(3):1082–1094.
- Ray, P. K., Mohanty, S. R., and Kishor, N. (2011). Disturbance detection in grid-connected distributed generation system using wavelet and S-transform. *Electric Power Systems Research*, 81(3):805–819.
- Redfern, M., Usta, O., and Fielding, G. (1993). Protection against loss of utility grid supply for a dispersed storage and generation unit. *IEEE Transactions on Power Delivery*, 8(3):948–954.
- Reigosa, D., Briz, F., Charro, C. B., García, P., and Guerrero, J. M. (2012). Active islanding detection using high-frequency signal injection. *IEEE Transactions on Industry Applications*, 48(5):1588–1597.
- Ribeiro, P. F., Duque, C. A., Ribeiro, P. M., and Cerqueira, A. S. (2013). *Power systems signal processing for smart grids*. John Wiley & Sons.
- Rilling, G., Flandrin, P., Goncalves, P., et al. (2003). On empirical mode decomposition and its algorithms. In *IEEE-EURASIP workshop on nonlinear signal and image processing*, volume 3, pages 8–11. IEEEER.
- Rish, I. (2001). An empirical study of the naive bayes classifier. In *IJCAI 2001 workshop on empirical methods in artificial intelligence*, volume 3, pages 41–46. IBM New York.
- Ropp, M., Begovic, M., and Rohatgi, A. (1999). Analysis and performance assessment of the active frequency drift method of islanding prevention. *IEEE Transactions on Energy conversion*, 14(3):810–816.
- Samantaray, S., El-Arroudi, K., Joos, G., and Kamwa, I. (2010a). A fuzzy rule-based approach for islanding detection in distributed generation. *IEEE Transactions on Power Delivery*, 25(3):1427–1433.

- Samantaray, S., Pujhari, T. M., and Subudhi, B. (2009). A new approach to islanding detection in distributed generations. In *Power Systems, 2009. ICPS'09. International Conference on*, pages 1–6. IEEE.
- Samantaray, S., Samui, A., and Babu, B. C. (2010b). S-transform based cumulative sum detector (CUSUM) for islanding detection in distributed generations. In *Power Electronics, Drives and Energy Systems (PEDES) & 2010 Power India, 2010 Joint International Conference on*, pages 1–6. IEEE.
- Samui, A. and Samantaray, S. (2013). Wavelet singular entropy-based islanding detection in distributed generation. *IEEE Transactions on Power Delivery*, 28(1):411–418.
- Sejdic, E., Djurovic, I., et al. (2008). Quantitative performance analysis of scalogram as instantaneous frequency estimator. *IEEE Transactions on Signal Processing*, 56(8):3837–3845.
- Shariatinasab, R. and Akbari, M. (2010). New islanding detection technique for DG using discrete wavelet transform. In *Power and Energy (PECon), 2010 IEEE International Conference on*, pages 294–299. IEEE.
- Sharma, R. and Singh, P. (2012). Islanding detection and control in grid based system using wavelet transform. In *Power India Conference, 2012 IEEE Fifth*, pages 1–4. IEEE.
- Simonyan, K. and Zisserman, A. (2014). Very deep convolutional networks for large-scale image recognition. *arXiv preprint arXiv:1409.1556*.
- Singam, B. and Hui, L. Y. (2006). Assessing sms and pjd schemes of anti-islanding with varying quality factor. In *Power and Energy Conference, 2006. PECon'06. IEEE International*, pages 196–201. IEEE.
- Specht, D. F. (1990). Probabilistic neural networks. *Neural networks*, 3(1):109–118.
- Stockwell, R. G., Mansinha, L., and Lowe, R. (1996). Localization of the complex spectrum: the S transform. *IEEE Transactions on Signal Processing*, 44(4):998–1001.

- Thomas, M. S. and Terang, P. P. (2010). Islanding detection using decision tree approach. In *Power Electronics, Drives and Energy Systems (PEDES) & 2010 Power India, 2010 Joint International Conference on*, pages 1–6. IEEE.
- Tsang, K. M. and Chan, W. L. (2013). Three-level grid-connected photovoltaic inverter with maximum power point tracking. *Energy Conversion and Management*, 65:221–227.
- Vahedi, H., Noroozian, R., Jalilvand, A., and Gharehpetian, G. (2010). Hybrid SFS and Q-f islanding detection method for inverter-based DG. In *Power and Energy (PECon), 2010 IEEE International Conference on*, pages 672–676. IEEE.
- Vatani, M., Amraee, T., Ranjbar, A. M., and Mozafari, B. (2015). Relay logic for islanding detection in active distribution systems. *IET Generation, Transmission & Distribution*, 9(12):1254–1263.
- Velasco, D., Trujillo, C., Garcera, G., and Figueres, E. (2011). An active anti-islanding method based on phase-pll perturbation. *IEEE Transactions on Power Electronics*, 26(4):1056–1066.
- Ventosa, S., Simon, C., Schimmel, M., Dañobeitia, J. J., and Mànuel, A. (2008). The S-transform from a wavelet point of view. *IEEE Transactions on Signal Processing*, 56(7):2771–2780.
- Wang, W., Kliber, J., Zhang, G., Xu, W., Howell, B., and Palladino, T. (2007). A power line signaling based scheme for anti-islanding protection of distributed generators—part ii: field test results. *IEEE Transactions on Power Delivery*, 22(3):1767–1772.
- Xu, W., Zhang, G., Li, C., Wang, W., Wang, G., and Kliber, J. (2007). A power line signaling based technique for anti-islanding protection of distributed generators—part i: Scheme and analysis. *IEEE Transactions on Power Delivery*, 22(3):1758–1766.
- Yin, G. (2005). A distributed generation islanding detection method based on artificial immune system. In *2005 IEEE/PES Transmission & Distribution Conference & Exposition: Asia and Pacific*, pages 1–4. IEEE.

- Zhao, C., He, M., and Zhao, X. (2004). Analysis of transient waveform based on combined short time fourier transform and wavelet transform. In *Power System Technology, 2004. PowerCon 2004. 2004 International Conference on*, volume 2, pages 1122–1126. IEEE.
- Zhu, Y., Yang, Q., Wu, J., Zheng, D., and Tian, Y. (2008). A novel islanding detection method of distributed generator based on wavelet transform. In *Electrical Machines and Systems, 2008. ICEMS 2008. International Conference on*, pages 2686–2688. IEEE.

PUBLICATIONS

Patents

1. Indian patent filed on “ A Method For Islanding Detection Based On Image Classification With Ensemble Convolution Neural Networks,” Sept. 2019 (Application No. 201941036379).

Papers in refereed journals

1. Santhosh K G Manikonda, Dattatraya N Gaonkar, “Comprehensive review of IDMs in DG systems” *IET Smart Grid*, vol. 2, no.1, pp. 11-24, Apr 2019. DOI: 10.1049/iet-stg.2018.0096
2. Santhosh K G Manikonda, Dattatraya N Gaonkar, “IDM based on image classification with CNN” *IET The Journal of Engineering*, May 13 2019. DOI: 10.1049/joe.2019.0025.
3. Santhosh K G Manikonda, Dattatraya N Gaonkar, “An islanding detection method based on image classification technique using histogram of oriented gradient features” *IET Generation, Transmission & Distribution - Accepted*.
4. Santhosh K G Manikonda, Dattatraya N Gaonkar, “Islanding Detection Method Based on Image Classification Technique Using Multiple CNN Classifiers” *Submitted to IET Renewable Power Generation - RPG-2019-1486*.
5. Santhosh K G Manikonda, Dattatraya N Gaonkar, “Islanding Detection Method Based on Image Classification Using Transfer Learning Classifiers” *Submitted to IEEE Systems Journal - ISJ-RE-19-08878*.

Book chapter

1. Santhosh K G Manikonda, Dattatraya N Gaonkar, “Islanding detection in microgrids: An overview” *Microgrids: Advances in Operation, Control, and Protection*, Springer, (Abstract Provisionally Accepted).

Papers published in refereed conference proceedings

1. Santhosh K G Manikonda, Joe Santhosh, Sanjayan Pradeep Kumar Sreekala, Siddharth Gangwani, Dattatraya N Gaonkar, "Power Quality Event Classification Using Long Short-Term Memory Networks" *IEEE Distributed Computing, VLSI, Electrical Circuits and Robotics (DISCOVER)2019*, Manipal Institute of Technology, Manipal, Karnataka, India, 11th to 12th August, 2019.
2. Santhosh K G Manikonda, Joe Santhosh, Sanjayan Pradeep Kumar Sreekala, Siddharth Gangwani, Dattatraya N Gaonkar, "Power Quality Event Classification Using Convolutional Neural Networks On Images" *IEEE International Conference on Energy, Systems and Information Processing (ICESIP)2019*, IITD&M Kancheepuram, Tamilnadu, India, 04th -06th July 2019.
3. Santhosh K G Manikonda, Joe Santhosh, Sanjayan Pradeep Kumar Sreekala, Siddharth Gangwani, Dattatraya N Gaonkar, "Power Quality Event Classification Using Transfer Learning On Images" *IEEE International Conference on Intelligent Techniques in Control, Optimization and Signal Processing (INCOS)2019*, Kalasalingam Academy of Research and Education, Srivilliputtur, Tamilnadu, India, 11th to 13th, April 2019.
4. Santhosh K G Manikonda, Dattatraya N Gaonkar, "A Novel Islanding Detection Method Based on Transfer Learning Technique Using VGG16 Network" *IEEE International Conference on Sustainable Energy Technologies and Systems (ICSETS)2019*, Kalinga Institute of Industrial Technology, Bhubaneswar, Odisha, India, 26th Feb to 01st March 2019.
5. Santhosh K G Manikonda, Dattatraya N Gaonkar, "A New Islanding Detection Method Using Transfer Learning Technique" *IEEE India International Conference on Power Electronics (IICPE)2018*, MNIT, Jaipur, Rajasthan, India, 13th - 15th Dec, 2018.
6. Santhosh K G Manikonda, Dattatraya N Gaonkar, "Influence of Various Load Types on Voltage at PCC and Islanding Detection in a Microgrid" *IEEE International Conference on Innovative Technologies in Engineering (ICITE)2018*, Osmania University, Hyderabad, Telangana, India, 11-13 April 2018.

Bio-data

Name : M Santhosh Kumar Goud

Date of birth: 22-02-1982

E-mail: santhosh.manikonda@gmail.com

Mobile: +91-9701723629

Education

- **MS**, Master of Science in Photonics (EMMP), University of St. Andrews and Heriot–Watt University, United Kingdom, 2008.
- **MS**, Master of Science in Photonics (EMMP), Vrije Universiteit Brussel (VUB), Brussels, Belgium, 2009.
- **B.Tech.**, Electrical & Electronics Engineering, Patnam Rajendar Reddy Memorial Engineering College, Shabad, Telangana, 2005.

Experience

- **Assistant Professor** in Jayaprakash Narayan College of Engineering, Mahabubnagar, Telangana, India from July 2013 to December 2015.
- **Research Assistant** in Vrije Universiteit Brussel, Belgium from September 2009 to December 2011.
- **Assistant Professor** in Jayaprakash Narayan College of Engineering, Mahabubnagar, Telangana, India from July 2006 to August 2007.

Address

H.No 18-182/9, Ayyappa Colony

Near Water Tank, Shadnagar

Telangana -509216, India.